Available online at www.sciencedirect.com
ScienceDirect
Journal of the European Ceramic Society 31 (2011) 941–976
www.elsevier.com/locate/jeurceramsoc

Review

Crystal chemistry of the monazite structure

Nicolas Clavier, Renaud Podor *, Nicolas Dacheux

Institut de Chimie Séparative de Marcoule, UMR 5257 CEA-CNRS-UM2-ENSCM, Site de Marcoule, BP17171, F-30207 Bagnols sur Cèze Cedex, France

Received 29 September 2010; received in revised form 7 December 2010; accepted 16 December 2010
Available online 5 February 2011

Abstract

The AXO_4 monazite-type compounds form an extended family that is described in this review in terms of field of stability versus composition. All the substitution possibilities on the cationic and anionic sites leading to the monazite structure are reported. The phosphate, vanadate, chromate, arseniate, sulphate and silicate families are described and the unit-cell parameters of pure compounds and solid solutions are gathered. The stability limits of the monazite-type structure are discussed versus several models generally correlated with geometric criteria. The effects of physico-chemical parameters such as pressure, temperature and irradiation on the monazite-type structure stability are also discussed. The structural relationships between the monazite structure and the related structures (zircon, anhydrite, barite, $AgMnO_4$, scheelite and monoclinic $BiPO_4$, $CaSeO_3$, rhabdophane and $SrNp(PO_4)_2$) are described.

Keywords: Phosphate; Monazite; Stability; Structure; Functional applications

Contents

* Corresponding author. Tel.: +33 4 66 33 92 02; fax: +33 4 66 79 76 11.
E-mail address: renaud.podor@cea.fr (R. Podor).

0955-2219/$ – see front matter © 2011 Elsevier Ltd. All rights reserved.
doi:10.1016/j.jeurceramsoc.2010.12.019

1. Introduction

Monazite is a natural light rare-earth element phosphate that generally contains large amounts of uranium and thorium.[1–5] Small crystals of this mineral are formed during the magma crystallization as an accessory phase. A review of the composition and geological occurrence of monazite in the accessory mineral assemblage of granitoids was given by Rapp and Watson.[6] Because of their high density, monazite minerals can concentrate in alluvial sands when released by the weathering of pegmatites. These so-called placer deposits are often beach or fossil beach sands and contain other heavy minerals of commercial interest such as zircon and ilmenite. These sands constitute the main world's thorium resource. During the 70s, several authors claimed that long-life superheavy elements ($Z = 124$, 126) were present in monazite inclusions in biotite. These minerals were characterized by giant halos, with radii up to 100 μm, that may be due to the radiation damage caused by the decay of superheavy elements.[7,8] However, no evidence for the existence of such elements was obtained.[9–11]

Due to some interesting physical and chemical properties (high fusion temperature, optical emissivity, high resistance to aqueous and molten glass corrosion or to radiation damage, . . .), five main applications for this material are already reported and under development.

Coatings and diffusion barrier: High fusion temperature and high temperature corrosion resistance in oxidizing environments yielded to propose the use of $LaPO_4$ as interface coatings in composites for high-temperature application, in the form of tape-cast laminates and fiber systems.[12–30]

Geochronology: Because natural monazites are often U and Th enriched minerals, radiogenic Pb accumulates quickly through the α, β decay sequences in the three natural radioactive families, and reaches, in about 100 Ma, a level where its analysis becomes possible by electron probe microanalysis (EPMA).[31] Assuming that common Pb is negligible, and that radiogenic Pb is kept in the structure all along the time excluding lead loss when ageing,[32,33] the simultaneous measurement of U, Th, and Pb allows to reach the geologically meaningful age from a single electron probe analysis. An easy to work/implement method was proposed and developed by Suzuki et al.[34] and Montel et al.[4,35,36] This method offers a large number of geologists to access an *in situ* dating technique with ±30–50 Ma final accuracy on ageing, for a 'normal' monazite.[3,37–40] The reliability of this method is linked to the structural properties of the monazite structure, in particular to its high chemical durability leading to small amounts of released elements[41–44] thus to the absence of lead loss during corrosion processes.

Luminophors, lasers and light emitters: Doped $LaPO_4$ crystals with Ce^{3+}, Eu^{3+}, Tb^{3+} or Yb^{3+} offer interesting optical properties.[45,46] Specific compositions were developed for applications in the field of electronic and optical applications.[47–49] The authors demonstrated that the light emission properties are directly linked to the doping elements substituted in the structure.[50,51] Most of the applications proposed are relative to the tetragonal form of $LaVO_4$,[52–54] and can depend on the crystal morphologies.[55–57] In this case, the main objectives are to avoid the formation of the monazite-type structure by addition of doping elements and to control the crystal growth process. This requires knowing the stability limits of both monazite and zircon structures.[58–71] The same objectives are required for the use of $LnVO_4$ and $LnCrO_4$ as catalysts.[72–77]

Ionic conductors: Specific applications in the field of ionic conductor materials are also proposed for several monazite-type compounds in the phosphate[78–81] and vanadate families.[58,82] Other particular compositions ($CaSeO_3$, $LaCrO_4$) can also potentially exhibit specific ionic or electronic conduction.[41,83]

Matrix for radioactive waste management: The resistance of natural monazites to geological events, its high chemical durability despite of the presence of usually mobile cations (e.g. calcium) and its capacity to incorporate large amounts of uranium and thorium yielded to propose their use in the field of long term storage of radioactive wastes.[5,84–93] In the same way, the high resistance of monazite-type structure to radiation damages (either in the synthetic and natural forms) is probably connected to the easy recovery of these distorted polyhedra for very low temperatures of annealing. A lot of compositions were synthesized, yielding to the incorporation of various elements in terms of ionic radii and oxidation state in the monazite structure.[94] Within this application, particular studies

are dedicated to the fabrication processes[95–104] or to the sintering of monazite compounds loaded with actinides or actinide surrogates.[105–110]

In these applications, the elementary incorporation in the structure is the key factor driving the material properties. The understanding and forecasting of elementary substitution in the monazite structure is of major interest to obtain designed materials. This objective could be achieved by the precise description of the crystal chemistry of the monazite structure-type compounds. During the last decades, few articles and reviews were devoted to this purpose but none of them were focussed on the substitution capabilities. In the light of the applied potentialities of monazite compounds and of the lack of general data on the monazite crystal chemistry, we decided to present this review paper based upon all the reported synthetic compounds adopting the monazite type structure dealing with the substitution mechanisms, structure stability domain and structural relationships with existing polymorphs. The aim of this work is mainly to explore the incorporation possibilities of the monazite structure thus to give the reader the keys for the design of new monazite compositions.

2. Description of the monazite structure

The monazite-type compounds crystallize in a monoclinic lattice with space group $P2_1/n$ ($Z=4$). This structure was first reported by Mooney in the framework of the Manhattan Project and latter published in 1948.[111] It was then refined from this date by several authors for various rare earth phosphates,[112–117] until Ni et al. provide a high precision structural determination.[118] As an example, the parameters reported for $LaPO_4$ reach $a=6.8313(10)$ Å; $b=7.0705(9)$ Å; $c=6.5034(9)$ Å and $b=103.27(1)^\circ$, leading to a cell volume of 305.73 Å^3 and a calculated density of about 5.08 g cm^{-3}.

A complete description of the structure and of the coordination polyhedra of the rare-earth element was reported by Beall et al.[117] and Mullica et al.[115,119] The structural arrangement is based on the nine-fold coordination of the metallic cation and is usually described as an equatorial pentagon (formed by 5 oxygen atoms belonging to monodentate anionic tetrahedrons) interpenetrated by a tetrahedron (built by 4 oxygen atoms belonging to two bidentate tetrahedrons) as shown in Fig. 1. The tetrahedrons located out of the equatorial plane could then be described as a link between the $REEO_9$ polyhedra, leading to the formation of infinite chains along the c axis ([0 0 1] direction).

Moreover, the values reported for the REE-O lengths evidence a longer bond (around 2.78 Å in $REEPO_4$) compared to the others (about 2.53 Å) which leads to a distortion of the $REEO_9$ polyhedron.[117,120] This induces a set of nine distinct bond distances between rare earth element and oxygen atoms.[118] This type of distortion is often correlated to the capability of the structure to accommodate a large variety of cations and polyoxoanions. Also, the irregular coordination around the metallic centre does not induce severe symmetry, size or charge constraints on cations.[84]

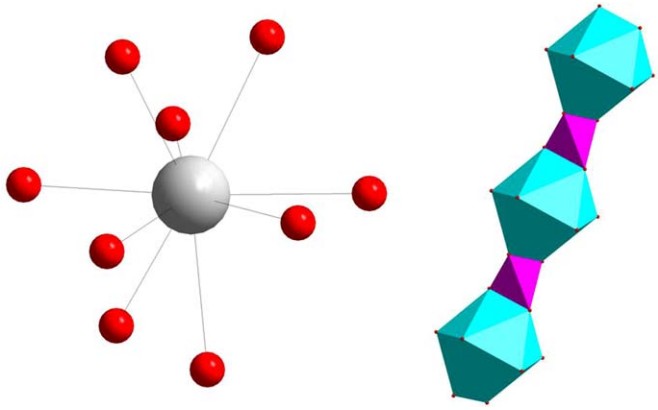

Fig. 1. Ninefold coordination of cerium and interlocking mechanism of the chain-like strands in $CePO_4$ monazite.[118]

3. AXO_4 compound series with the monazite-type structure

All the compounds that can be stabilized with the monazite structure are reported in this section and associated crystallographic data are collected in Tables 1–8. The wide variety of compositions that can be stabilized with the monazite structure yields us to treat separately the phosphate family from the other series (vanadates, arsenates, etc.).

3.1. Phosphates with the monazite structure

3.1.1. $M^{III}PO_4$ compounds

All the light lanthanide phosphates (typically from lanthanum to gadolinium, including promethium[121]) crystallize in the $P2_1/n$ space group of monazite[122–129] while the heavier (from Tb to Lu) adopt the zircon-type structure of xenotime.[118,130–132] Nevertheless, for the rare earth elements located in the middle of the series, the limit between both families appears to be strongly dependent on the chemical way of synthesis. Indeed, several authors report the formation of $TbPO_4$[133–135] monazites from the heat treatment of the corresponding rhabdophane ($REEPO_4$, 0.5 H_2O) precursor. Such a transformation is described for several rare earth elements and generally occurs with the formation of an anhydrous phosphate with rhabdophane structure before the phase transition to the monoclinic monazite.[136,137] On the other hand, the direct preparation of monazites through flux method[138] or during precipitation in organic media[139] as well as the use of solid state reactions[140] led to a tetragonal lattice for the terbium phosphate. Moreover, the structure of $TbPO_4$ is also dependent on the precursor used during the precipitation processes as demonstrated by Boakye et al.[141] who obtained the monazite form only in the presence of citrate ions.

The formation of monazite-type compounds was also reported for trivalent actinides phosphates. As instance, the preparation of $PuPO_4$ was mentioned using wet chemistry methods, mostly involving the initial precipitation of rhabdophane as starting precursors,[142] or solid state syntheses.[140,143] Ponderable amounts of monazite were also obtained for americium,[144,145] ^{248}Cm curium[146] as well as for ^{249}Bk berkelium, ^{249}Cf cal-

Table 1
Unit-cell parameters of the $M^{III}PO_4$ monazite-type compounds.

	a (Å)	b (Å)	c (Å)	β (°)	V (Å^3)	Ref.
$LaPO_4$	6.8413	7.078	6.513	103.322	306.89	122
$LaPO_4$	6.825	7.057	6.482	103.21	303.94	115
$LaPO_4$	6.8406	7.0736	6.5126	103.31	306.66	123
$LaPO_4$	6.836	7.076	6.509	103.23	306.49	112
$LaPO_4$	6.8313	7.0705	6.5034	103.27	305.73	118
$LaPO_4$	6.841	7.079	6.508	103.33	306.67	135
$LaPO_4$	6.8313	7.0705	6.5034	103.27	305.73	118
$LaPO_4$	6.8242	7.0792	6.4919	103	305.58	133
$CePO_4$	6.7777	6.993	6.445	103.54	296.98	114
$CePO_4$	6.7804	6.9967	6.4482	103.52	297.43	123
$CePO_4$	6.7989	7.0226	6.4735	103.4755	300.57	124
$CePO_4$	6.788	7.0163	6.465	103.43	299.49	118
$CePO_4$	6.803	7.03	6.472	103.6	300.85	135
$CePO_4$	6.7968	7.0258	6.4743	103.5	300.62	133
$CePO_4$	6.7989	7.0226	6.4735	103.4755	300.57	124
$PrPO_4$	6.741	6.961	6.416	103.63	292.59	125
$PrPO_4$	6.7596	6.9812	6.4344	103.53	295.21	118
$PrPO_4$	6.7687	6.99	6.4439	103.5	296.46	133
$PrPO_4$	6.7623	6.9785	6.4304	103.516	295.05	126
$NdPO_4$	6.722	6.933	6.39	103.72	289.30	127
$NdPO_4$	6.7426	6.9574	6.4097	103.6624	292.18	124
$NdPO_4$	6.7352	6.95	6.4049	103.68	291.31	118
$NdPO_4$	6.7392	6.9621	6.4053	103.6	292.10	133
$NdPO_4$	6.7426	6.9574	6.4097	103.6624	292.18	126
$SmPO_4$	6.669	6.868	6.351	103.92	282.35	128
$SmPO_4$	6.6818	6.8877	6.3653	103.86	284.42	118
$SmPO_4$	6.6891	6.8958	6.377	103.9	285.54	133
$EuPO_4$	6.639	6.823	6.318	104	277.69	128
$EuPO_4$	6.6613	6.8618	6.3491	103.96	281.64	118
$EuPO_4$	6.666	6.8684	6.3486	103.9	282.16	133
$GdPO_4$	6.621	6.823	6.31	104.16	276.39	128
$GdPO_4$	6.6503	6.8466	6.3333	104.007	279.79	123
$GdPO_4$	6.652	6.845	6.334	104	279.84	112
$GdPO_4$	6.6435	6.8414	6.3281	103.976	279.10	118
$GdPO_4$	6.6435	6.8414	6.3281	103.976	279.10	118
$GdPO_4$	6.6511	6.8471	6.3343	104	279.90	133
$GdPO_4$	6.732	6.93	6.383	103.61	289.42	129
$TbPO_4$	6.6115	6.8131	6.3143	104.1	275.86	133
$BiPO_4$	6.7626	6.9516	6.4822	103.74	296.01	151
$PuPO_4$	6.73	7	6.42	103.8	293.72	142
$PuPO_4$	6.7641	6.9841	6.4536	103.64	296.28	124
$PuPO_4$	6.73	7	6.42	103.8	293.72	144
$PuPO_4$	6.74	6.95	6.42	103.7	292.18	107
$PuPO_4$	6.76	6.98	6.44	103.66	295.27	107
$PuPO_4$	6.772	6.968	6.427	103.7	294.64	143
$AmPO_4$	6.73	6.93	6.41	103.50	290.29	144
$AmPO_4$	6.74	6.96	6.43	103.75	292.99	107
$CmPO_4$	6.72	6.93	6.37	104.63	287.70	146

ifornium and ^{251}Es einsteinium.[147–149] The precipitation of UPO_4 in formic acid media was also reported[150] but appears strongly doubtful regarding to the oxidation states generally stabilized for uranium in presence of phosphates (*i.e.* IV and VI).

Bismuth phosphate also adopts the monazite structure even if a second tetragonal phase can be obtained from precipitation between 25 °C and 200 °C, the nature of the solid stabilized being mostly dependent on the heating time.[151–153] Nevertheless, the stability of monazite-type $BiPO_4$ appears to be limited to a smaller temperature range compared to lanthanide phosphates since it decomposes above 600 °C to adopt another monoclinic structure.[154]

On the basis of these data, the ionic radii of trivalent elements that can be incorporated in the monazite structure ranges from 1.095 Å (terbium) to 1.216 Å (lanthanum) (note that the ionic

Table 2
Unit-cell parameters of REE′REE″PO_4 solid solutions with the monazite structure.

REE′REE″$(PO_4)_3$ series	a (Å)	b (Å)	c (Å)	β (°)	V (Å^3)	Ref.
$(Ce_{0.50}Tb_{0.50})PO_4$	6.7272	6.944	6.4176	103.726	291.23	170
$(Ce_{0.50}Tb_{0.50})PO_4$	6.670	6.878	6.373	104.8	282.67	48
$(Nd_{0.50}Tb_{0.50})PO_4$	6.681	6.886	6.366	103.89	284.29	170
$(Nd_{0.50}Tb_{0.50})PO_4$	6.670	6.870	6.365	104.0	283.0	48
$(Sm_{0.50}Tb_{0.50})PO_4$	6.6500	6.8534	6.3412	103.99	280.42	170
$(Sm_{0.50}Tb_{0.50})PO_4$	6.630	6.820	6.333	104.1	277.73	48
$(La_{0.91}Ce_{0.09})PO_4$	6.8275	7.0609	6.5005	103.31	304.96	221
$LaPO_4$	6.837	7.078	6.507	103.28	306.50	135
$(La_{0.95}Gd_{0.05})PO_4$	6.806	7.02	6.467	103.61	300.30	135
$(La_{0.90}Gd_{0.10})PO_4$	6.797	7.015	6.452	103.6	299.00	135
$(La_{0.80}Gd_{0.20})PO_4$	6.786	7.013	6.457	103.42	298.90	135
$(La_{0.65}Gd_{0.35})PO_4$	6.765	6.99	6.448	103.66	296.20	135
$(La_{0.50}Gd_{0.50})PO_4$	6.737	6.947	6.408	103.69	291.30	135
$(La_{0.35}Gd_{0.65})PO_4$	6.72	6.925	6.393	103.76	288.80	135
$(La_{0.20}Gd_{0.80})PO_4$	6.684	6.883	6.353	103.84	282.80	135
$GdPO_4$	6.653	6.847	6.331	103.96	279.90	135
$(La_{0.85}Ce_{0.15})PO_4$	6.82814	7.06114	6.50125	103.297	305.05	158
$(La_{0.80}Tb_{0.20})PO_4$	6.82653	7.05615	6.50049	103.344	304.67	158
$(La_{0.65}Ce_{0.15}Tb_{0.20})PO_4$	6.81656	7.05175	6.49545	103.357	303.78	158
$CePO_4$	6.767	7.03	6.474	103.44	299.55	156
$(Ce_{0.8}La_{0.2})PO_4$	6.775	7.036	6.481	103.39	300.54	156
$(Ce_{0.6}La_{0.4})PO_4$	6.8	7.045	6.488	103.35	302.42	156
$(Ce_{0.4}La_{0.6})PO_4$	6.813	7.053	6.495	103.32	303.7	156
$(Ce_{0.2}La_{0.8})PO_4$	6.821	7.062	6.512	103.3	305.46	156
$LaPO_4$	6.833	7.072	6.516	103.25	306.49	156
$NdPO_4$	6.7448	6.9552	6.4140	103.669	292.368	172
$(Nd_{0.95}Y_{0.05})PO_4$	6.7363	6.9495	6.4058	103.701	291.347	172
$(Nd_{0.90}Y_{0.10})PO_4$	6.7345	6.9471	6.4070	103.728	291.190	172
$(Nd_{0.80}Y_{0.20})PO_4$	6.7187	6.9290	6.3962	103.765	289.216	172
$(Nd_{0.70}Y_{0.30})PO_4$	6.7030	6.9109	6.3850	103.809	287.228	172
$(Nd_{0.90}Yb_{0.10})PO_4$	6.7221	6.9339	6.4007	103.728	289.816	172
$(La_{0.60}Y_{0.40})PO_4$	6.7273	6.9445	6.4244	103.697	291.598	172
$(La_{0.9}Pu_{0.1})PO_4$	6.8396	7.0777	6.5008	103.2	306.38	177
$(La_{0.9}Gd_{0.1})PO_4$	6.8234	7.0582	6.4949	103.33	304.37	177

radii reported in the paper are all given for the nine-fold coordination, unless specifically advised in the text).[155] The unit-cell parameters of the APO_4 monazite-type compounds are gathered in Table 1.

3.1.2. $M'_{1-x}M''_xPO_4$ solid solutions

As mineral ores, natural monazites generally incorporate all the lanthanide elements from lanthanum to lutetium with various chemical compositions, La and Ce being almost always predominant.[6] On this basis, several studies were undertaken about the possibility to incorporate simultaneously several rare earth elements in phosphate-based monazite-type compounds. These samples are generally obtained through wet chemistry methods since solid state routes hardly promote the formation of homogeneous solid solutions due to some differences in the temperature reaction of the various elements.[140]

Two cases could be distinguished in the family. On the one hand, several authors studied some mixtures of two light rare earth elements, namely from La to Gd, which usually adopt the

Table 3
$(M^{II}_{0.5}M^{IV}_{0.5})PO_4$ phases with the monazite structure reported in the literature.

M^{IV}	M^{II}						
	Mg	Ca	Sr		Cd	Ba	Pb
Ce	210	210 140, 207, 208	210	207	210	210 207	
Th	210	140, 202, 203, 210, 171, 213, 216	210, 213		213, 215	213, 215	213, 215
U	210	140, 202, 203, 210, 212, 216	210				
Np		204, 205, 206					
Pu		107, 204					

Note: The shaded cells indicate unsucceeded syntheses.

Table 4
Unit-cell parameters of $(M^{II}_{0.5}M^{IV}_{0.5})PO_4$ compounds with the monazite structure.

	a (Å)	b (Å)	c (Å)	β (°)	V (Å^3)	Ref.
$(Ca_{0.5}Th_{0.5})PO_4$	6.675	6.889	6.392	103.57	285.72	210
$(Ca_{0.5}Th_{0.5})PO_4$	6.695	6.907	6.41	103.609	288.09	215
$(Ca_{0.5}Th_{0.5})PO_4$	6.714	6.921	6.424	103.683	290.04	215
$(Ca_{0.5}Th_{0.5})PO_4$	6.705	6.918	6.415	103.65	289.16	171
$(Ca_{0.5}Th_{0.5})PO_4$	6.706	6.916	6.417	103.72	289.12	171
$(Ca_{0.5}Th_{0.5})PO_4$	6.7088	6.9166	6.4158	103.7031	289.23	124
$(Ca_{0.5}Th_{0.5})PO_4$	6.7085	6.916	6.4152	103.71	289.16	205
$(Mg_{0.5}Th_{0.5})PO_4$	6.523	6.83	6.261	102.18	272.66	210
$(Sr_{0.5}Th_{0.5})PO_4$	6.792	7.017	6.501	103.514	301.26	215
$(Sr_{0.5}Th_{0.5})PO_4$	6.825	7.047	6.535	103.64	305.44	210
$(Ba_{0.5}Th_{0.5})PO_4$	6.944	7.161	6.67	102.88	323.33	215
$(Pb_{0.5}Th_{0.5})PO_4$	6.848	7.081	6.565	103.8	309.15	215
$(Ca_{0.5}U_{0.5})PO_4$	6.661	6.851	6.36	104.134	281.45	212
$(Ca_{0.5}U_{0.5})PO_4$	6.673	6.852	6.364	104.068	282.26	212
$(Ca_{0.5}U_{0.5})PO_4$	6.653	6.845	6.356	104.025	280.82	212
$(Ca_{0.5}U_{0.5})PO_4$	6.639	6.852	6.362	103.8	281.06	210
$(Mg_{0.5}U_{0.5})PO_4$	6.548	6.785	6.284	103.5	271.47	210
$(Sr_{0.5}U_{0.5})PO_4$	6.803	6.965	6.42	103.62	295.64	210
$(Sr_{0.5}U_{0.5})PO_4$	6.803	6.965	6.42	103.62	295.7	204
$(Ca_{0.5}Np_{0.5})PO_4$	6.6509	6.839	6.3537	104.12	280.27	205
$(Ca_{0.5}Np_{0.5})PO_4$	6.666	6.854	6.370	104.11	282.23	204
$(Ca_{0.50}Np_{0.35}Pu_{0.15})PO_4$	6.649	6.840	6.351	104.14	280.07	204
$(Ca_{0.50}Ce_{0.50})PO_4$	6.759	6.992	6.438	103.43	295.90	210,211
$(Mg_{0.50}Ce_{0.50})PO_4$	6.788	7.004	6.449	103.46	298.20	210,211
$(Ba_{0.50}Ce_{0.50})PO_4$	6.776	7.016	6.437	103.42	297.60	210,211,240
$(Ba_{0.50}Ce_{0.50})PO_4$	6.8	7.027	6.475	103.46	300.90	201
$(Sr_{0.50}Ce_{0.50})PO_4$	6.768	7.007	6.443	103.39	297.00	210,211
$(Cd_{0.50}Ce_{0.50})PO_4$	6.764	7.002	6.446	103.39	297.00	210,211
$(Ca_{0.5}Th_{0.5})PO_4$	6.713	6.916	6.418	103.74	289.4	216
$(Ca_{0.5}Th_{0.5})PO_4$	6.71	6.914	6.414	103.73	289.1	216
$(Ca_{0.5}Th_{0.4}U_{0.1})PO_4$	6.706	6.906	6.411	103.8	288.3	216
$(Ca_{0.5}Th_{0.4}U_{0.1})PO_4$	6.707	6.906	6.412	103.79	288.4	216
$(Ca_{0.5}Th_{0.3}U_{0.2})PO_4$	6.697	6.893	6.401	103.86	286.9	216
$(Ca_{0.5}Th_{0.2}U_{0.3})PO_4$	6.689	6.882	6.395	103.91	285.7	216
$(Ca_{0.5}Th_{0.1}U_{0.4})PO_4$	6.68	6.873	6.385	103.97	284.5	216
$(Ca_{0.5}U_{0.5})PO_4$	6.673	6.862	6.38	104.03	283.4	216
$(Ca_{0.5}U_{0.5})PO_4$	6.673	6.858	6.381	104.04	283.3	216

monazite structure. In these conditions, the unit cell parameters vary linearly with the substitution rate x and the solid solution can be obtained in the whole composition range between the two end-members. Several examples are reported in the literature for La–Ce,[156–158] La–Sm,[159] La–Eu,[13,160,161] La–Gd[135] or Gd–Eu.[162] These data can then be plotted along with the lattice parameters of the pure REE monazites as a function of the average ionic radius leading to a linear variation. The same type of complete solid solutions are reported in the $(La_{1-x}REE_x)PO_4$ (REE = Nd, Gd, Eu) systems by Popa et al.[163] The unit-cell parameters of the obtained compounds are not reported in their study.

On the other hand, several authors investigated the formation of solid solutions with one light rare earth (La–Gd) and one heavy lanthanide (Tb–Lu). For this kind of compounds, three distinct domains of composition could be defined, the first one corresponding to the stabilization of the monazite structure. Such samples are particularly studied for photoluminescence applications, where the incorporation of terbium or thulium in $LaPO_4$ allows obtaining green or blue light emission, respectively. In this framework, the monazite structure is maintained up to 15% of Tb[50,157,164,165,166] and 1% of Tm.[50] $(Ce_{1-x}Tb_x)PO_4$ $(0 < x < 0.4)$ crystallized compounds with the monazite structure were obtained by Li et al.[167] However, no specific analyses were performed to precisely determine the composition of the studied compounds. The authors only reported that no additional phase was observed in the XRD patterns. Up to 5% of erbium or ytterbium were also incorporated in $LaPO_4$ without any structural modification by Jung et al.[168] while Han et al. reported the formation of $La_{0.9}Dy_{0.1}PO_4$.[169] Finally, Mullica et al.[170] also prepared the (1:1) Ce–Tb, Nd–Tb and Sm–Tb phosphates with the monazite structure. On the other hand, the tetragonal xenotime crystallizes as the most stable phase in the case of the (1:1) Nd–Er, Sm–Er, Sm–Yb and Sm–Lu phosphates which present average ionic radii from 1.082 Å ($Sm_{0.5}Lu_{0.5}PO_4$) to 1.125 Å ($Nd_{0.5}Er_{0.5}PO_4$). Indeed, these values stand at the border or out of the monazite structure stability range defined by Podor and Cuney[171] which will be discussed later.

Table 5
Unit-cell parameters of $M^{II}M^{III}M^{IV}(PO_4)_3$ series with the monazite structure.

	a (Å)	b (Å)	c (Å)	β (°)	V (Å^3)	Ref.
$(Mg_{1/3}Sm_{1/3}Zr_{1/3})PO_4$	6.67	6.88	6.35	103.8	283.10	210
$(Ba_{1/3}Sm_{1/3}Zr_{1/3})PO_4$	6.71	7.05	6.44	102.8	297.60	210
$(Mg_{1/3}Eu_{1/3}Zr_{1/3})PO_4$	6.74	6.91	6.44	103	292.20	210
$(Ca_{1/3}Eu_{1/3}Zr_{1/3})PO_4$	6.78	6.9	6.41	102.9	292.30	210
$(Ba_{1/3}Eu_{1/3}Zr_{1/3})PO_4$	6.76	6.92	6.48	103.1	295.20	210
$(Mg_{1/3}Gd_{1/3}Zr_{1/3})PO_4$	6.78	6.9	6.44	102.7	293.90	210
$(Ca_{1/3}Gd_{1/3}Zr_{1/3})PO_4$	6.77	6.91	6.45	103.2	292.80	210
$(Sr_{1/3}Gd_{1/3}Zr_{1/3})PO_4$	6.76	6.93	6.43	102.9	293.60	210
$(Ba_{1/3}Gd_{1/3}Zr_{1/3})PO_4$	6.76	6.92	6.43	103.2	292.80	210
$(Mg_{1/3}Nd_{1/3}Ce_{1/3})PO_4$	6.731	6.98	6.425	103.6	293.80	210
$(Ca_{1/3}Nd_{1/3}Ce_{1/3})PO_4$	6.76	6.973	6.419	103.7	293.90	210
$(Sr_{1/3}Nd_{1/3}Ce_{1/3})PO_4$	6.75	6.983	6.429	103.62	294.50	210
$(Ba_{1/3}Nd_{1/3}Ce_{1/3})PO_4$	6.763	6.989	6.433	103.62	295.50	210
$(Cd_{1/3}Nd_{1/3}Ce_{1/3})PO_4$	6.759	6.986	6.431	103.56	295.30	210
$(Mg_{1/3}Gd_{1/3}Ce_{1/3})PO_4$	6.717	6.916	6.399	103.95	288.50	210
$(Ca_{1/3}Gd_{1/3}Ce_{1/3})PO_4$	6.721	6.931	6.404	103.93	289.50	210
$(Sr_{1/3}Gd_{1/3}Ce_{1/3})PO_4$	6.729	6.949	6.418	103.77	291.50	210
$(Ba_{1/3}Gd_{1/3}Ce_{1/3})PO_4$	6.73	6.96	6.414	103.9	291.70	210
$(Cd_{1/3}Gd_{1/3}Ce_{1/3})PO_4$	6.742	6.954	6.426	103.9	292.50	210
$(Mg_{1/3}Gd_{1/3}Th_{1/3})PO_4$	6.572	6.799	6.313	104.2	273.40	210
$(Ca_{1/3}Gd_{1/3}Th_{1/3})PO_4$	6.674	6.882	6.379	103.8	284.50	210
$(Ba_{1/3}Gd_{1/3}Th_{1/3})PO_4$	6.709	6.898	6.487	104.38	290.90	210
$(Cd_{1/3}Gd_{1/3}Th_{1/3})PO_4$	6.658	6.85	6.362	104.04	281.50	210
$(Ca_{1/3}Nd_{1/3}U_{1/3})PO_4$	6.677	6.889	6.373	103.7	284.80	210
$(Sr_{1/3}Nd_{1/3}U_{1/3})PO_4$	6.697	6.933	6.388	103.5	288.40	210
$(Ba_{1/3}Nd_{1/3}U_{1/3})PO_4$	6.722	6.923	6.405	103.91	289.30	210
$(Cd_{1/3}Nd_{1/3}U_{1/3})PO_4$	6.696	6.917	6.372	103.8	286.60	210
$(Ca_{1/3}Gd_{1/3}U_{1/3})PO_4$	6.648	6.839	6.347	103.99	280.00	210
$(Sr_{1/3}Gd_{1/3}U_{1/3})PO_4$	6.646	6.859	6.345	104.03	280.90	210
$(Ba_{1/3}Gd_{1/3}U_{1/3})PO_4$	6.644	6.895	6.344	104.08	281.90	210
$(Cd_{1/3}Gd_{1/3}U_{1/3})PO_4$	6.653	6.835	6.333	103.8	279.60	210
$(Nd_{0.716}Th_{0.151}Ca_{0.146})PO_4$	6.774	7.002	6.469	103.59	298.24	227
$LaPO_4$	6.83	7.067	6.5	103.275	305.36	215
$LaPO_4$	6.827	7.062	6.499	103.28	304.95	215
$(La_{0.808}Ba_{0.096}Th_{0.096})PO_4$	6.851	7.075	6.518	103.399	307.33	215
$(La_{0.757}Ba_{0.121}Th_{0.121})PO_4$	6.854	7.085	6.538	103.295	308.98	215
$(La_{0.690}Ba_{0.155}Th_{0.155})PO_4$	6.849	7.081	6.535	103.306	308.42	215
$(La_{0.541}Ba_{0.229}Th_{0.229})PO_4$	6.856	7.065	6.575	103.08	310.21	215
$(La_{0.521}Ba_{0.239}Th_{0.2401})PO_4$	6.868	7.094	6.567	103.363	311.29	215
$(La_{0.479}Ba_{0.260}Th_{0.261})PO_4$	6.868	7.091	6.562	103.387	310.89	215
$(Ba_{0.5}Th_{0.5})PO_4$	6.95	7.162	6.675	102.885	323.89	215
$(Ba_{0.5}Th_{0.5})PO_4$	6.944	7.161	6.67	102.88	323.33	215
$LaPO_4$	6.825	7.065	6.497	103.258	304.93	215
$(La_{0.202}Sr_{0.399}Th_{0.399})PO_4$	6.793	7.021	6.498	103.439	301.43	215
$(La_{0.382}Sr_{0.309}Th_{0.309})PO_4$	6.801	7.03	6.5	103.383	302.33	215
$(La_{0.562}Sr_{0.219}Th_{0.219})PO_4$	6.809	7.039	6.499	103.341	303.08	215
$(La_{0.738}Sr_{0.131}Th_{0.131})PO_4$	6.817	7.051	6.501	103.306	304.09	215
$(Sr_{0.5}Th_{0.5})PO_4$	6.786	7.001	6.498	103.505	300.18	215
$(Sr_{0.5}Th_{0.5})PO_4$	6.792	7.017	6.501	103.514	301.26	215
$(Sr_{0.5}Th_{0.5})PO_4$	6.801	7.027	6.51	103.562	302.44	215
$(Sr_{0.5}Th_{0.5})PO_4$	6.791	7.013	6.518	103.515	301.83	215
$LaPO_4$	6.825	7.065	6.497	103.258	304.93	215
$(La_{0.857}Pb_{0.071}Th_{0.072})PO_4$	6.825	7.063	6.503	103.288	305.08	215
$(La_{0.801}Pb_{0.099}Th_{0.100})PO_4$	6.823	7.058	6.504	103.295	304.82	215
$(La_{0.725}Pb_{0.137}Th_{0.138})PO_4$	6.823	7.06	6.507	103.314	305.02	215
$(La_{0.722}Pb_{0.139}Th_{0.139})PO_4$	6.822	7.056	6.508	103.349	304.81	215
$(La_{0.539}Pb_{0.230}Th_{0.230})PO_4$	6.823	7.057	6.516	103.392	305.21	215
$(La_{0.519}Pb_{0.240}Th_{0.241})PO_4$	6.825	7.061	6.517	103.387	305.53	215
$(La_{0.322}Pb_{0.339}Th_{0.339})PO_4$	6.823	7.054	6.527	103.495	305.47	215
$(La_{0.311}Pb_{0.344}Th_{0.345})PO_4$	6.83	7.063	6.531	103.501	306.35	215
$(Pb_{0.5}Th_{0.5})PO_4$	6.848	7.071	6.565	103.8	308.72	215

Table 5 (*Continued*)

	a (Å)	b (Å)	c (Å)	β (°)	V (Å^3)	Ref.
$(Pb_{0.5}Th_{0.5})PO_4$	6.831	7.057	6.549	103.694	306.73	215
$(Pb_{0.5}Th_{0.5})PO_4$	6.849	7.076	6.56	103.793	308.75	215
$(Pb_{0.5}Th_{0.5})PO_4$	6.848	7.078	6.568	103.716	309.27	215
$LaPO_4$	6.825	7.065	6.497	103.258	304.93	215
$(La_{0.774}Cd_{0.113}Th_{0.113})PO_4$	6.798	7.027	6.474	103.4	300.84	215
$(La_{0.613}Cd_{0.193}Th_{0.194})PO_4$	6.776	7.001	6.456	103.502	297.80	215
$(La_{0.407}Cd_{0.296}Th_{0.297})PO_4$	6.74	6.957	6.427	103.702	292.79	215
$(La_{0.241}Cd_{0.379}Th_{0.380})PO_4$	6.714	6.924	6.407	103.877	289.15	215
$(Cd_{0.5}Th_{0.5})PO_4$	6.67	6.879	6.384	104.165	284.01	215
$LaPO_4$	6.829	7.065	6.501	103.278	305.27	215
$(La_{0.753}Ca_{0.123}Th_{0.124})PO_4$	6.797	7.027	6.479	103.368	301.07	215
$(La_{0.603}Ca_{0.198}Th_{0.199})PO_4$	6.775	7	6.464	103.437	298.16	215
$(La_{0.429}Ca_{0.285}Th_{0.286})PO_4$	6.756	6.976	6.45	103.521	295.56	215
$(La_{0.235}Ca_{0.382}Th_{0.383})PO_4$	6.734	6.95	6.438	103.613	292.84	215
$(Ca_{0.5}Th_{0.5})PO_4$	6.697	6.904	6.402	103.712	287.57	215
$(Ca_{0.5}Th_{0.5})PO_4$	6.695	6.907	6.41	103.609	288.09	215
$(Ca_{0.5}Th_{0.5})PO_4$	6.695	6.9	6.402	103.66	287.38	215
$LaPO_4$	6.845	7.082	6.512	103.29	307.54	212
$(La_{0.894}Ca_{0.053}U_{0.053})PO_4$	6.823	7.057	6.498	103.316	304.441	212
$(La_{0.87}Ca_{0.065}U_{0.065})PO_4$	6.83	7.064	6.491	103.375	304.637	212
$(La_{0.756}Ca_{0.122}U_{0.122})PO_4$	6.811	7.049	6.479	103.411	302.561	212
$(La_{0.728}Ca_{0.136}U_{0.136})PO_4$	6.79	7.015	6.476	103.424	300.035	212
$(La_{0.644}Ca_{0.178}U_{0.178})PO_4$	6.756	7.004	6.44	103.446	296.446	212
$(La_{0.580}Ca_{0.210}U_{0.210})PO_4$	6.766	6.982	6.446	103.598	295.974	212
$(La_{0.546}Ca_{0.227}U_{0.227})PO_4$	6.742	6.955	6.431	103.664	293.029	212
$(La_{0.538}Ca_{0.231}U_{0.231})PO_4$	6.733	6.951	6.432	103.614	292.547	212
$(La_{0.532}Ca_{0.234}U_{0.234})PO_4$	6.757	6.966	6.456	103.69	295.24	212
$(La_{0.532}Ca_{0.234}U_{0.234})PO_4$	6.733	6.958	6.42	103.565	292.383	212
$(La_{0.488}Ca_{0.256}U_{0.256})PO_4$	6.734	6.947	6.43	103.603	292.388	212
$(La_{0.484}Ca_{0.258}U_{0.258})PO_4$	6.732	6.948	6.432	103.72	292.24	212
$(La_{0.456}Ca_{0.272}U_{0.272})PO_4$	6.718	6.948	6.426	103.723	291.374	212
$(La_{0.334}Ca_{0.333}U_{0.333})PO_4$	6.725	6.939	6.422	103.897	289.925	212
$(La_{0.206}Ca_{0.397}U_{0.397})PO_4$	6.688	6.883	6.38	104.073	284.828	212
$(Ca_{0.5}U_{0.5})PO_4$	6.661	6.851	6.36	104.134	281.438	212
$(Ca_{0.5}U_{0.5})PO_4$	6.673	6.852	6.364	104.068	282.274	212
$(Ca_{0.5}U_{0.5})PO_4$	6.653	6.845	6.356	104.025	280.797	212
$(La_{0.4}Ca_{0.3}U_{0.3})PO_4$	6.725	6.938	6.415	103.7	290.796	224
$(La_{0.3}Ca_{0.35}U_{0.35})PO_4$	6.716	6.925	6.408	103.76	289.472	224
$LaPO_4$	6.824	7.056	6.495	103.31	304.343	171
$(La_{0.944}Ca_{0.028}Th_{0.028})PO_4$	6.838	7.076	6.51	103.31	306.53	171
$(La_{0.890}Ca_{0.055}Th_{0.055})PO_4$	6.839	7.075	6.51	103.31	306.56	171
$(La_{0.812}Ca_{0.094}Th_{0.094})PO_4$	6.818	7.047	6.497	103.34	303.77	171
$(La_{0.600}Ca_{0.20}Th_{0.20})PO_4$	6.792	7.019	6.478	103.4	300.46	171
$(La_{0.56}Ca_{0.22}Th_{0.22})PO_4$	6.79	7.016	6.476	103.42	300.09	171
$(La_{0.398}Ca_{0.301}Th_{0.301})PO_4$	6.769	6.991	6.461	103.5	297.35	171
$(La_{0.374}Ca_{0.313}Th_{0.313})PO_4$	6.768	6.992	6.458	103.51	297.16	171
$(La_{0.230}Ca_{0.385}Th_{0.385})PO_4$	6.738	6.953	6.439	103.6	293.19	171
$(La_{0.204}Ca_{0.398}Th_{0.398})PO_4$	6.741	6.959	6.44	103.59	293.66	171
$(Ca_{0.5}Th_{0.5})PO_4$	6.705	6.918	6.415	103.65	289.15	171
$(Ca_{0.5}Th_{0.5})PO_4$	6.706	6.916	6.417	103.72	289.03	171
$LaPO_4$	6.8391	7.0772	6.509	103.27	306.63	228
$(La_{0.90}Ca_{0.05}Th_{0.05})PO_4$	6.8269	7.0618	6.5006	103.27	305.03	228
$(La_{0.80}Ca_{0.10}Th_{0.10})PO_4$	6.816	7.0451	6.4917	103.34	303.32	228
$(La_{0.70}Ca_{0.15}Th_{0.15})PO_4$	6.8025	7.0304	6.4831	103.39	301.62	228
$(La_{0.60}Ca_{0.20}Th_{0.20})PO_4$	6.7905	7.0135	6.4745	103.42	299.93	228
$(La_{0.50}Ca_{0.25}Th_{0.25})PO_4$	6.7777	6.9986	6.4656	103.43	298.31	228
$(La_{0.40}Ca_{0.30}Th_{0.30})PO_4$	6.7647	6.9821	6.4561	103.52	296.48	228
$(La_{0.30}Ca_{0.35}Th_{0.35})PO_4$	6.7516	6.9657	6.4468	103.53	294.78	228
$(La_{0.20}Ca_{0.40}Th_{0.40})PO_4$	6.7376	6.9489	6.4375	103.62	292.92	228

Table 5 (*Continued*)

	a (Å)	*b* (Å)	*c* (Å)	*β* (°)	*V* (Å^3)	Ref.
$(La_{0.10}Ca_{0.45}Th_{0.45})PO_4$	6.7259	6.9327	6.4279	103.67	291.23	228
$(Ca_{0.5}Th_{0.5})PO_4$	6.7116	6.9153	6.4179	103.73	289.36	228
$CePO_4$	6.787	7.029	6.468	103.18	300.43	219
$(Ce_{0.950}Ca_{0.025}Th_{0.025})PO_4$	6.784	7.02	6.468	103.21	299.88	219
$(Ce_{0.90}Ca_{0.05}Th_{0.05})PO_4$	6.782	7.015	6.462	103.22	299.29	219
$(Ce_{0.850}Ca_{0.075}Th_{0.075})PO_4$	6.77	7.008	6.460	103.23	298.35	219
$(Ce_{0.80}Ca_{0.10}Th_{0.10})PO_4$	6.763	7.000	6.458	103.27	297.56	219
$(Ce_{0.750}Ca_{0.125}Th_{0.125})PO_4$	6.733	6.971	6.441	103.26	294.25	219
$(Ce_{0.50}Ca_{0.25}Th_{0.25})PO_4$	6.711	6.949	6.433	103.44	291.79	219
$(Ca_{0.5}Th_{0.5})PO_4$	6.681	6.926	6.421	103.54	288.86	219
$CePO_4$	6.8035	7.0274	6.4761	103.46	301.12	228
$(Ce_{0.90}Ca_{0.05}Th_{0.05})PO_4$	6.7944	7.0163	6.4703	103.41	300.04	228
$(Ce_{0.80}Ca_{0.10}Th_{0.10})PO_4$	6.7858	7.0057	6.4649	103.44	298.92	228
$(Ce_{0.70}Ca_{0.15}Th_{0.15})PO_4$	6.7789	6.9941	6.4589	103.46	297.82	228
$(Ce_{0.60}Ca_{0.20}Th_{0.20})PO_4$	6.7761	6.9828	6.4532	103.54	296.46	228
$(Ce_{0.50}Ca_{0.25}Th_{0.25})PO_4$	6.767	6.9719	6.4486	103.58	295.33	228
$(Ce_{0.40}Ca_{0.30}Th_{0.30})PO_4$	6.7578	6.9606	6.4424	103.59	293.77	228
$(Ce_{0.30}Ca_{0.35}Th_{0.35})PO_4$	6.7398	6.9495	6.4364	103.6	292.61	228
$(Ce_{0.20}Ca_{0.40}Th_{0.40})PO_4$	6.7304	6.9381	6.4309	103.67	291.39	228
$(Ce_{0.10}Ca_{0.45}Th_{0.45})PO_4$	6.7211	6.9269	6.4241	103.7	290.16	228
$(Ca_{0.5}Th_{0.5})PO_4$	6.7116	6.9153	6.4179	103.73	289.36	228
$(Nd_{0.716}Th_{0.151}Ca_{0.146})PO_4$	6.743	6.96	6.426	103.68	293.03	227
$CePO_4$	6.800	7.023	6.471	103.46	300.5	229
$(Ce_{0.90}Ba_{0.05}Zr_{0.05})PO_4$	6.801	7.024	6.474	103.47	300.7	229
$(Ce_{0.80}Ba_{0.10}Zr_{0.10})PO_4$	6.802	7.025	6.478	103.48	301.0	229
$(Ce_{0.90}Ba_{0.05}Hf_{0.05})PO_4$	6.803	7.028	6.484	103.07	301.4	229
$(La_{0.73}Ce_{0.09}Th_{0.09}Ca_{0.09})PO_4$	6.8088	7.0407	6.48774	103.353	302.61	221
$(Pu^{III}_{0.4}Pu^{IV}_{0.3}Ca_{0.3})PO_4$	6.67	6.87	6.36	103.99	282.79	107
$(La_{0.73}Pu_{0.09}Th_{0.09}Ca_{0.09})PO_4$	6.8101	7.0387	6.4815	103.39	302.24	218
$(La_{0.80}Ca_{0.10}Th_{0.08}U_{0.02})PO_4$	6.8179	7.0469	6.4965	103.370	303.7	216
$(La_{0.60}Ca_{0.20}Th_{0.16}U_{0.04})PO_4$	6.7923	7.0138	6.4775	103.47	300.1	216
$(La_{0.40}Ca_{0.30}Th_{0.24}U_{0.06})PO_4$	6.7635	6.9789	6.4563	103.57	296.2	216
$(La_{0.20}Ca_{0.40}Th_{0.32}U_{0.08})PO_4$	6.7297	6.9363	6.4301	103.713	291.6	216

Between the domain of existence of monazite and xenotime, a miscibility gap[172] is generally observed and its extend will be discussed further. The same behaviour is observed in the binary system between light rare earth phosphates and YPO_4. The limit of incorporation of Y in $LaPO_4$ was found between 12% at 1000 °C (while it is equal to 40% for Maslennikova et al.[173]) and 40–42% at 1600 °C.[174,175] On this basis, Rovnyi et al. reported the preparation of monazite sample incorporating all light rare earth elements and yttrium with the following composition $Nd_{0.31}Sm_{0.18}Ce_{0.15}La_{0.15}Pr_{0.08}Y_{0.07}Gd_{0.06}PO_4$.[176]

Table 6
Unit-cell parameters of $M^{II}_{0.5}M^{IV}_2(PO_4)_3$ series with the monazite structure.

$B_{0.5}M_2(PO_4)_3$-M^{4+} series	*a* (Å)	*b* (Å)	*c* (Å)	*β* (°)	*V* (Å^3)	Ref.
$Mg_{0.5}Ce_{2.0}(PO_4)_3$	6.769	7.011	6.458	103.4	298.10	209,211
$Ca_{0.5}Ce_{2.0}(PO_4)_3$	6.788	7.005	6.461	103.42	298.80	209,211
$Sr_{0.5}Ce_{2.0}(PO_4)_3$	6.77	6.998	6.438	103.52	296.60	209,211
$Cd_{0.5}Ce_{2.0}(PO_4)_3$	6.777	7.014	6.447	103.39	298.10	209,211
$Mg_{0.5}Ce_{2.0}(PO_4)_3$	6.769	7.011	6.458	103.4	298.10	210
$Ca_{0.5}Ce_{2.0}(PO_4)_3$	6.788	7.005	6.461	103.42	298.80	210
$Sr_{0.5}Ce_{2.0}(PO_4)_3$	6.77	6.998	6.438	103.52	296.60	210
$Ba_{0.5}Ce_{2.0}(PO_4)_3$	6.795	7.022	6.473	103.52	300.30	210,211
$Cd_{0.5}Ce_{2.0}(PO_4)_3$	6.777	7.014	6.447	103.39	298.10	210
$Mg_{0.5}Np_{2.0}(PO_4)_3$	6.755	6.987	6.394	103.5	293.40	210
$Ca_{0.5}Np_{2.0}(PO_4)_3$	6.737	6.953	6.412	103.84	291.60	210
$Sr_{0.5}Np_{2.0}(PO_4)_3$	6.737	6.961	6.406	103.51	292.10	210
$Ca_{0.5}Pu_{2.0}(PO_4)_3$	6.712	6.931	6.361	103.91	287.70	210

Table 7
Unit-cell parameters of $M^{I}M^{IV}_{2}(PO_4)_3$ and $M^{I}_{2}M^{IV}(PO_4)_2$ series with the monazite structure.

	a (Å)	b (Å)	c (Å)	β (°)	V (Å^3)	Ref.
$LiCe_2(PO_4)_3$	6.794	7.021	6.469	103.48	300.1	211
$NaCe_2(PO_4)_3$	6.799	7.010	6.444	103.42	297.8	209,211
$KCe_2(PO_4)_3$	6.799	7.031	6.475	103.50	301.0	211
$RbCe_2(PO_4)_3$	6.791	7.015	6.466	103.46	299.6	211
$CsCe_2(PO_4)_3$	6.788	7.012	6.452	103.56	298.6	211
$Li_2Ce(PO_4)_2$	6.775	7.006	6.441	103.41	297.4	211
$Na_2Ce(PO_4)_2$	6.783	7.003	6.435	103.40	297.4	211
$K_2Ce(PO_4)_2$	6.780	6.984	6.433	103.57	296.1	211

As for mixed samples involving light REE, various compounds based on a mixture between light lanthanides and trivalent actinides were reported. Particularly, several authors reported the preparation of $La_{1-x}Pu_xPO_4$ and $La_{1-x}Am_xPO_4$ solid solutions with x values ranging from 0.01 to 0.1.[95,177–180]

3.1.3. Incorporation of monovalent elements

The incorporation of monovalent elements in the monazite structure could occur through substitution mechanisms or by direct incorporation in the lattice defects of the structure. For this latter, a recent study undertaken in the (La:Li)PO_4 system showed that the weight loading is limited to only 1–2%.[181] This limit was contradicted by Li and Lee[182] who synthesized samples with lithium contents up to 10% in La–Eu–Li systems. However, this author did not observe any shift in the position of the XRD lines, suggesting that Li^+ ions could have not been incorporated in the crystal lattice.

On the other hand, the formation of defined compounds through substitution mechanisms was found to lead to families with general composition $M^{I}_{3}REE^{III}_{2}(PO_4)_3$ or $M^{I}_{3}REE^{III}(PO_4)_2$. For example, Schwarz et al.[183] reported the formation of $Na_3La(PO_4)_2$ and isotype compounds in the Na–Gd, K–La, K–Gd and K–Y systems but did not provide any crystallographic data. In the Na_2O–Ce_2O_3–P_2O_5 system, the existence of a monazite phase incorporating Na and Ce(III) was excluded by Szczygiel and Znamierowska[184] who systematically obtained the $NaCeP_2O_7$ diphosphate. Other $M_3R_2(PO_4)_3$ samples incorporating several lanthanides (M^{I} = Na, K; REE = Ce, Pr, Nd, Sm, Eu, Gd),[185] or actinides (M^{I} = Na M^{III} = Pu, Am and M^{I} = K; M^{III} = Am, Cm))[186,187] were prepared and characterized through XRD but without any growth of single crystals. For this kind of compounds, Orlova generally observed a dimorphism with the NZP structural type.[188] The main difference lies in the position of the alkaline cations which are located in structural voids for NZP compounds while they belong to the framework in the monazite structure.

Finally, the incorporation of monovalent cations in the monazite structure was also evidenced with the preparation of $Li_3Sc_{0.3}Ce_{1.7}(PO_4)_3$.[189] Despite these various examples, no precise mechanism was proposed by any of the authors concerning the incorporation of monovalent elements in the monazite structure.

3.1.4. Incorporation of divalent elements

The incorporation of divalent elements in the monazite structure was studied without the help of coupled substitution mechanisms in the field of the preparation of compounds with mixed protonic-electronic transport properties[78,79,81,159,190,191] and also of the development of novel pigments.[80] The studies dedicated to protonic conductors were mainly focussed on the incorporation of Sr^{2+} in various $LnPO_4$ compounds. When the incorporation rates ranged from 1 to 2%, no additional phase was detected with Ln = Pr, Nd and Sm.[190] Gomez del Moral et al.[191] reported the doping of $CePO_4$ with strontium up to 5%. In this case, the charge is counterbalanced by the formation of oxygen vacancies. For higher strontium loadings, the formation of $Sr_3Ce(PO_4)_3$ as secondary phase was evidenced by XRD.

Additionally, several authors claimed that the incorporation of divalent elements in the monazite structure is achievable for higher rates without any coupled substitution. For example, Gallini et al.[78,79] reported the preparation of $La_{1-x}Sr_xPO_4$ nanopowders up to $x = 0.1$ while Sivakumar and Varadaraju[80] argue for the obtention of $Pr_{1-x}Ca_xPO_4$ with $x \leq 0.4$. Nevertheless, in this last case, the authors confess that the formation of additional α-$Ca_2P_2O_7$ could be difficult to evidence due to some interferences in the XRD line positions with those of monazite.

Actually, only Amezawa et al.[81] performed a complete study on the direct incorporation of divalent elements in the monazite

Table 8
Unit-cell parameters of complex compounds with the monazite structure.

Complex compositions	a (Å)	b (Å)	c (Å)	β (°)	V (Å^3)	Ref.
$Ca_{0.525}Gd_{0.130}(Hf_{0.150}Ti_{1.329}U_{0.273}Pu_{0.138})(PO_4)_3$	6.667	6.828	6.347	103.64	280.78	223
$(Ca_{0.304}Cd_{0.174})Gd_{0.044}(U_{0.116}Ce_{0.362})PO_4$	6.775	7.031	6.46	103.6	299.09	223
$(Ca_{0.304}Cd_{0.174})Gd_{0.044}(U_{0.116}Ce_{0.304}Pu_{0.058})PO_4$	6.72	6.965	6.42	103.5	292.18	223
$(La_{0.16}Nd_{0.02}Gd_{0.02}Th_{0.32}U_{0.08})PO_4$	6.7290	6.9357	6.4291	103.711	291.5	216
$KMgLa(PO_4)_2$	6.839	7.066	6.523	103.42	306.61	243

structure through the preparation of Mg, Ca, Sr and Ba-doped $LaPO_4$. From XRD analyses, the solubility limit of calcium in $LaPO_4$ was determined to be equal to 4.2 mol% for calcium, while the values determined for Sr and Ba are reported to be 1.9 and 0.4 mol%, respectively. These authors also determined that Mg^{2+} cannot be incorporated in $LaPO_4$. The variation of the solubility limit of the alkaline earth metals in $LaPO_4$ seems to be related with the difference in the ionic radii between La and the alkaline earth element,[81] the closer the alkaline earth element ionic radius to that of La^{3+} in the ninefold coordination, the higher the solubility. Furthermore, the solubility limit of the divalent element in $LaPO_4$ determined at $T = 1350\,^{\circ}C$ is lower than that reported at $T = 1200\,^{\circ}C$.

Finally, Ravindran Nair et al.[192] mentioned the formation of pure $M^{II}M^{III}P_3O_{10}$ compounds with the monazite structure from solid state reaction at high temperature for M^{II} = Ba or Ca and M^{III} = La, Ce or Sm. Nevertheless, no indication on the unit cell parameters was supplied by the authors.

3.1.5. Incorporation of tetravalent elements

The direct substitution of trivalent elements by tetravalent actinides with the formation of vacancies is reported to occur in natural and synthetic monazites.[193] The proposed mechanism corresponds to[194]:

$$4REE^{3+} \leftrightarrow 3(Th, U)^{4+} + \text{vacancy} \quad (1)$$

The formation of vacancies seems to limit the U and Th content to a few weight percent in natural monazites. This limit was determined to be equal to 17.68 wt% ThO_2 (*i.e.* $La_{0.83}Th_{0.17}PO_4$) on synthetic materials. Furthermore, Boatner et al. and Kelly et al. argue for the direct incorporation of up to 10 wt% of UO_2, PuO_2 or NpO_2 in $LaPO_4$.[195,196]

3.1.6. Coupled substitutions M^{2+}/M^{4+}

Type 1: Natural monazites that constitute the main source of thorium on earth since mineral samples were found to incorporate up to 31.5 wt.% ThO_2[1] and 15.64 wt% UO_2.[1] One of the incorporation mechanism of tetravalent elements in the structure of the monazite is described by the mean of coupled substitution:

$$REE^{III}PO_4 + xM^{2+} + xM^{4+} = (REE^{III}_{1-2x}M^{II}_xM^{IV}_x)PO_4 + 2x\,REE^{3+} \quad (2)$$

The full substitution leads to the formation of the cheralite family[197] (formerly called brabantite[198]) with general formulae $A_{0.5}B_{0.5}PO_4$. These compounds adopt the monazite structure for big tetravalent cations, generally including cerium and tetravalent actinides. For smaller B^{4+} ions, another monoclinic structure, isotypic of the $KFe(SO_4)_2$ yavapaïte, is stabilized as evidenced for the $BaM^{IV}(PO_4)_2$ series with M^{IV} = Ti, Zr, Hf, Ge, Sn, Mo.[199–201]

On this basis, the formation of cheralite was mainly investigated for tetravalent actinides. While wet chemistry methods generally failed to obtain single phase samples, solid state reactions at high temperature allow the preparation of pure $CaM^{IV}(PO_4)_2$ with M^{IV} = Th, U[140,202,203] or Np.[204–206] Tabuteau et al.[204] also succeeded to incorporate tetravalent plutonium in the monazite lattice as a mixture with tetravalent neptunium, leading to the final $Ca_{0.5}Np_{0.35}Pu_{0.15}PO_4$ composition. Conversely, all the attempts to form pure $Ca_{0.5}Pu^{IV}{}_{0.5}PO_4$, as well as analogous $Ca_{0.5}Ce^{IV}{}_{0.5}PO_4$, failed due to the partial reduction of plutonium (or cerium) into Pu^{3+} (resp. Ce^{3+}).[207–209] Only Kitaev et al.[210] and Orlova et al.[211] reports the formation of several $M^{II}{}_{0.5}Ce^{IV}{}_{0.5}PO_4$ compounds but did not provide any evidence arguing for the absence of trivalent cerium. The preparation of single crystals of actinides-bearing cheralites ($(Ca^{II}_{0.5}M^{IV}_{0.5})PO_4$, where M^{IV} = Th and U) was also reported by Podor et al. under hydrothermal conditions.[171,212]

Besides calcium, several other divalent cations were employed for the formation of cheralites. Particularly, Devidal and Montel[213] prepared the $M^{II}Th(PO_4)_2$ series with M^{II} = Ca, Cd, Sr, Pb and Ba while Quarton et al.[214] reported the synthesis of $PbTh(PO_4)_2$. For cadmium and barium, which lead to average ionic radius at the limit of the stability range, different structures could be stabilized. Nevertheless, Montel et al.[215] succeeded to prepare pure single phase samples by varying the temperature and pressure conditions applied during hydrothermal syntheses. Indeed, $Cd_{0.5}Th_{0.5}PO_4$ was obtained at $T = 1200\,^{\circ}C$ and $P = 1$ bar, while pure $Ba_{0.5}Th_{0.5}PO_4$ crystallizes at $T = 700\,^{\circ}C$ and $P = 2500$ bar.

From a general point of view, this coupled substitution does not lead to important deformation of the unit cell compared to the values reported for REE phosphates. Moreover, three defined compounds mentioned in the literature, *i.e.* $(Mg_{0.5}Th_{0.5})PO_4$, $(Mg_{0.5}U_{0.5})PO_4$ and $(Ba_{0.5}Th_{0.5})PO_4$ present average ionic radii out of the stability range defined in a forthcoming section of the review. In these conditions, the ratio between M^{2+} and M^{4+} ionic radius appears as an additional parameter to stabilize the monazite structure. The $M^{II}M^{IV}(PO_4)_2$ phases with the monazite structure reported in the literature are gathered in Table 4.

Only one complete solid solution between two end-members of the cheralite family, $Ca_{0.5}U_{0.5}PO_4$ and $Ca_{0.5}Th_{0.5}PO_4$, was reported by Terra et al.[216] The results reported in this study did not evidence any specific ordering of elements in the cationic site.

The formation of solid solutions between $REEPO_4$ and $(M^{II}_{0.5}M^{IV}_{0.5})PO_4$ compounds was also widely investigated through the past decades. Among these studies, several works were dedicated to samples incorporating simultaneously tri- and tetravalent actinides as such materials could be used as radwaste matrices [217]. On this basis, the incorporation of plutonium under both +III and +IV oxidation states was mentioned[218] and correlated to the partial reduction of Pu(IV) in Pu(III) in phosphate media. Similar compounds were also obtained with cerium.[140,208] Nevertheless, most of the tetravalent actinides-bearing solids reported are based on thorium[171,219–221] or uranium.[140,212,222,223]

Moreover, specific compositions, generally with the formulae $REE^{III}_{1/3}M^{II}_{1/3}M^{IV}_{1/3}PO_4$, were synthesized and characterized by several authors.[210,218,224–227] Compositions in specific $REE^{III}_{1-2x}M^{II}_xM^{IV}_xPO_4$ series are also reported.[171,212,215,216,219,228]. The incorporation of Zr^{4+} and Hf^{4+} through this substitution type involving Ba^{2+} as

a charge compensator was obtained by Popa et al.[229] The $Ce_{1-2x}M^{IV}_xBa_xPO_4$ monazite-like compounds were obtained only for $x \leq 0.2$ (M^{IV} = Zr) and $x \leq 0.1$ (M^{IV} = Hf).

As it will be described later in this paper, the miscibility between monazite and cheralite depends on steric constraints and could be determined from the ionic radii of the cations. For example, a total miscibility was demonstrated for the $LaPO_4$–$SrTh(PO_4)_2$[213] and $LaPO_4$–$CaU(PO_4)_2$[212] systems while a miscibility gap was observed for $LaPO_4$–$BaTh(PO_4)_2$.[213] In all these studies, no specific ordering on the cation site was reported. Podor demonstrated from Raman spectra that REE, Ca and U elements are randomly distributed in the cation site for $La_{1-2x}{}^{3+}Ca_x{}^{2+}$(Th or U)$_x{}^{4+}PO_4$.[230] Moreover, Konings et al. performed calorimetry measurements in the $LnPO_4$–$CaTh(PO_4)_2$ binaries and concluded to a deviation of the solid solutions formed from the ideality, this deviation increasing with the size of the Ln^{3+} cation.[228]

Type 2: Another mechanism for the coupled incorporation of divalent elements and large tetravalent cations (*i.e.* cerium and actinides) was described in the literature through the preparation of single phase $M^{II}_{0.5}M^{IV}_2(PO_4)_3$ compounds by the Russian team of Orlova et al.[209,210,231–234]. In this case, the charge is counterbalanced by the creation of a vacancy on the cation site through the following reaction:

$$M^{III}PO_4 + \frac{x}{6}M^{2+} + \frac{2x}{3}M^{4+} + \frac{x}{6}\square = (M^{III}_{1-x}M^{II}_{x/6}M^{IV}_{2x/3}\square_{x/6})PO_4 + xM^{3+} \quad (3)$$

The first pure compounds prepared within this family were simply obtained through the heat treatment of the gelatinous phase obtained after adding phosphoric acid to a mixture of nitrate or chloride salts of metallic cations in the corresponding acidic solution. By this way, $M^{II}_{0.5}Ce_2(PO_4)_3$ powdered samples were synthesized for M^{II} = Mg, Ca, Sr and Cd[209,231] and the XRD powder pattern was refined for $Cd_{0.17}Ce_{0.68}\square_{0.32}PO_4$.[232,233]

Similar compounds were also prepared using actinides as tetravalent cations.[210] Single phases were obtained for neptunium with M^{II} = Mg, Ca or Sr while only the use of calcium led to a monazite structure for tetravalent plutonium. For thorium and uranium, no phase with the monazite structure was obtained, probably due to the too high ionic radius of these elements.[234,235]

3.1.7. Coupled substitutions M^+/M^{4+}

Phosphates of tetravalent *f* elements with monovalent cations belong to two distinct formula types, namely $M^IM^{IV}_2(PO_4)_3$ and $M^I_2M^{IV}(PO_4)_2$[209–211,233] (Table 7). $M^IM^{IV}_2(PO_4)_3$ are the more numerous compounds available but only few present the monazite structure. Indeed, pure monazite phases were only reported for M^{IV} = Ce with M^I = Li–Cs,[211,236] and for M^{IV} = Np with M^I = Na[237–239] while other compounds of this family generally belong to the NZP structural type.[185,240] Particularly, it is to note that in this series, neptunium is the only tetravalent actinide that adopt the monazite structure since Th, U and Pu generally exhibit a dimorphism between a low-temperature rhombohedral modification and the NZP type.[241,242] In this case, the substitution can be described as follows[233]:

$$M^{III}PO_4 + \frac{x}{3}M^+ + \frac{2x}{3}M^{4+} = (M^{III}_{1-x}M^I_{x/3}M^{IV}_{2x/3})PO_4 + xM^{3+} \quad (4)$$

On the other hand, $M^I_2M^{IV}(PO_4)_2$ monazites were only reported for Ce(IV) with M^I = Li, Na and K.[211,233] As for $M^IM^{IV}_2(PO_4)_3$ compounds, their unit cell parameters appear very close to that of pure $CePO_4$ which accounts for a substitution model involving the formation of anionic vacancies as follows[233]:

$$Ce^{3+} = M^+ + \frac{1}{2}\square + \frac{1}{2}Ce^{4+} \quad (5)$$

3.1.8. Correlated substitutions

Considering all the substitutions mentioned above, complex compounds incorporating rare earth elements, alkaline and alkaline earth as well as tetravalent cations were prepared as solid solutions with the monazite structure.

The $M^IM^{II}REE(PO_4)_2$ family was studied by several authors due to some interesting optical properties. Even if the major part of the compounds adopt an hexagonal structure, some defined compounds were reported to belong to the monazite structural type such as $KMgLa(PO_4)_2$,[243] $KCaY(PO_4)_2$ and $KCaEu(PO_4)_2$[244] or related $NaCaNd_2(PO_4)_3$.[238]

Syntheses of complex compounds containing rare-earth, alkali-earth and tetravalent elements (including Th and Ti) were reported by Volkov et al.[223] Samples of $Ca_{0.525}Gd_{0.130}(Hf_{0.150}Ti_{1.329}U_{0.273}Pu_{0.138})(PO_4)_3$, $(Ca_{0.304}Cd_{0.174})Gd_{0.044}(U_{0.116}Ce_{0.362})PO_4$, and $(Ca_{0.304}Cd_{0.174})Gd_{0.044}(U_{0.116}Ce_{0.304}Pu_{0.058})PO_4$ were obtained with the monazite structure. Their cristallographic parameters are gathered in Table 8.

3.2. AXO_4 monazite-type compounds ($X \neq P$)

The elements present in the anion site can also be substituted. This contributes to the formation of $REEXO_4$ or $A^{n+}XO_4$ monazite-type materials. Two types of substitutions were already evidenced by several authors. The first one corresponds to the direct replacement of the $PO_4{}^{3-}$ group by another anionic group with the same total anionic charge: $VO_4{}^{3-}$, $AsO_4{}^{3-}$ and $Cr^VO_4{}^{3-}$. This substitution allows the formation of monazite-like materials with the $REEXO_4$ general composition.

The second mechanism is associated to a double substitution occurring on both anionic and cationic sites. In these cases, the charge of the cation site remains equal to the charge of the anion group. The better known example of this type of substitution is the huttonitic one, first described by Hutton.[245] This substitution occurs in natural monazite minerals and yields to the formation of the end-member $ThSiO_4$ with the monazite structure (huttonite). Other substitutions involving $Cr^{VI}O_4{}^{2-}$, $SeO_4{}^{2-}$ or $SO_4{}^{2-}$ groups can also be considered due to the sta-

bility of $SrCrO_4$, $PbSeO_4$ or $CaSO_4$ with the monazite structure. On the contrary, all the reported germanates do not crystallize with the monazite structure.

These different substitution mechanisms will be described in the following part of the review.

3.2.1. $M^{III}(V, Cr^{V}, As)O_4$ type compounds

Many compounds containing trivalent elements on the cation site and vanadate, arsenate and chromate groups on the cationic one are reported in the literature to be stable with the monazite structure. Two recent reviews were devoted to the description of the crystal chemistry of $REEXO_4$[246] and $M^{III}AsO_4$.[247]

The crystallographic data concerning all the $M^{III}XO_4$ ($X \neq P$) compounds are reported in Tables 9–11, leading to their classification into three distinct families.

3.2.1.1. Vanadates. No evidence for a monazitic natural mineral containing vanadium has been reported yet. Only wakefieldite-(Ce) ("$CeVO_4$")[248] and the La-analogue ("$LaVO_4$")[249] were reported to crystallize with the zircon structure.

The $LaVO_4$ compound prepared by high-temperature solid-state synthesis or flux growth methods is the only $REEVO_4$ type-compound crystallizing with the monazite-type structure[250–252] while all the other REE members (Ce–Lu) as well as Y and Sc exhibit the zircon-type structure.[253] Furthermore, the structure of $LaVO_4$ depends on the chemical way of preparation.[52,246,254–257] However, monazite-type $REEVO_4$ (REE = Ce, Pr, Nd) could be obtained by the atmospheric oxidation of $REEVO_3$ compounds at 350–400 °C.[255] Similarly, metastable monazite-type $CeVO_4$ was observed by Yoshimura and Sata[258] as an oxidation product of $CeVO_3$.

Varma et al.[60] synthesised mixed vanadates $La_{1-x}Ce_xVO_4$ by solid-state route at 600 °C, and demonstrated that the monazite-type $LaVO_4$ phase was prepared for $x \leq 0.2$, while the zircon-type $CeVO_4$ was stabilised for $x \geq 0.5$. In the intermediate range ($0.2 < x < 0.5$), both $La_{1-x}Ce_xVO_4$ and $La_{0.5}Ce_{0.5}VO_4$ (zircon-type) coexisted. Recently, Park et al.[54] reported that $LaVO_4$:Eu^{3+} is stable with the monazite structure up to 0.05 mol% Eu^{3+}. When the Eu^{3+} concentration is equal or higher than 0.05 mol%, monoclinic and tetragonal $LaVO_4$ phases coexist. Attempts to stabilize $LaVO_4$:xFe^{3+} with the monazite structure reported by Zhao et al.[259] only yielded to mixtures between monoclinic $LaVO_4$ and tetragonal Fe^{3+}-doped $LaVO_4$. Lanthanum can be also partially substituted by lithium. $Li_{3x}La_{1-x}VO_4$ ($0 \leq x \leq 0.3$) solid solutions were obtained in the temperature range of 320–600 °C. The maximum Li-substitution was obtained for the compound $Li_{0.15}La_{0.95}VO_4$ that adopts a distorted monazite-type structure.[58]

Bismuth vanadate $BiVO_4$ was first reported by Schwarz[260] to exist in a low-temperature modification of huttonite type and still another unknown form. Latter, Sleight et al.[261] as well as Tokugana et al.[262] obtained a monoclinic form of $BiVO_4$ but these authors described it with another structure than that of monazite (the β angle is much smaller than in the monazite structure).

Mixed vanadates of general formula $(Cd,REE,M^{IV})VO_4$ and $(Ca,REE,M^{IV})VO_4$ are reported to be unstable with the monazite structure.[246,263] However, several mixed compounds are reported in the literature. $Pb_{0.5}Th_{0.5}VO_4$ was stabilized with the scheelite-, zircon- and monazite-type structures.[264] Similarly, $(Ba_{1/3}La_{1/3}Th_{1/3})VO_4$ and $(Ba_{1/3}Pr_{1/3}Th_{1/3})VO_4$ were prepared by Nabar and Mhatre[265] and stabilized with the monazite-structure. A partial substitution of Ba by Ca in $(Ca_{x/3}Ba_{(1-x)/3}La_{1/3}Th_{1/3})VO_4$ was also reported.[266] The maximum substitution rate to maintain the compound with the monazite structure corresponds to $x = 0.2$. When Th is replaced by Ce in $(Ba_{1/3}La_{1/3}Th_{1/3})VO_4$, the obtained $(Ba_{1/3}La_{1/3}Ce_{1/3})VO_4$ compound, as well as the series where La is replaced by Pr, Nd and Sm, crystallizes with the zircon structure.[265]

Studies on the substitution possibilities in the anionic site have been only described so far for synthetic $REE(P_{1-x}V_x)O_4$ solid-solution members.[263,57] Aldred[267] concluded to the existence of partial solid solutions with the monazite and zircon structure which extend depends on the rare earth element. This point will be described latter in Section 4.1.2. These results clearly evidence the existence of a miscibility gap between both monazite and zircon structures as already described in the phosphate structures.[174,175,268–270] No specific ordering on the anionic site, between P and V atoms, was reported. The $Gd(P_{1-x}V_x)O_4$:0.05 mol%Eu^{3+} compounds obtained by Xiao et al.[271] exhibit a large extend in the zircon domain (from $GdVO_4$:Eu^{3+} to $GdP_{0.9}V_{0.1}O_4$:Eu^{3+}) while $GdPO_4$ is monazite-structured, in good agreement with Aldred's data.

3.2.1.2. Arsenates. Two different minerals with respective compositions "$LaAsO_4$"[272] and "$CeAsO_4$"[273,274] were found to be isomorphs with the monazite. Pure phases were synthesized by several authors (Table 10). In the REE series, only the La, Ce, Pr and Nd end-members exhibit the monazite structure.[275–281] Escobar and Baran[282] and Ropp and Carroll[254] predicted that only $PmAsO_4$ exhibits a monazite–zircon dimorphism, although so far only zircon-type modification of $PmAsO_4$ was reported.[283] Arsenates of other trivalent elements are reported to be isotype with monazite: $PuAsO_4$, $AmAsO_4$[144] and $BiAsO_4$ (also called Rooseveltite). The case of $BiAsO_4$ is particular since Bedlivy and Mereiter[284] describes the effect of the lone electron pair of Bi^{3+} as the cause of significant deviations in the cation coordination from rare-earth monazite-type structures. The result of this is the modification of the Bi–O distances in the coordination polyhedron and a shift of the Bi position compared to that of La in $LaAsO_4$.

No study reporting the existence of solid solutions between these end-members is reported. Only Nabar and Mangaonkar[285] demonstrated the possibility to incorporate divalent and tetravalent cations in the cationic site according to a $2REE^{3+} \leftrightarrow M^{2+} + M^{4+}$ substitution mechanism identical to that already reported in phosphate-based materials. Several compounds of the $(M^{II}_{1/3}REE^{III}_{1/3}Th^{IV}_{1/3})AsO_4$ family were synthesized and characterized by XRD.[286] Among all the compounds presented in this study, the X-ray diffractograms of the

Table 9
Unit-cell parameters of vanadate compounds with the monazite structure.

	a (Å)	b (Å)	c (Å)	β (°)	V (Å^3)	Ref.
$CeVO_4$	6.98	7.22	6.76	105.02	329.04	258
$La_{0.6}Ce_{0.4}VO_4$	7.042	7.278	6.722	104.9	332.93	60
$La_{0.7}Ce_{0.3}VO_4$	7.04	7.278	6.72	104.9	332.74	60
$La_{0.8}Ce_{0.2}VO_4$	7.034	7.266	6.704	104.8	331.27	60
$La_{0.9}Ce_{0.1}VO_4$	7.036	7.276	6.719	104.9	332.41	60
$LaVO_4$	7.0434	7.2801	6.7224	104.865	333.17	250
$LaVO_4$	7.043	7.279	6.717	104.9	332.78	60
$LaVO_4$	7.047	7.826	6.725	104.85	358.50	251
$LaVO_4$	7.07	7.29	6.77	105	337.04	252
$LaVO_4$	7.047	7.286	6.725	104.85	333.76	58
$Li_{0.15}La_{0.95}VO_4$	7.047	7.283	6.726	104.86	333.66	58
$Li_{0.30}La_{0.90}VO_4$	7.042	7.28	6.717	104.84	332.87	58
$Li_{0.60}La_{0.80}VO_4$	7.038	7.272	6.715	104.84	332.21	58
$Li_{0.90}La_{0.70}VO_4$	7.034	7.268	6.712	104.83	331.71	58
$(Ba_{1/3}La_{1/3}Th_{1/3})VO_4$	7.070	7.323	6.810	104.96	340.63	265
$(Ba_{1/3}Pr_{1/3}Th_{1/3})VO_4$	7.066	7.315	6.801	104.94	339.65	265
$(Ba_{0.5}Th_{0.5})VO_4$	7.046	7.3089	6.8066	105.8	338.29	264
$([Ca_{0.00}Ba_{1.00}]_{1/3}La_{1/3}Th_{1/3})VO_4$	7.071	7.324	6.81	104.96	340.72	266
$([Ca_{0.10}Ba_{0.90}]_{1/3}La_{1/3}Th_{1/3})VO_4$	7.065	7.319	6.803	104.93	339.90	266
$([Ca_{0.20}Ba_{0.80}]_{1/3}La_{1/3}Th_{1/3})VO_4$	7.059	7.307	6.796	104.9	338.75	266

compounds with Sr, Ba, Cd and Pb as divalent ions containing the lanthanide ions La, Pr, Nd and Sm were indexed in the monoclinic system, similarly to that found for $LnAsO_4$. On the contrary, arsenate compounds with Mg and Cd as divalent ions and heavier lanthanide ions such as Sm, Gd, Tb, Dy, and Y, reveal their isostructurality with the zircon structure. From a previous study, it has been demonstrated that $(Cd_{1/3}Nd_{1/3}Th_{1/3})AsO_4$ possesses temperature dependent dimorphism, the low temperature monazite form converting to scheelite structure at high temperature.[287] $(Cd_{1/3}Bi_{1/3}Th_{1/3})AsO_4$ is also stabilized with the monazite-type structure at low-temperature,[285] while its high-temperature form corresponds to the zircon structure.

Table 10
Unit-cell parameters of arsenate compounds with the monazite structure.

	a (Å)	b (Å)	c (Å)	β (°)	V (Å^3)	Ref.
$LaAsO_4$	7.0056	7.2103	6.7615	104.507	330.65	276
$LaAsO_4$	6.7646	7.2184	7.004	104.51	331.09	278
$LaAsO_4$	6.7615	7.2103	7.0056	104.507	330.65	276
$CeAsO_4$	6.975	7.177	6.759	104.69	327.29	279
$PrAsO_4$	7.011	7.125	6.57	104.3	318.02	280
$NdAsO_4$	6.6852	7.0885	6.8935	104.91	315.67	281
$BiAsO_4$	6.879	7.159	6.732	104.84	320.47	284
$PuAsO_4$	6.92	7.09	6.66	105.5	314.87	144
$AmAsO_4$	6.89	7.06	6.62	105.3	310.61	144
$(Ba_{1/3}La_{1/3}Th_{1/3})AsO_4$	7.027	7.227	6.839	107.79	330.71	286
$(Ba_{1/3}Nd_{1/3}Th_{1/3})AsO_4$	6.995	7.213	6.815	104.67	332.64	286
$(Ba_{1/3}Pr_{1/3}Th_{1/3})AsO_4$	7.005	7.217	6.816	104.75	333.23	286
$(Cd_{1/3}Bi_{1/3}Th_{1/3})AsO_4$	6.89	7.08	6.73	105.3	316.66	285
$(Cd_{1/3}La_{1/3}Th_{1/3})AsO_4$	6.852	7.023	6.655	104.81	309.65	286
$(Cd_{1/3}Nd_{1/3}Th_{1/3})AsO_4$	6.824	6.983	6.628	104.61	305.62	286,287
$(Cd_{1/3}Pr_{1/3}Th_{1/3})AsO_4$	6.844	7.022	6.649	104.74	309.01	286
$(Pb_{1/3}La_{1/3}Th_{1/3})AsO_4$	6.984	7.178	6.765	104.56	328.25	286
$(Pb_{1/3}Nd_{1/3}Th_{1/3})AsO_4$	6.939	7.143	6.749	104.8	323.42	286
$(Pb_{1/3}Pr_{1/3}Th_{1/3})AsO_4$	6.944	7.156	6.755	104.82	324.50	286
$(Pb_{1/3}Sm_{1/3}Th_{1/3})AsO_4$	6.908	7.129	6.742	104.91	320.85	286
$(Sr_{1/3}La_{1/3}Th_{1/3})AsO_4$	6.951	7.152	6.947	104.63	334.16	286
$(Sr_{1/3}Nd_{1/3}Th_{1/3})AsO_4$	6.888	7.088	6.681	104.52	315.76	286
$(Sr_{1/3}Pr_{1/3}Th_{1/3})AsO_4$	6.917	7.096	6.714	104.73	318.85	286
$(Ce.La.Nd)(As_{0.71}P_{0.29})O_4$	6.929	7.129	6.697	104.46	320.33	274
$(Ce_{0.47}La_{0.20}Nd_{0.18})AsO_4$	6.937	7.7137	6.738	104.69	348.76	281

Table 11
Unit-cell parameters of chromate compounds with the monazite structure.

	a (Å)	b (Å)	c (Å)	β (°)	V (Å^3)	Ref.
$LaCrO_4$	7.08	7.27	6.71	104.98	333.64	296
$LaCrO_4$	6.793	7.273	6.551	103.211	315.09	293
$LaCrO_4$	7.0369	7.2348	6.6918	104.95	329.15	294
$LaCrO_4$	7.041	7.237	6.693	104.94	329.52	297
$LaCrO_4$	7.08	7.27	6.71	107.98	328.51	296
$LaCrO_4$	7.038	7.023	6.689	104.98	319.39	292
$LaCrO_4$	7.0399	7.2344	6.6921	104.974	329.25	292
$SrCrO_4$	7.065	7.375	6.741	103.08	342.12	304
$SrCrO_4$	7.083	7.388	6.771	103.4	344.67	303
$SrCrO_4$	7.083	7.388	6.771	103.4	344.67	308
$SrCrO_4$	7.089	7.393	6.755	103.2	344.67	305
$PbCrO_4$	7.10	7.40	6.80	102.27	349.11	310
$PbCrO_4$	7.12	7.43	6.79	102.42	350.80	73
$PbCrO_4$	7.12	7.44	6.8	102.4	351.81	75
$PbCrO_4$	7.145	7.436	6.795	102.42	352.57	306
$PbCrO_4$	7.127	7.438	6.79	102.43	351.51	304
$PbCrO_4$	7.021	7.386	6.649	101.77	337.55	309
$PbCrO_4$	7.063	7.384	6.744	102.24	343.73	303
$PbCrO_4$	6.98	7.16	6.63	105.22	319.72	296
$PbCrO_4$	7.125	7.431	6.796	102.44	351.37	319
$PbCrO_4$	7.126	7.440	6.800	nd		320
$Pb(Cr_{0.90}S_{0.10})O_4$	7.117	7.452	6.792	nd		320
$Pb(Cr_{0.80}S_{0.20})O_4$	7.100	7.401	6.771	nd		320
$Pb(Cr_{0.70}S_{0.30})O_4$	7.082	7.374	6.763	nd		320
$Pb(Cr_{0.60}S_{0.40})O_4$	7.068	7.036	6.744	nd		320
$PbCrO_4$	7.128	7.439	6.796	102.42	351.93	319
$Pb(Cr_{0.96}S_{0.04})O_4$	7.125	7.435	6.495	102.44	335.99	319
$Pb(Cr_{0.89}S_{0.11})O_4$	7.133	7.446	6.797	102.42	352.56	319
$Pb(Cr_{0.81}S_{0.19})O_4$	7.134	7.449	6.797	102.44	352.72	319
$Pb(Cr_{0.78}S_{0.22})O_4$	7.098	7.397	6.771	102.39	347.22	319
$Pb(Cr_{0.70}S_{0.30})O_4$	7.097	7.388	6.764	102.39	346.39	319
$Pb(Cr_{0.64}S_{0.34})O_4$	7.08	7.382	6.756	102.42	344.84	319

Schwarz[288] also reports a charge compensation mechanism corresponding to the replacement of La by Ca and Th in $LaAsO_4$. The obtained $CaTh(AsO_4)_2$ compound exhibits a phase transition from monazite to zircon structure between 850 and 900 °C. The mean ionic radii of the cations in the cation site remains in the limits defined by Fukunaga and Yamaoka.[289]

No experimental evidence for the existence of AsO_4–PO_4 substitution was reported. However, Kolitsch et al.[246,274] reported that 10% of the As atoms can be substituted by P in natural Ce-gasparite. These authors also assumed through the comparison of the unit-cell parameters of natural gasparites with that of synthetic $CePO_4$ and $CeAsO_4$, that the substitution of P for As lead to the substantial decrease of the c-parameter, while the other a and b unit-cell parameters only slightly decrease. From a crystal chemistry point of view, they explained this observation by the arrangement of the XO_4 groups in the structure, these groups being stacked along the [0 0 1] direction and not along the other two main axes.

3.2.1.3. Chromates. Lanthanum chromium tetraoxide, $LaCrO_4$, is one of a few Cr^V compounds that can be stabilized and isolated.[290] No natural analogue of $LaCrO_4$ is reported in the literature. The rare-earth element chromates were mainly studied for their electronic properties (paramagnetism due to a single unpaired electron in Cr^V), mainly due to the $Cr^V \leftrightarrow Cr^{III}$ transition with oxygen fugacity and/or temperature.[83,291,292] Konno et al.[83] determined that the unpaired electron is occupying the dz^2 orbital of the Cr^V atoms. Furthermore, covalency

Table 12
Unit-cell parameters of sulphate, seleniate and other compounds with the monazite structure.

	a (Å)	b (Å)	c (Å)	β (°)	V (Å^3)	Ref.
$YbBeF_4$	6.674	6.911	6.402	103.87	286.68	347
$CaSO_4$	6.3769	6.6439	6.1667	102.22	255.35	315
$CaSeO_3$	6.402	6.791	6.681	102.78	283.27	312
$CaSeO_4$	6.85661	7.04962	6.68817	104.2675	313.31	313
$PbSeO_4$	7.154	7.407	6.954	103.14	358.84	304
$SrSeO_4$	7.101	7.34	6.874	103.48	348.41	304
$SrSeO_4$	7.102	7.352	6.853	103.43	348.04	311

is assumed to play a significant role in the Cr–O bonds of the CrO_4^{3-} tetrahedral structure in $LaCrO_4$, and to contribute to the stabilization of the tetrahedral CrO_4^{3-} groups.

Only $LaCrO_4$ crystallizes with the monoclinic structure.[293,294] All the other $REECrO_4$ exhibit the zircon-type structure.[292–296] The $LaCrO_4$ monazite-type compound becomes unstable and turns to perovskite-type $LaCrO_3$ at temperature above $680 \pm 10\,^{\circ}C$[72,297] according to the $LaCrO_4 \rightarrow LaCrO_3 + 1/2O_2$ reaction. This transformation, as well as the solid-solution possible field of existence, were studied for possible use of $LaCrO_3$ perovskite in solid oxide fuel cells[298] or as catalysts.[299] The transformation between the two crystal structures is complex and not well understood, but a comparison of the monazite to the perovskite structure[300] shows that La atoms turn from a 9-fold to a 12-fold oxygen coordination and Cr atoms change from the tetrahedral to the octahedral coordination. According to electrical neutrality conditions, the Cr atoms are reduced from a +5 to +3 valence, and one O atom per formula unit diffuses out of the bulk crystal to a free surface then is released. These crystallographic changes cause a unit cell volume decrease from 0.33 to 0.23 nm^3.[297]

$LaCrO_4$ can incorporate Ca to form a partial solid solution $(La_{1-x}Ca_x)CrO_4$ with $0.1 \leq x \leq 0.2$ at%.[72,297] The Ca incorporation is associated with a change in the Cr valence; this element adopts both V to VI valences, the Cr^{VI} content increasing with increasing the Ca substitution. Similarly, Miyoshi et al.[301] report the incorporation of Sr into $LaCrO_4$ and the formation of $La_{1-x}Sr_xCrO_4$ solid solution where Cr presents both V and VI oxidation states. No value for the maximum limit of composition for this solid solution is given in this work but Wagner et al.[302] reports the formation of $(La_{0.84}Sr_{0.16})CrO_4$ with the monazite structure.

Unsuccessful attempts to prepare the $M^{II}_{0.5}Th^{IV}_{0.5}Cr^{V}O_4$ (M^{II} = Cd, Ca, Sr and Pb) compounds by thermal decomposition of suitable compound mixture are reported by Schwarz.[288]

3.2.2. $M^{II}(Cr^{VI}, S, Se)O_4$ type compounds

Two chromates, where Cr is stabilized with the VI oxidation state, are known to crystallize with the monazite-type structure. Pistorius and Pistorius[303] and Effenberger and Pertlik[304] report the synthesis of both $SrCrO_4$ and $PbCrO_4$. $PbCrO_4$ was extensively studied since the early 2000s for its optical properties in the nanorods form.[75,305,306] Crystallographic data are available in the works performed by Jacob and Abraham,[307] Yin et al.,[308] Knight[309] and Wang et al.[75] Jacob and Abraham[307] extensively studied the thermodynamic properties in the SrO–CrO_3 binary system, and more particularly those of $SrCrO_4$, while Yin et al.[308] studied the $SrCrO_4$ compound for its photocatalytic efficiency. From a crystallographic point of view, Effenberger and Pertlik[304] described the coordination polyhedra of Sr in the ten-fold coordination, eight Sr–O bond lengths being short, the two others being longer in this polyhedron. $PbCrO_4$ appears as the synthetic analogue of crocoite mineral that is rarely found in the oxidation zones of lead deposits. Crystallographic data were first determined by Brill.[310] The $PbCrO_4$ structure is reported from single crystal study by Effenberger and Pertlik.[304] In this compound, Cr remains at the same oxidation state VI while lead is divalent. The lead coordination polyhedron is similar to that of Sr in $SrCrO_4$. It must be noted that the Cr–O bond length in the CrO_4^{3-} entities in $SrCrO_4$ (1.626 Å) is significantly shorter than the Cr–O average bond length in $PbCrO_4$ (1.663 Å).

Syntheses of $SrSeO_4$ and $PbSeO_4$ were also reported by Effenberger and Pertlik.[304] These authors preferred to describe the CN polyhedron of cation in the ten-fold coordination. On the contrary, Prevost-Czeskleba and Endres[311] considered that Sr atoms are surrounded by nine O atoms belonging to seven different SeO_4 tetrahedra in $SrSeO_4$. For both authors, the structure may be described in terms of nearly regular SeO_4^{2-} tetrahedra linked by Sr^{2+} ions. Furthermore, the geometry of the selenate groups is the same in both $SrSeO_4$ and $PbSeO_4$ structures, the average Se–O bond lengths being 1.640 Å and 1.642 Å, respectively.[304]

Wildner and Giester[312] report the $CaSeO_3$ compound to be stable with the monazite structure. This particular structure is described with Ca in the sevenfold coordination and pyramidal SeO_3 groups comprising a lone electron pair. This structure will be more precisely described regarding the monazite structure in part 5.1 of this review. Recently, Crichton et al.[313] have reported the structure of the high-temperature form of $CaSeO_4$, formed by dehydration of the gypsum-type. This material is equivalent to that described previously as a $P2_12_12_1$ form, but is however, a monazite with a monoclinic unit cell in space group $P2_1/n$.

During the study of the high pressure/high temperature forms of $CaSO_4$, Parise et al.,[314] Crichton et al.,[315] Ma et al.[316] and Bradbury and Williams,[317] confirmed the existence of a monazite-type form of $CaSO_4$, first reported by Borg and Smith,[318] and stabilized for $P \geq 11.8$ GPa and $T \geq 295$ K.[314,315]

Only one example of mixed distribution in the anionic group is reported in the literature. Incorporation of sulphate ions in $PbCrO_4$ can occur up to an extend of 38 mol% of sulphate at 25 °C.[319,320] These authors determined that the variation of the unit-cell parameters in the $PbCr_{1-x}S_xO_4$ series decreases linearly when increasing the substitution rate x. Crane et al.[320] stabilized the $PbCr_{1-x}S_xO_4$ compounds with an orthorhombic structure. However, the obtained solid was found to be thermodynamically unstable and slowly turns into the monazite-type structure. This substitution was observed on synthetic materials but was never reported for natural materials.

Schenker et al.[321] synthesized MnO_4^{2-}-doped crystals of $SrCrO_4$ by a flux method. The MnO_4^{2-} concentration in the solid phase was found to be 45 ppm by measuring the absorption spectrum in the visible, while the amount of $KMnO_4$ in the flux (that is reduced to MnO_4^{2-} during reaction) varied between 0.8 and 5 mol% with respect to $SrCrO_4$. This clearly indicates that the monazite domain of $SrCrO_4$ is very thin.

The cristallographic data available in the literature are reported in Tables 11 and 12.

3.2.3. $M^{iv}SiO_4$ type compounds

Only two silicates of tetravalent elements (Th and Pa) are reported to form monazite-type compounds, *i.e.* $PaSiO_4$[322,323] and $ThSiO_4$.[245] $USiO_4$, $NpSiO_4$, $PuSiO_4$ and $AmSiO_4$ crystallize with the zircon-type structure[322,324,325] as well as zirconium and hafnium.[326] They occur as natural and highly durable mate-

Table 13
Unit-cell parameters of silicate compounds with the monazite structure.

	a (Å)	b (Å)	c (Å)	β (°)	V (Å^3)	Ref.
$ThSiO_4$	6.8	6.96	6.54	104.55	299.60	329
$ThSiO_4$	6.78	6.97	6.5	104.92	296.81	331
$ThSiO_4$	6.784	6.974	6.5	104.92	297.16	334
$ThSiO_4$	6.774	6.962	6.495	105	295.87	335
$PaSiO_4$	6.76	6.92	6.54	104.53	296.15	322,323
$LaPO_4$	6.825	6.981	6.495	nd		346
$La_{0.914}Th_{0.086}(SiO_4)_{0.086}(PO_4)_{0.914}$	6.819	6.981	6.495	nd		346
$La_{0.869}Th_{0.131}(SiO_4)_{0.131}(PO_4)_{0.869}$	6.816	6.981	6.502	nd		346
$La_{0.878}Th_{0.122}(SiO_4)_{0.122}(PO_4)_{0.870}$	6.830	6.981	6.501	nd		346
$La_{0.799}Th_{0.201}(SiO_4)_{0.201}(PO_4)_{0.799}$	6.833	6.981	6.509	nd		346
$La_{0.790}Th_{0.210}(SiO_4)_{0.210}(PO_4)_{0.790}$	6.822	6.981	6.509	nd		346
$La_{0.736}Th_{0.264}(SiO_4)_{0.264}(PO_4)_{0.736}$	6.829	6.981	6.519	nd		346
$La_{0.697}Th_{0.303}(SiO_4)_{0.303}(PO_4)_{0.697}$	6.826	6.981	6.510	nd		346
$La_{0.646}Th_{0.354}(SiO_4)_{0.354}(PO_4)_{0.646}$	6.829	6.981	6.521	nd		346
$La_{0.598}Th_{0.402}(SiO_4)_{0.402}(PO_4)_{0.598}$	6.829	6.981	6.521	nd		346
$La_{0.556}Th_{0.444}(SiO_4)_{0.444}(PO_4)_{0.556}$	6.828	6.981	6.517	nd		346
$La_{0.501}Th_{0.499}(SiO_4)_{0.499}(PO_4)_{0.501}$	6.825	6.980	6.533	nd		346
$La_{0.502}Th_{0.498}(SiO_4)_{0.498}(PO_4)_{0.502}$	6.834	6.980	6.529	nd		346
$La_{0.447}Th_{0.498}(SiO_4)_{0.498}(PO_4)_{0.447}$	6.829	6.980	6.529	nd		346
$La_{0.403}Th_{0.597}(SiO_4)_{0.597}(PO_4)_{0.403}$	6.828	6.980	6.534	nd		346
$La_{0.334}Th_{0.666}(SiO_4)_{0.666}(PO_4)_{0.334}$	6.831	6.980	6.548	nd		346
$La_{0.307}Th_{0.693}(SiO_4)_{0.693}(PO_4)_{0.307}$	6.827	6.980	6.541	nd		346
$La_{0.274}Th_{0.726}(SiO_4)_{0.726}(PO_4)_{0.274}$	6.828	6.980	6.542	nd		346
$La_{0.201}Th_{0.799}(SiO_4)_{0.799}(PO_4)_{0.201}$	6.830	6.980	6.549	nd		346
$La_{0.139}Th_{0.861}(SiO_4)_{0.861}(PO_4)_{0.139}$	6.836	6.980	6.549	nd		346
$La_{0.102}Th_{0.898}(SiO_4)_{0.898}(PO_4)_{0.102}$	6.832	6.979	6.559	nd		346
$La_{0.082}Th_{0.918}(SiO_4)_{0.918}(PO_4)_{0.082}$	6.831	6.980	6.553	nd		346
$ThSiO_4$	6.831	6.979	6.558	nd		346
$CePO_4$	6.787	7.029	6.468	103.18	300.29	219
$Ce_{0.95}Th_{0.05}(SiO_4)_{0.05}(PO_4)_{0.95}$	6.788	7.029	6.473	103.19	300.54	219
$Ce_{0.90}Th_{0.10}(SiO_4)_{0.10}(PO_4)_{0.90}$	6.788	7.025	6.474	103.27	300.25	219
$Ce_{0.85}Th_{0.15}(SiO_4)_{0.15}(PO_4)_{0.85}$	6.789	7.018	6.479	103.32	300.12	219
$Ce_{0.80}Th_{0.20}(SiO_4)_{0.20}(PO_4)_{0.80}$	6.79	7.014	6.485	103.4	300.15	219
$Ce_{0.75}Th_{0.25}(SiO_4)_{0.25}(PO_4)_{0.75}$	6.79	7.01	6.489	103.43	300.05	219
$Ce_{0.50}Th_{0.50}(SiO_4)_{0.50}(PO_4)_{0.50}$	6.792	6.993	6.498	104.24	298.94	219
$ThSiO_4$	6.797	6.962	6.546	104.54	299.35	219

rials such as zircon ($ZrSiO_4$) and hafnon ($HfSiO_4$). $USiO_4$ and YPO_4 do not adopt the monoclinic structure but must be defined as virtual end-members of the monazite solid solutions to describe the chemical composition of natural monazites.[215]

The substitution of $ThSiO_4$ in natural monazites was first described by Frondel.[327,328] The existence of the $ThSiO_4$ end-member was first reported by Hutton[245] and Pabst et al.,[329] while Frondel and Collette[330] described the first way of preparation of this compound. $ThSiO_4$ can be stabilized with the monazite structure (huttonite)[331] but also with the zircon structure (called thorite).[332] On the basis of the full-potential linearized augmented-plane-wave method with the generalized gradient approximation for the exchange-correlation potential (FLAPW-GGA), Shein et al.[333] determined that the tetragonal cell of thorite became more favorable than huttonite with monoclinic structure. These calculations also yielded the authors to conclude that at zero temperature and zero pressure approximation, these phases are unstable in comparison with mechanical mixture of constituent binary oxides. The zircon-type structure is formed at low temperature while huttonite is stable at high temperature. The thorite–huttonite phase transition was extensively studied by Taylor and Ewing[334] and Mazeina et al.[335] This latter determined the variation of enthalpy of formation from elements $\Delta H^0_{f,el}$ and the variations of enthalpy and entropy of reaction, $\Delta H^0_{R,ox}$ and $\Delta S^0_{R,ox}$, from oxides (relative to quartz and MO_2), and the molar volume of thorite and huttonite. The temperature of the phase transition at atmospheric pressure reaches $1210 \pm 10\,^{\circ}C$.[336] This value is in good agreement with that reported by Finch et al.[337] *i.e.* $1225 \pm 10\,^{\circ}C$ but disagrees with that noted by Dachille and Roy[338] (1000 °C). The phase transformation from tetragonal $ThSiO_4$ (thorite) to monoclinic $ThSiO_4$ (huttonite) is unconsistent with the general expectation that the less dense modification exists at higher temperatures[335] and to what is generally observed with monazite-structured compounds.[118,339] Protactinium silicate, $PaSiO_4$, shows similar behaviour than $ThSiO_4$.[322]

The Th/Si mole ratio being constantly equal to 1 also supports the existence of the straightforward solid-solution along the binary join $REEPO_4$–$ThSiO_4$ in natural monazites, as suggested

by Starynkevitch.[340] Later confirmation by Bowie and Horne[341] and Pavlenko et al.[342] did not enjoy wide acceptance, possibly because they were based on average wet chemical analyses with no indication of the sample homogeneity. Kucha[343] argued that the huttonite-monazite series cannot be explained solely by the simple coupled substitution $Th^{4+} + SiO_4^{4-} \leftrightarrow REE^{3+} + PO_4^{4-}$ and concluded that there must be an electrostatic compensation by the concomitant incorporation of Ca, F and OH, leading to a formula for intermediate members of the series of (REE,Th,M^{2+},U)(SiO_4,PO_4,OH,F), similar to cheralite.[341] Data reported by Kucha[343] and Della Ventura et al.[344] leave no doubt about the continuity of the monazite-huttonite series to a maximal extend of 30 at% huttonite in natural monazites, while Della Ventura et al.[344] suggested that the substitution can be written without requiring any electrostatic compensation by divalent cations, or anionic groups.

Only few studies were devoted to the syntheses and studies of monazite-huttonite solid solutions. Peiffert and Cuney[345] and Montel et al.[346] reported the synthesis of several compounds in the $LaPO_4$–$ThSiO_4$ system, indicating the formation of a complete solid solution between both end-members, under hydrothermal conditions. The a, b and c unit-cell parameters decrease linearly with increasing thorium content in the $La_{1-x}Th_x(SiO_4)_x(PO_4)_{1-x}$ while β angle parameter decreases. Hikichi et al.[219] determined that a complete solid solution exists between the two end-members $CePO_4$ and $ThSiO_4$, all the compounds being obtained with the monazite structure. The same variations of the unit-cell parameters than those determined by Montel et al.[346] are reported in this work.

The only available data corresponding to the simultaneous incorporation of uranium and silicate in $LaPO_4$ were reported by Montel et al.[346] The field of existence of the monazite solid solution with $USiO_4$ is limited to $La_{0.87}U_{0.13}(SiO_4)_{0.13}(PO_4)_{0.87}$, corresponding to 14.25 UO_2 wt%.

3.2.4. Particular case of $YbBeF_4$

$YbBeF_4$ is the only monazitic compound which does not belong to the AXO_4 (*i.e.* oxide) family. It is also the first, and the only one, reported fluoroberyllate that adopts the monazite-type structure.[347] The structure was described as the classical $CePO_4$ monazite structure: Be is tetrahedrally coordinated by four F atoms between 1.55 and 1.59 Å, and Yb is surrounded by nine F with Yb–F bond distances ranging from 2.40 to 2.80 Å. The YbF_9 polyhedron can be described as a pentagon capped by two additional F atoms from two sides each. The YbF_9 polyhedron forms infinite chains with the BeF_4 tetrahedron *via* common edges.

4. Criteria for the AXO_4 monazite-type structures stability

As described in the two previous chapters, monazite is known to be a very flexible structure that can accept various elements with various oxidation states in its bulk. To evaluate the factors affecting the structural stability of this structure according to the elements incorporated, few authors tried to define systematic schemes and potentially predictive models. Physicochemical parameters such as temperature or pressure can also modify the frontiers between two structural domains.

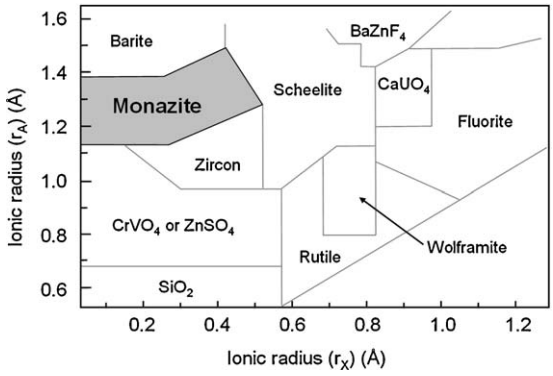

Fig. 2. Composite structure field map for AXO_4 structures proposed by Muller and Roy.[348]

4.1. Composition dependence of the stability domain of the monazite structure

4.1.1. The structure-field map model

The usefulness of structure-field map concept[348] was proved in systematizing the occurrence of different structures among a range of fixed stoichiometry compounds of the $A_xX_yO_z$ type, here AXO_4. A binary phase diagram is built in which the axes represent the crystal radii of the A and X ions.[155] The first diagram proposed by Muller and Roy[348] is reported in Fig. 2. From this figure, one can see the relative stability domains of the $A_xX_yO_z$ compounds, and particularly, the stability field that is related with the monazite structure. It has been used by Kohler[347] to determine the structural stability of $YBeF_4$.

A similar approach was developed by Fukunaga and Yamaoka.[289] Their classification diagram of the AXO_4 type compounds with respect to their crystal structures at normal pressure versus both k and t parameters ($k = r_A/r_X$ and $t = (r_A + r_X)/2r_O$) is reported in Fig. 3. In this representation, the cation with the larger coordination number and/or smaller valency is chosen as the A cation. It must be noted that when two compounds have the same X cation, the AXO_4 type compounds lie on the same line described as $k = (2r_O/r_X)t - 1$. Main (XO_4) lines are shown in the diagram. The compounds with the same X cation often crystallize in the same structure even if the radius of A cation varies to some extent. Therefore, the classified area of a specific structure type tends to extend toward larger k and t. The extend of the monazite stability domain is very large and covers a wide variety of anionic families. This representation can be potentially extremely useful to predict the structure of an AXO_4 compound to be synthesized and to describe the substitution possibilities in the monazite structure.[349] Similar diagrams to that of Fukunaga and Yamaoka[289] were developed by Bastide,[350] (Fig. 4) Finch and Hanchar[351] and Errandonea and Manjón[352] for the prediction of the AXO_4 phase stability.

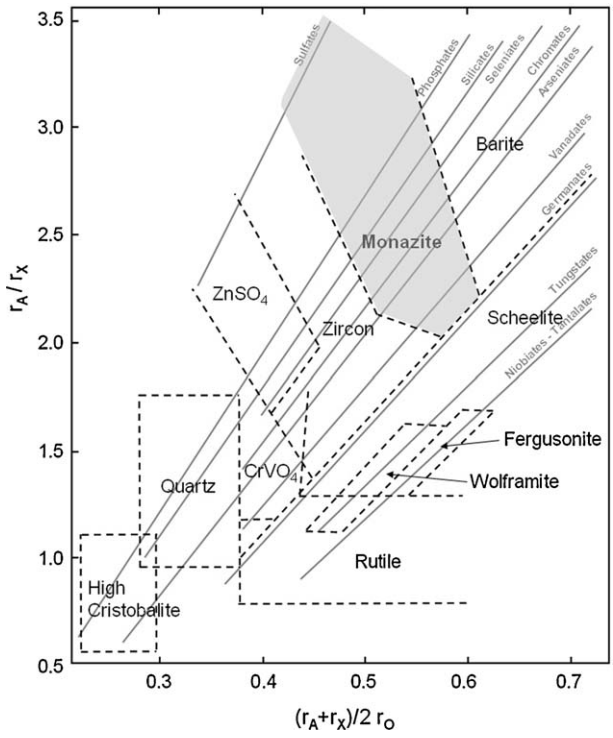

Fig. 3. Classification diagram of AXO_4 type compounds proposed by Fukunaga and Yamaoka.[289] The monazite stability domain is represented in grey.

4.1.2. Stability domain of the monazite-type structure

These types of representation offer the possibility to predict the structure of a compound. However, the problem of the limits of the field stability domain remains open. The possibilities of incorporation of elements as solid solution within the monazite structure and the extent of these solid solutions were extensively studied by several authors. Their attention was generally paid on specific compositions. Some of them tried to identify systematics and to propose comprehensive models in order to predict if one compound could adopt the monazite structure.

4.1.2.1. Preliminary studies. A first attempt to correlate the ionic radii to structures in the monazite/xenotime families was reported by Carron et al.[353] On the basis of the ratio between the (X–O) bond length (in the AXO_4 compounds) and the ionic radius of A, noted X/A, these authors calculated that a value of 1.86 seems to specify the size limit of both the cation and the anion at the xenotime–monazite structural frontier. This ratio yielded to propose the stability of silicates and the possibility of isomorphous substitution of the anions among the rare-earth phosphates, silicates, arsenates and vanadates. More recently, Macey[354] completed this work by determining that the structural border between zircon and monazite corresponds to a X/A ratio equal to 1/1.56. Monazite and zircon structures are obtained for X/A < 1/1.56 and X/A > 1/1.56, respectively. Even if systematic variations between the unit-cell parameters and chemical compositions were evidenced in this work, no predictive model for the structural stability limits was proposed.

4.1.2.2. Criteria for the stability of the monazite structure. Podor and Cuney[171] focussed their attention on the stability domain of the monazite structure, and more precisely on that of the $(M^{III}_{1-2x}M^{II}_xM^{IV}_x)PO_4$ compounds. These compounds are described by two parameters $r_{average} = (1-2x)^{[9]}r_{M^{3+}} + x^{[9]}r_{M^{2+}} + x^{[9]}r_{M^{4+}}$ and $r_{ratio} = [(1-x)^{[9]}r_{M^{3+}} + x^{[9]}r_{M^{2+}}]/[(1-x)^{[9]}r_{M^{3+}} + x^{[9]}r_{M^{4+}}]$ (where $^{[9]}r_M$ is the ionic radius of the M element in the ninefold coordination[155]). The upper and lower values of these parameters are $1.216\,\text{Å} \geq r_{average} \geq 1.107\,\text{Å}$ and $1.238 \geq r_{ratio} \geq 1$. The stability range of the $(M^{III}_{1-2x}M^{II}_xM^{IV}_x)PO_4$ compounds is plotted as a function of the three parameters x, $r_{average}$ and

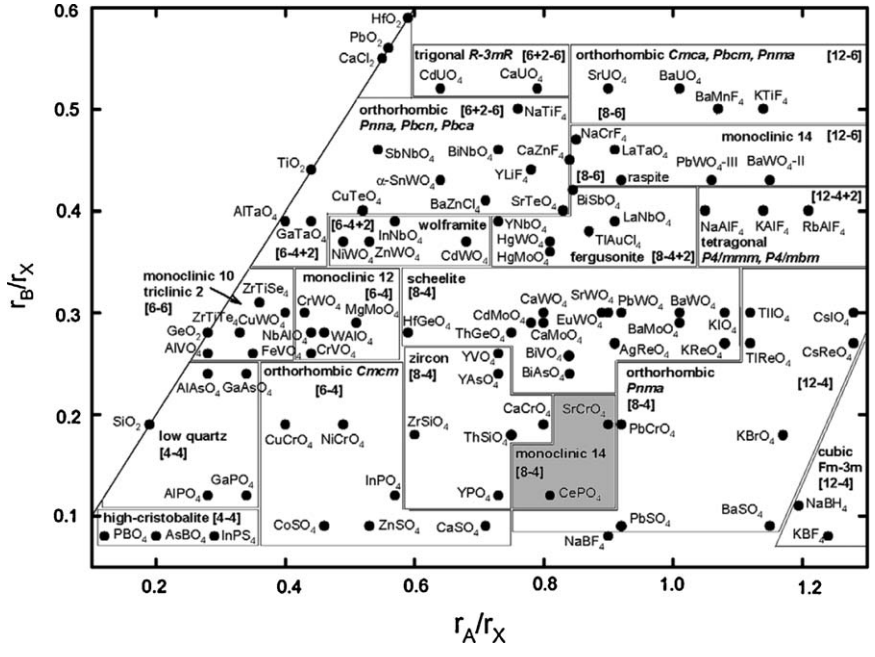

Fig. 4. Updated Bastide's diagram for AXO_4 compounds proposed by Errandonea and Manjón.[352] The monazite stability domain is reported in grey.

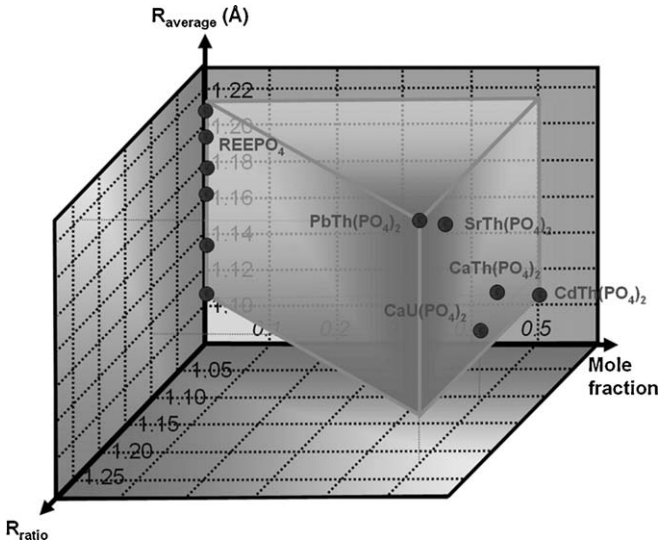

Fig. 5. Stability domain of the $(A_{1-2x}^{3+}B_x^{2+}C_x^{4+})PO_4$ compounds in the monazite structure-type versus mole fraction of B^{2+} or C^{4+}, $r_{average}$ and r_{ratio} (after Podor and Cuney[171]).

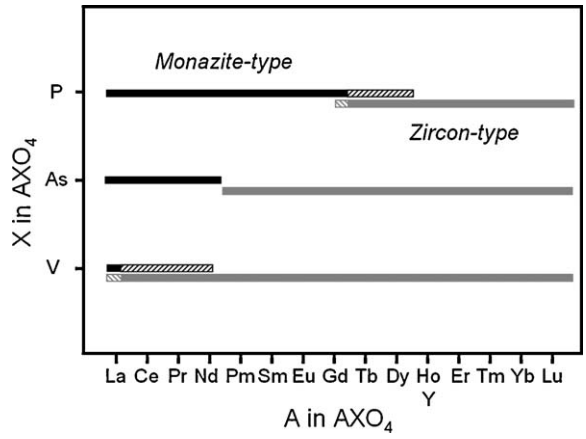

Fig. 6. Stability fields of the monazite and zircon structure types among $REEXO_4$ (X = P, As, V) compounds (dotted lines = metastable regions (after Kolitsch and Holtstam[246]).

r_{ratio} (Fig. 5). The volume obtained is a prism that describes the stability domain of monazites. Each point included in this volume corresponds to the composition of a product that crystallizes with the monazite structure. A line segment joining two points in this volume represents a solid solution between the two compositions. This model is more accurate to describe the limit of chemical compositions in the border line than the field stability domains reported in Section 4.1. Some authors used this model to predict the maximum solubility of one element in monazite-type compounds[216,355] or the way of incorporation of other ones (such as cerium, neptunium and plutonium).[107,140,206] However, some discrepancies with reality remain possible, especially in the case of miscibility gaps.

4.1.2.3. Monazite to zircon transition. Due to its importance in the earth sciences, several authors paid a great attention on the monazite to zircon transition. This limit was clearly established in the case of pure compounds, but is difficult to characterize in the case of mixed rare-earth elements systems, with the formation of a miscibility gap.

In a recent review, Kolitsch and Holtstam[246] constructed a schematic diagram showing the stability fields of the monazite and zircon-type structures, on the basis of available data for $REEXO_4$ (X = P, As, V) compounds. This diagram describes what occurs in one $REEXO_4$ family. The conclusions were as follows:

(i) within a single series of REE phosphates, arsenates or vanadates, the monazite structure type is stable for the large(st) REE^{3+} cations while the small(est) REE^{3+} cations form the zircon structure;
(ii) the stability field of the monazite structure type in $REEXO_4$ (X = P, As, V) compounds narrows with increasing size of the XO_4 group (Fig. 6). This structural influence of the XO_4 group agrees with earlier conclusions of Losutov et al.[356] who stated that an increase of the ionic radius of the X atom in AXO_4 compounds leads to the structure types of scheelite and, for very large X atoms, of wolframite;
(iii) metastable phase fields are evident for the areas left and right of the monazite–zircon structure-type limit (Fig. 6). These metastable regions are largest for the phosphates and absent for the arsenates. Ropp and Carroll[254] found, in an early comparison of the dimorphic forms of $REEXO_4$ compounds (*i.e.* $TbPO_4$ and $LaVO_4$), a linear correlation between the REE^{3+} radius and the X^{5+} radius of the $(XO_4)^{3-}$ tetrahedral oxyanion rather than with the X–O bond length or the tetrahedral volume of the oxyanion. Their observation[254] was based on the assumption that $PmAsO_4$ is also dimorphic. However, the existence of monazite-type $PmAsO_4$ has not been demonstrated yet.

This diagram is useful to overview the stability field of the monazite structure, but is insufficient to describe correctly the partial solid solutions between two $REEXO_4$ compounds, particularly between a light and a heavy rare-earth element, and the existence of a miscibility gap.

A similar behaviour is described by Nabar and Mhatre[266] in the $Ca_{1-x}Ba_xLaTh(VO_4)_3$ system. The structure of the obtained compound depends on barium substitution fraction and temperature, as illustrated in Fig. 7.

A description of the inter-family compounds $REE(X_{1-x}X'_x)O_4$ was proposed by Aldred[267] on the basis of a systematic study of the $REE(P_{1-x}V_x)O_4$ compounds (REE = La to Yb). The conclusions were that:

(i) Complete solid solution behaviour is observed when the end members are isostructural ($LaPO_4$–$LaVO_4$-monazite-type, $YbPO_4$–$YbVO_4$-zircon-type).
(ii) When the end-members are not isostructural, a systematic change in the solubility range in both structures is found as REE is modified. At large REE ionic radius (Ce or Pr) the two-phase field is narrow and dominated by a monazite solid-solution field. For intermediate REE ionic radius (*i.e.* Nd or Sm), the two-phase field is broad with little solu-

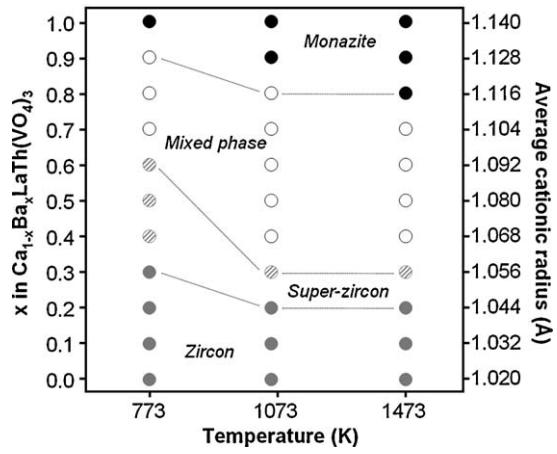

Fig. 7. Structure of some phases in the $Ca_{1-x}Ba_xLaTh(VO_4)_3$ system as a function of x at various temperatures (after Nabar and Mhatre[266]).

bility in either the monazite or zircon structures. At small REE ionic radius (Gd), the two-phase field is again narrow with extensive solid solubility in the zircon phase. These conclusions support the fact that the miscibility gap also exists with inter-family compounds. The obtained diagram (reported in Fig. 8) allows the representation of the miscibility gap existing between the monazite and zircon-type compounds.

In the (REE′REE″)PO_4 family, when both end-members crystallize with the monazite-type structure, the solid solution is complete, as demonstrated by Gratz and Heinrich[357] and Terra et al.[135] in the $Ce_xGd_{1-x}PO_4$ and $La_xGd_{1-x}PO_4$ systems, respectively. This was also confirmed by the calculations performed by Mogilevsky.[174,175] When both end-members are not isostructural, only few experimental data are available but all tends to demonstrate that only restricted solubility ranges are observed. Gratz and Heinrich[357] report a temperature-dependent miscibility gap between $CePO_4$ and YPO_4 under hydrothermal

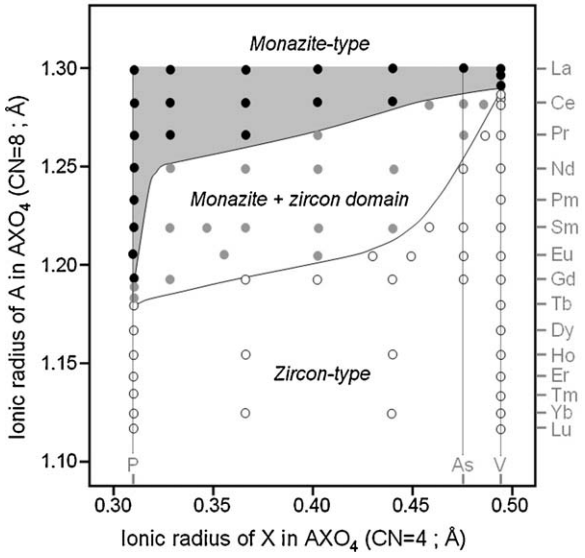

Fig. 8. Structure field map for AXO_4 compounds (after Aldred[267]).

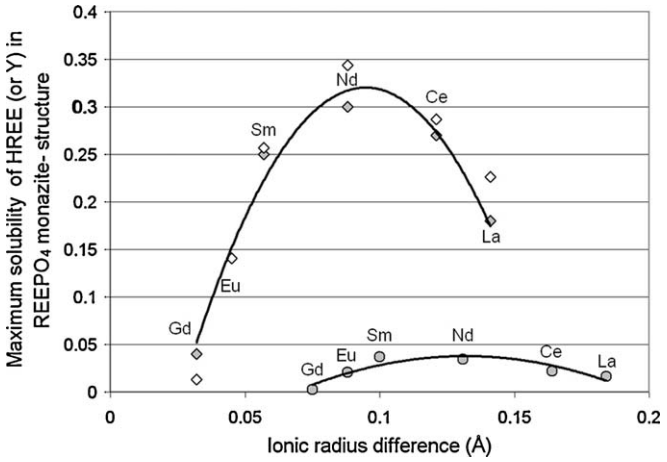

Fig. 9. Maximum solubility of Lu and Y in the $REEPO_4$ monazite-structure series (values at $T = 1200\,^{\circ}C$). Open losange = Y in $REEPO_4$ (experimental data), grey losange = Y in $REEPO_4$ (calculated data after Mogilevski), grey circle = Lu in $REEPO_4$ (data after Mogilevsky[174]).

conditions: the higher the synthesis temperature/pressure synthesis, the higher the Y content in $CePO_4$. Similar results were reported by Andrehs and Heinrich[268] and Pyle[3] in a similar study performed with natural minerals. Seydoux-Guillaume et al.[270] also concluded to an increase of the YPO_4 solubility in $CePO_4$ when increasing the experimental temperature. Furthermore, these authors determined that this solubility increases with increasing the thorium and silicate contents in $CePO_4$. All the available data were gathered by Spear and Pyle.[358] The same trends were observed in the $LaPO_4$–YPO_4,[172,175] $NdPO_4$–YPO_4, $SmPO_4$–YPO_4 and $NdPO_4$–$YbPO_4$ systems[172] with materials obtained by direct high temperature synthesis. Moreover, the solubility of $DyPO_4$ in $GdPO_4$ was estimated to be less than 40 mol% at 1200 °C by Boakye et al.[141] Solubility of Tb in $CePO_4$, $NdPO_4$ and $SmPO_4$ was determined to be higher than 50 mol% at 1350 °C by Mullica et al.[170] A regular solution model was applied by Mogilevsky and Boakye[175] to describe the solid solubility in monazite–xenotime systems and its pressure dependence. The comparison between the experimental data in the $REEPO_4$–YPO_4 system with the calculated solubilities in the $REEPO_4$–YPO_4 and $REEPO_4$–$LuPO_4$ systems at 1200 °C are reported as a function of the ionic radii difference between REE and Y (Lu respectively) in Fig. 9. This figure clearly illustrates that there is a good agreement between the model and the available experimental data, suggesting that the model could be used to predict the solubility in all the monazite–xenotime systems. Furthermore, this figure illustrates the fact that the solid state solubility of one HREE in the monazite structure does not linearly decrease from $LaPO_4$ to $GdPO_4$. This solubility goes through a maximum value centered between $PrPO_4$ and $NdPO_4$. It must be noted that at the border between the monazite and zircon (*i.e.* xenotime) structures, the solubility of Gd in $HREEPO_4$ is higher than the solubility of HREE (and YPO_4) in $GdPO_4$.[174,269,359,360] These results indicate that only 4 at.% of HREE elements (or Y) are sufficient to fully transform $GdPO_4$ to the xenotime structure.

4.2. Structural effect of external parameters

The limits of the stability domain of the monazite structure vary with temperature, pressure and radiation dose. These particular effects were specifically studied by several authors. The main results are reported in this section.

4.2.1. Influence of temperature

Depending on the temperature of synthesis, an hemihydrated hexagonal form[361] (stable at "low" temperature) of $REEPO_4$ (REE = La to Dy[134,135,362]) or $M^{III}PO_4$ (M^{III} = Pu,[142] Am[145]), called rhabdophane, can be stabilized.[363–365] As an example, du Fou de Kerdaniel et al.[363] reported that for light rare earth elements (La,Ce), the hexagonal rhabdophane is obtained from ions in solution below 90 °C while monazite is directly stabilized for higher temperatures. This "transition" temperature increases along the REE series to reach about 160 °C for $GdPO_4$.

Rhabdophane transforms into monoclinic form by heating at high temperature. First, an anhydrous form of the hexagonal phase is obtained between 100 and 400 °C, the transformation temperature depending on the considered cation, then the transition to monoclinic monazite is observed.[136,137,366–369] The transition temperatures are in the range 400–500 °C for $LaPO_4$,[136,137,366] about 600 °C for $CePO_4$[136,366,370,371] and $EuPO_4$,[372] 700 °C for $SmPO_4$[136] then reach up to 900 °C for $DyPO_4$.[136] Moreover, it is to note that monazite compounds could be obtained from rhabdophane by mechanical treatment, typically milling.[373–375]

The rhabdophane → monazite transition was also reported for compounds incorporating both light and heavy lanthanides such as $(La,Y)PO_4$,[173] $(Ce,Y)PO_4$[376] or $(La,Lu)PO_4$[377] solid solutions. On the other hand, two polymorphic modifications were found for the transitional compounds $GdPO_4$, $TbPO_4$, and $DyPO_4$: from hexagonal to monoclinic form and from monoclinic to tetragonal form. The first transition temperatures are 550 °C for $GdPO_4$ and 600 °C for $TbPO_4$ and $DyPO_4$[367] while the second ones are found above 1200 °C for $GdPO_4$, between 800 and 1100 °C for $TbPO_4$ and approximately 800 °C for $DyPO_4$.[368,378] For heavier rare earth elements (Yb, Lu), the rhabdophane directly turns to tetragonal form when heating above 860 °C.[379] These modifications occur on the $r_{average}$ parameter defined by Podor and Cuney.[171] Moreover, hexagonal hydrated forms of $BiPO_4$,[151] $CaTh(PO_4)_2$ (called brockite),[380] $CaU(PO_4)_2$ (called tristramide)[381] and $Nd_{1-2x}Ca_xTh_{x-y}U_yPO_4$[382] are also mentioned and led to monazite-type compounds after heating.

Another effect of the temperature lies in the solubility of heavy lanthanides in the monazite structure. Indeed, several authors[172,174,269] report the increase of the solid state solubility of $HREEPO_4$ (and YPO_4) in $LREEPO_4$ compounds with increasing temperature. This particular point fits well with the model developed by Mogilevsky.[174]

The limits of the r_{ratio} parameter defined by Podor and Cuney[171] also vary with temperature. The zircon to monazite structural transformation is observed in only a few compounds such as $ThSiO_4$, $PaSiO_4$, $Pb_{0.5}Th_{0.5}VO_4$,[264] and $CeVO_4$.[339] Dusausoy et al.[339] showed that synthetic $(Ca_{0.5}U_{0.5})PO_4$ compound have an irreversible polymorphic transition from orthorhombic to monoclinic above 1000 °C in standard pressure conditions. The $(Ca_{0.5}Th_{0.5})PO_4$ compound does not undergo this type of phase transformation. In these five transformations, a temperature increase yields to the stabilization of the monazite structure.

A special attention was paid to $ThSiO_4$. Mazeina et al.[335] determined the enthalpies of formation of thorite and huttonite (equal to -2117.6 ± 4.2 kJ/mol and to -2110.9 ± 4.7 kJ/mol, respectively). These values indicate that $ThSiO_4$ (thorite or huttonite forms) are metastable relative to SiO_2 (quartz) and ThO_2 (thorianite) at standard conditions. Although metastable at room temperature, $ThSiO_4$ stabilizes at higher temperatures compared to its binary oxides, owing to the entropy contribution for huttonite/thorite relative to cristobalite and ThO_2.

4.2.2. Influence of pressure

The influence of very high pressure on the $CePO_4$ structure was studied by Huang et al.[383] The structure deformation of monazite can be linked to the higher compressibility of the CeO_9 polyhedron compared to that of the PO_4 tetrahedron. X-ray diffraction data suggested a structural distortion at ~11.5 GPa.

Pressure can also influence the limits of the stability domain of the monazite structure. The solid state solubility of elements in the monazite structure can vary with pressure. Gratz and Heinrich[269] and Mogilevsky[174] report the increase of the HREE and Y incorporation in $CePO_4$ when increasing the operating pressure during synthesis. Thus, variation of the pressure can involve the stabilization of polymorphs. The increase of pressure can yield to the stabilization of the monazite structure. Many authors[315,317,318,335,384] have observed $CaSO_4$ undergoing phase transitions from its ambient anhydrite structure to the monazite type at $P = 2$ GPa, then at higher pressure and temperature to crystallize in the barite-type structure. Bradbury and Williams[317] conducted X-ray diffraction and infrared spectroscopy on $CaSO_4$ to pressures of 28 and 25 GPa, respectively. A reversible phase transition to the monazite-type structure occurs gradually between 2 and ~5 GPa with a highly pressure-dependent volume change of ~6–8%. In the case of $NdAsO_4$, a pressure increase yields to the destabilization of the monazite structure and to the formation of a scheelite-type polymorph.[385] The same behaviour was observed by Range et al.[386] for the $CeVO_4$ compound. Recently, Lacomba-Perales et al.[387] found evidence of a reversible pressure-induced structural phase transformation from zircon to a monazite-type structure in the xenotimes. The onset of the transition is at 19.7 GPa in YPO_4 and 17.3 GPa in $ErPO_4$. A similar transition is described for $TbPO_4$ by Lopez-Solano et al.[388]

A hypothetical schematic phase diagram for the AXO_4 compounds, indicating the temperature and pressure dependence of the structure transformations, was proposed by Finch and Hanchar[351] (Fig. 10).

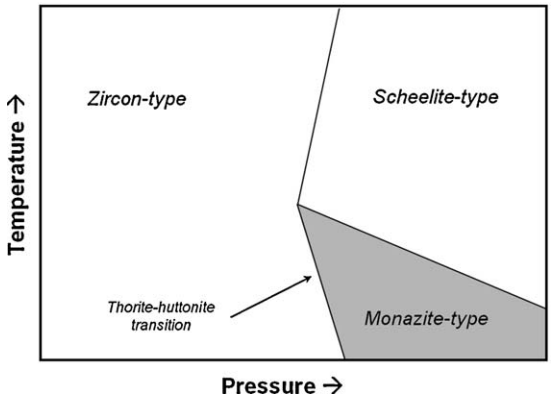

Fig. 10. Hypothetical schematic phase diagram for the AXO_4 compounds (from Fig. 15 of Finch and Hanchar[351]).

4.2.3. Effect of irradiation on the monazite structure

The last parameter of importance reported in the literature as influent on the stability domain of the monazite structure is irradiation. The majority of the studies developed in this field was dedicated to phosphate-based compounds. Natural monazites, as well as synthetic compounds, are known to recover from irradiation damages at low temperature.[84,120,389] Natural monazite analogues of several hundred millions years old are found to remain crystallized despite of high thorium and/or uranium weight loadings contrarily to other minerals such as zirconolite that become metamict under irradiation. Although monazite is apparently always found in a crystalline state in nature, it is possible to produce a metamict state by bombarding the material with heavy ions at fluences higher than 4×10^{14} ions/cm^2. However, the cristallinity of monazite can be restored by annealing the material at low temperature (400 K).[85,389] The same behaviour is described for huttonite by Meldrum et al.[389] Furthermore, these authors reported that the critical amorphization temperature above which amorphization did not occur increased from huttonite to thorite. At temperatures below 500 K, the tetragonal and monoclinic polymorphs of $ThSiO_4$ required approximately the same ion fluence for amorphization. However, they noted that the monoclinic $ThSiO_4$ is not "more resistant" to radiation damage than the tetragonal-symmetry form, but its amorphous phase recrystallizes at a lower temperature.

The irradiation dose required to get amorphization of synthetic $CePO_4$ samples is found to be very important at 400 K compared to that required to amorphize apatites or zircons. Moreover, above this temperature, the amorphization of the structure cannot be obtained even for very high amorphization doses (higher than 3 dpa) probably due to an efficient annealing of the defects in this structure.[390] In the same way, Burakov et al.[391] reported that lanthanum phosphate monazites (La,Pu)PO_4 containing 8.1 wt.% of plutonium ^{238}Pu remain crystallized at ambient temperature up to a cumulative radiation dose of 1.19×10^{25} α/m^3 (*i.e.* 2×10^{18} α/g) while the sample changed in color from initial light blue to grey under self-irradiation. It was assumed that self irradiation is accompanied by two processes: accumulation of defects in monazite crystalline structure and self-annealing of these defects at ambient temperature. On the contrary, $PuPO_4$ (7.2 wt.% of ^{238}Pu) became nearly amorphous above 4.2×10^{24} α/m^3. Swelling and crack formation due to the α decay damage was observed in the $PuPO_4$ ceramic.[391] With the same objective, samples of (La,Am)PO_4 with 23 wt.% ^{243}Am were prepared.[179,180] Goubard et al.[392] reports the experimental studies by X-ray diffraction of irradiation damage from alpha decay in neptunium and americium vanadates versus cumulative dose. The isotopes used were the ^{237}Np α-emitter and the ^{241}Am α, γ-emitter. The data reveal that the irradiation has no apparent effect on the neptunium phases while the americium vanadate swells and becomes metamict when increasing the cumulative dose.

5. Structural relationships between the monazite structure and other related structures

Many compounds exhibit polymorphic transitions between the monazite structure and another structure: zircon (or xenotime), scheelite, anhydrite, rhabdophane and barite. These possible transformations correspond to the structures that are at the monazite stability limits evidenced in the structure-map model developed by Fukunaga and Yamaoka.[289] The transformation of one isomorph to another can be obtained through the action of temperature or pressure increase (or decrease). The transitions can be displacive or reconstructive. The structural relationships, as well as the transition mechanisms, have been described by several authors and are reported in this part of the review.

5.1. Monazite derivative structures

The monazite structure of the AXO_4 compounds was described in part 2. The distribution of the A element in the cationic site occurs in AO_9 coordination polyhedra. Three derived structures were reported in the literature.

Wildner and Giester[312] reported that the $CaSeO_3$ compound is stable with a structure that is very similar to monazite. The main difference lies in the fact that the Ca atom is in the sevenfold coordination instead of the ninefold coordination for Ce in $CePO_4$. $CaSeO_3$ provides an example for the stereochemical equivalence of a pyramidal SeO_3 group comprising a lone electron pair E with a tetrahedral TO_4 group. The authors claimed that $CaSeO_3$ belongs to a new structure type but is 'quasi-isotypic' to the monazite structure, where the lone electron pair E is formally replaced by an additional oxygen ligand. This results in polyhedral rotations and in a change from the sevenfold coordination of Ca in $CaSeO_3$ to the ninefold coordination of the large Me cations in monazite type compounds.

On a similar way, the structure of the $Li_{3x}La_{1-x}VO_4$ ($0 \leq x \leq 0.3$) compounds is described by Isasi et al.[58] as a distorted monazite-type structure. The structure is described by means of VO_4 tetrahedra, LaO_9 polyhedra and LiO_5 units. The rare-earth element adopts the "classical" nine-fold coordination while the lithium atoms are coordinated to five oxygen atoms. The LiO_5 polyhedron is described as a distorted square pyramid that is rather unusual for lithium. The authors note that around the

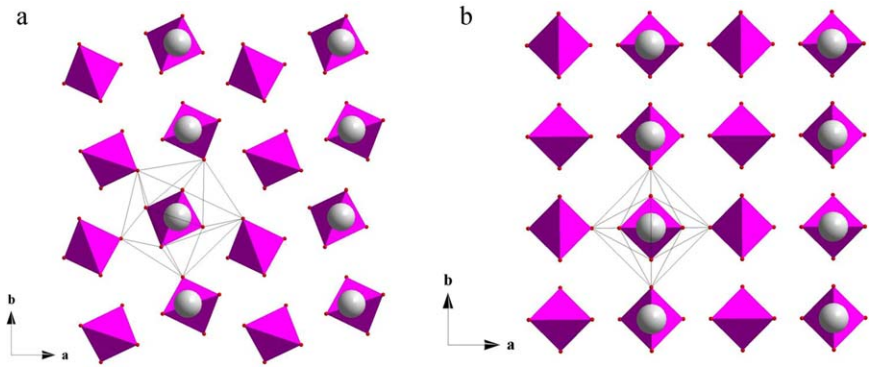

Fig. 11. Comparison of monazite (a) and xenotime (b) phases projected down [0 0 1]. The diagrams illustrate the changes in RE–O bonds that occur during the "transition" between the monazite and xenotime phases. Larger open circles represent RE atoms; smaller circles represent O atoms (after Ni et al.[118]).

lithium occupied positions there are vacant sites toward which this cation could migrate and unsure a good ionic conduction.

The structure of $SrNp(PO_4)_2$ is described in the orthorhombic system, *Cmca* space group.[355] In spite of the higher symmetry, the cell is related to the monazite one, showing alternate layers of SrO_{10} and NpO_8 polyhedra instead of the disordered array of MO_9 units. The authors explained this particular arrangement by the ionic radii differences between Sr^{2+} and Np^{4+}. The structure is seen as an ordered modification of the cheralite type. This structural model allows explaining the narrow limits of the cheralite domain in terms of cation size and suggests that transuranium-loaded compounds could also be derivatives of the archetype.

5.2. Monazite–zircon structural relationships

Numerous examples of monazite and zircon polymorphs are reported in the literature ($ThSiO_4$, $TbPO_4$, $CeVO_4$, etc.). The structure of zircon ($ZrSiO_4$)[351] is tetragonal and crystallizes in space group $I4_1/amd$. The SiO_4 tetrahedra share corners and edges with ZrO_8 dodecahedra while this latter share edges with each other to form chains parallel to [1 0 0] such that each ZrO_8 polyhedron shares edges with four adjacent ZrO_8 polyhedra, two in each of the crystallographically equivalent directions [1 0 0] and [0 1 0]. These [1 0 0] chains of ZrO_8 polyhedra are cross linked by sharing corners with SiO_4 tetrahedra. The Si and Zr polyhedra also form an edge-connected chain of alternating ZrO_8 and SiO_4 polyhedra parallel to [0 0 1], between which lie unoccupied channels, also parallel to [0 0 1]. The [0 0 1] edge-connected chains of Zr and Si polyhedra comprise an especially strongly connected feature in the structure, generally expressed in the prismatic habit and (1 1 0) cleavage of zircon minerals. Several minerals (xenotime, thorite, coffinite, pretulite, etc.[351]) are associated to the zircon-group.

The structural relationships between monazite and xenotime were elucidated by Ni et al.[118] The relationship between the atomic arrangements is evidenced in the juxtaposition of [0 0 1] projections of the two structures (Fig. 11). The phosphate tetrahedra in both structures exist in planes perpendicular to *a* (Fig. 11a), with two such planes in the unit cell of each phase; each of these tetrahedra represents the projection of a polyhedron–tetrahedron chain. In monazite, the tetrahedra in adjacent (1 0 0) planes are offset from each other principally along [0 1 0], and O–O edges of the tetrahedra are inclined to the crystallographic axes; in xenotime, the tetrahedra are in rows parallel to *a* and *b*, and the shared edges of the tetrahedron are parallel to *a* or *b*. The structures are related by these shifts of the (1 0 0) planes (for example it reaches 2.23 Å along [0 1 0] and $1/2\,a\cos\beta = 0.79$ Å along [0 0 1] between $GdPO_4$ and $TbPO_4$) and a slight rotation of the tetrahedron about [0 0 1]. As illustrated in Fig. 11, the change in coordination of the REE polyhedron from the xenotime to the monazite atomic arrangements is accomplished by breaking a REE–O bond in the xenotime structure and adding two REE–O bonds in the monazite structure. The transformation of a zircon-structured material into the monazite-type compounds was observed in the case of $Ca_{0.5}U_{0.5}PO_4$,[339] $CeVO_4$,[386] $PaSiO_4$ and $ThSiO_4$[322,335] compounds. This transition also generates a contraction of the unit-cell volume.[118,335,339]

5.3. Anhydrite–monazite structural relationships

The anhydrite to monazite transformation was reported only in the case of $CaSO_4$. Even if Chen et al.[393] does not evidence the $CaSO_4$ monazite-type in their work, monazitic $CaSO_4$ is obtained by high pressure room-temperature compression of anhydrite.[318,335] The main structural features of the anhydrite are reported by Kirfel and Will.[394] The anhydrite structure is built up of chains of alternating SO_4 tetrahedra and CaO_8 dodecahedra, running along [0 0 1]. Thus each S atom is coordinated by four O atoms with two unique S–O bonds, and each Ca^{2+} cation is coordinated by eight O atoms with four unique Ca–O distances. While the SO_4 tetrahedron is almost regular, the CaO_8 dodecahedron is considerably distorted with strongly contracted edges shared with the SO_4 groups.[395]

A plausible anhydrite to monazite phase transition is proposed by Borg and Smith.[318] A significant feature in the anhydrite structure is the chains of AO_8 and XO_4 polyhedra linked by shared edges. The tetrahedral orientations alternatively rotate ±45° about the chain axis. The reversibility of the anhydrite–monazite transition in $CaSO_4$ suggests it is mostly displacive in nature and the chains are probably retained. Rotation as well as displacement of the chains relative to each other is required (Fig. 12). To preserve the chains, the two structures

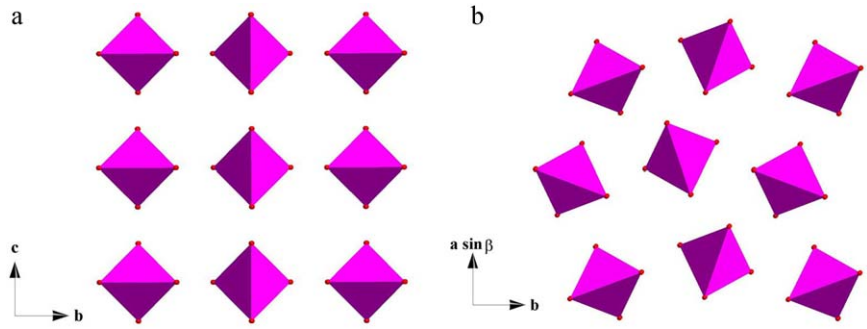

Fig. 12. Projection of anhydrite[395] (a) and monazite[118] (b) structures along the chain direction (after Borg and Smith[318]).

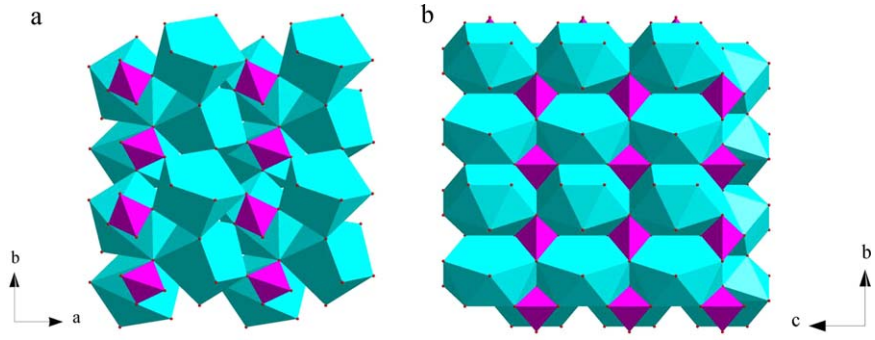

Fig. 13. Comparison of $CePO_4$ monazite[118] (a) and $CaSO_4$ barite[311] (b) (after Crichton et al.[313]).

are related through axial transformation, $a_{Anhydrite} \rightarrow c_{Monazite}$, $b_{Anhydrite} \rightarrow b_{Monazite}$ and $c_{Anhydrite} \rightarrow a_{Monazite}$. The requisite displacements suggest a shear or twinning mechanism as proposed for martinistic transformations, e.g., monoclinic-tetragonal ZrO_2.

5.4. Monazite–barite structural relationships

The monazite to $BaSO_4$ barite-type transformation is reported to occur during heating of the $CaSO_4$ high pressure monazitic form at $T = 1250\,^{\circ}C$.[314,315] This phase transformation is also suggested by Lacomba-Perales et al.[387] for the high pressure form of $LaPO_4$. This seems to be a reasonable proposition since the monazite-barite transition involves an important atomic rearrangement. In particular, the barite-type structure implies an increase of the coordination of the La cation. La is nine-fold coordinated in monazite while it is twelve coordinated in barite. In contrast the PO_4 tetrahedra remain essentially unchanged in both structure types (Fig. 13).

5.5. Monazite–$AgMnO_4$ structural relationships

No direct monazite to $AgMnO_4$ structural transformation is reported in the literature. However, the monazite and the $AgMnO_4$ structures[396] reported in Fig. 14a and b, respectively,[315] are closely related. It is evident from this diagram that a notional shear of the monazite structure parallel to a, reducing the β angle, would produce a topology close to

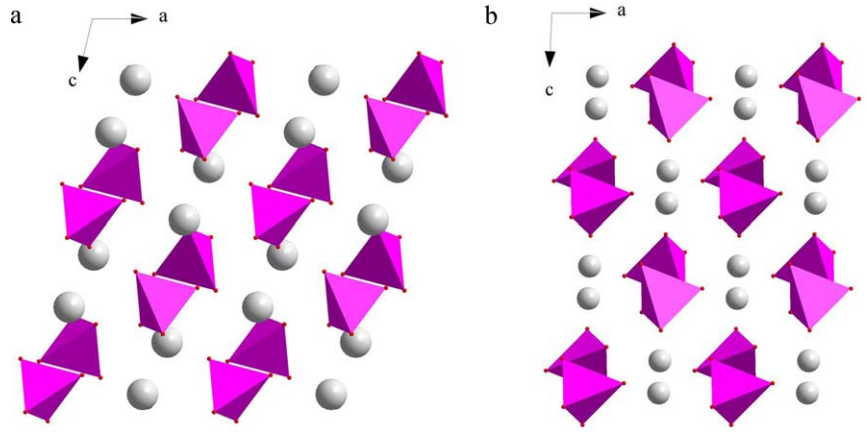

Fig. 14. Comparison of (0 1 0) planes of $CePO_4$ monazite[118] (a) and $AgMnO_4$[390] (b) (after Crichton et al.[313]).

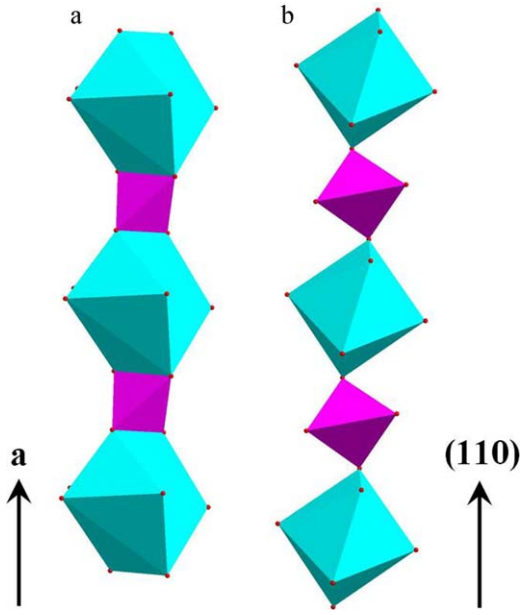

Fig. 15. Portions of polyhedral chains in the $CePO_4$ monazite[118] (a) and $CaWO_4$ scheelite[397] (b) structures (after Macey[354]).

that of $AgMnO_4$. This description corresponds to the description of two high-pressure forms of $CaSO_4$. The SO_4-tetrahedra and cation positions are shown, with non-bonded oxygen removed for clarity.

5.6. Monazite–scheelite structural relationships

The monazite to scheelite transformation is another rarely observed transformation that takes place for $LaVO_4$, $PrAsO_4$, $NdAsO_4$[385] and $BiAsO_4$.[284] The pressure is the driving force for this transformation that can be proceeded by both temperature and pressure paths for these compounds. Nabar and Sakhardande[287] reports the existence of a monazite to scheelite transition, that is irreversible and endothermic, for the $(Cd_{1/3}Nd_{1/3}Th_{1/3})AsO_4$ compound. This transition occurs at 900 °C and is only induced by the heat treatment of the material.

Macey[354] describes the monazite to scheelite transformation as follows. The plane parallel to (0 0 1) and the plane parallel to (0 1 0) of monazite are shared to become the closest packed cation planes in the scheelite form (Fig. 15). Atomic movements within the planes are also necessary to reach the scheelite packing. The transformation is reconstructive in nature as evidenced by the fact that the transformed product is metastable[284] and that the monazite has tetrahedral sharing edges with nine coordinated polyhedra while scheelite has tetrahedral sharing corners with adjacent dodecahedra.[397]

$Pb_{0.5}Th_{0.5}VO_4$ has polymorphs in both scheelite and monazite structures, as well as in the zircon structure.[264] In this case, the structure sequence that is observed when heating this compound from room temperature is scheelite ($T = 600$ °C) → zircon ($T = 920$ °C) → monazite.

5.7. Monazite–HT monoclinic $BiPO_4$ structural relationships

The case of the low temperature monazite form of $BiPO_4$ to a high temperature monoclinic form is unique and completely described by Romero et al.[151] The monoclinic high-temperature modification of $BiPO_4$ is very similar to the monazite type although this similarity is partially concealed by the choice of the cell parameters (Fig. 16).[398] The transformation from the low-temperature monazite-type to the high-temperature form is irreversible and requires a small rotation of the tetrahedra to adopt a more symmetric (and slightly more volume-consuming) arrangement, with no modification of the essential topological features. A consequence of the increase in symmetry of the tetrahedra network is that an approximate P-centering present in the monazite structure now becomes exact, and hence a smaller primitive unit cell can be selected.

5.8. Monazite–rhabdophane structural relationships

As previously described, monazite can be easily obtained by heating the rhabdophane hexagonal hydrated form.[136,361] Hikichi et al. emphasized the weak differences existing between both structures, especially concerning the arrangement of oxygen atoms around the P^{5+} ion as well as the REE–O distances.[373] The main modification lies in the presence of larger channels along the c axis in the case of rhabdophane which host the water molecules that stabilize the structure.[247] The comparison of the structural features was also reported by Romero et al. in the case of $BiPO_4$ which presents a similar hexagonal modification.[151]

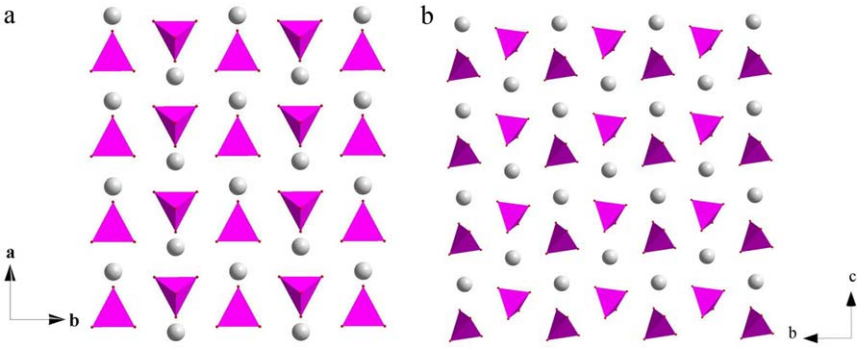

Fig. 16. Orthogonal projections of $CePO_4$ monazite structure[118] onto the (1 0 0) plane (a) and of high-temperature monoclinic form of $BiPO_4$[398] onto the (−1 0 1) plane (b) (after Romero et al.[151]).

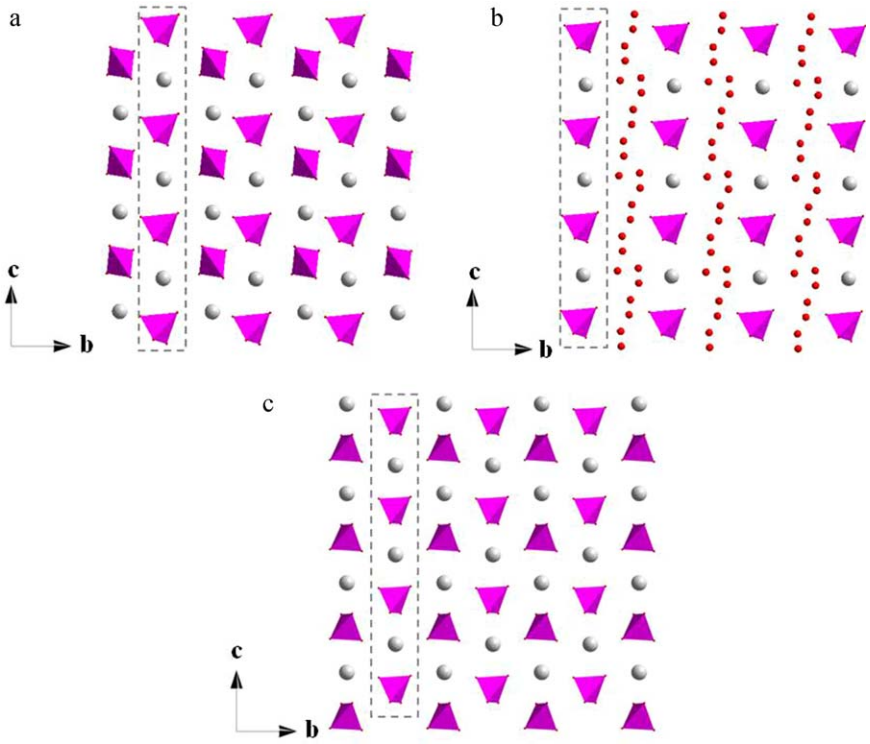

Fig. 17. Orthogonal projections onto the (1 0 0) plane of the rhabdophane-type hexagonal modification of $BiPO_4$, with layers located at $x = 0.5$ (a) and $x = 0$ (b) and of monazite (c) (after Romero et al.[151]). The frames indicate the common cation/PO_4 chains.

They described rhabdophane as an alternance of two types of layers parallel to the (1 0 0) plane. The first one (at $x = 0.5$), formed by bismuth atoms and phosphate tetrahedrons (Fig. 17a) appears very close to monazite arrangement, while the second one (located at $x = 0$) consists in alternate chains formed by water molecules then by bismuth and phosphates groups (Fig. 17b). This alternance of layers led to a looser stacking than the monazite type structure (Fig. 17c).

6. Conclusions

Based on the diversity of the chemical composition of the obtained samples, the monazite structure appears to be strongly flexible. Such chemical variety can explain why the number of scientific projects dealing with the use of monazite-type compounds for various applications remains significant and clearly shows that new opportunities for material composition design are always open.

One of the explanations of this chemical flexibility is probably due to the presence of the cationic pentagonal interpenetrating tetrahedral polyhedron that allows the structure to accommodate chemically diverse cations. This irregular coordination existing around the lanthanide ion does not place severe symmetry, size or charge constraints for the incorporated cation and allows large domains of chemical compositions for the prepared solid solutions. Such structural aspect can be also connected to several properties of interest of the monazite structure. Among them, one can note, as instance, the high chemical durability, resistance to radiation damage (properties of interest for geochemical chronology, for radwaste storage matrices, etc.) or high temperature thermal conductivity (for coating and diffusion barrier designs).

As a summary, the literature dealing with the preparation and the characterization of monazite samples is very rich. A complete database of the existing monazite compounds and the possible substitutions in the structure is reported herein. The stability domains of the existing compounds are also reported as well as the structural relationships between the monazite structure and related structures. All the data that are gathered together for the first time offer an unique view of the versatility of the monazite structure regarding the possibilities for elemental substitution or incorporation. New coupled substitutions on the anionic and cationic sites are now conceivable, although possibly with limited solid solution extend. As instance, limited incorporation of niobiate or tantalate groups in replacement of phosphate entities could probably be achieved.

References

1. Gramaccioli CM, Segalstad TV. A uranium- and thorium rich monazite from a south-alpine pegmatite at Piona, Italy. *Am Mineral* 1978;**63**:757–61.
2. Overstreet WC. The geological occurrence f monazite. US' Geol Surv. Prof. pap. 530.
3. Pyle JM, Spear FS, Rudnick RL, McDonough WF. Monazite–xenotime–garnet equilibrium in metapelites and a new monazite–garnet thermometer. *J Petrol* 2001;**42**(11):2083–107.
4. Montel JM, Foret S, Veschambre M, Nicollet C, Provost A. Electron microprobe dating of monazite. *Chem Geol* 1996;**131**:37–53.
5. Oelkers EH, Montel JM. Phosphates and nuclear waste storage. *Elements* 2008;**4**(2):113–6.

6. Rapp RP, Watson EB. Monazite solubility and dissolution kinetics—implications for the thorium and light rare-earth chemistry of felsic magmas. *Contrib Mineral Petrol* 1986;**94**:304–16.
7. Gentry RV, Cahill TA, Fletcher NR, Kaufman HC, Medsker LR, Nelson JW, Floechini RG. Evidence for primordial superheavy elements. *Phys Rev Lett* 1976;**37**:11–5.
8. Kapoor SS, Ramamurthy VS, Lal M, Kataria SK. Search for superheavy elements in monazite from beach sands of South India. *Pramana J Phys* 1977;**9**(5):515–21.
9. Stephan C, Epherre M, Cieslak E, Sowinski M, Tys J. Search for superheavy elements in monazite ore from Madagascar. *Phys Rev Lett* 1976;**37**(23):1534–6.
10. Bosch F, E1 Goresy A, Kritschmer W, Martin B, Povh B, Nobiling R, Traxel K, Schwalm D. On the possible existence of superheavy elements in monazite. *Z Phys A* 1977;**280**:39–44.
11. Ketelle BH, O'Kelley GD, Stoughton RW, Halperin J. Search for superheavy-element decay in samples of Madagascar monazite. *Phys Rev Lett* 1976;**37**(26):1734–7.
12. Kuo DH, Kriven WM. Chemical stability, microstructure and mechanical behavior of $LaPO_4$-containing ceramics. *Mater Sci Eng A* 1996;**210**(1/2):123–34.
13. Fisher MJ, Wang W, Dorhout PK, Fisher ER. Synthesis of $LaPO_4$:Eu nanostructures using the sol–gel template method. *J Phys Chem C* 2008;**112**(6):1901–7.
14. Davis JB, Marshall DB, Housley RM, Morgan PED. Machinable ceramics containing rare-earth phosphates. *J Am Ceram Soc* 1998;**81**(8):2169–75.
15. Davis JB, Marshall DB, Oka KS, Housley RM, Morgan PED. Ceramic composites for thermal protection systems. *Composites A* 1999;**30**(4):483–8.
16. Davis JB, Marshall DB, Morgan PED. Oxide composites of Al_2O_3 and $LaPO_4$. *J Eur Ceram Soc* 1999;**19**:2421–6.
17. Davis JB, Marshall DB, Morgan PED. Monazite-containing oxide/oxide composites. *J Eur Ceram Soc* 2000;**20**:583–7.
18. Hay RS, Marshall DB. Deformation twinning in monazite. *Acta Mater* 2003;**51**:5235–54.
19. Hay RS. Twin-dislocation interaction in monazite (monoclinic $LaPO_4$). *Philos Mag* 2005;**85**(2/3):373–86.
20. Hwang TJ, Hendrick MR, Shao H, Hornis HG, Hunt AT. Combustion chemical vapor deposition (CCVD) of $LaPO_4$ monazite and beta-alumina on alumina fibers for ceramic matrix composites. *Mater Sci Eng A* 1998;**244**:91–6.
21. Seung-Ho K, Sekino T, Kusunose T, Hirvonen AT. Thermal properties and microstructure of zirconia/monazite-type $LaPO_4$ composites for powder preparation methods. *Mater Sci Forum* 2007;**544–545**:909–12.
22. Konishi Y, Kusunose T, Morgan PED, Sekino T, Niihara K. Fabrication and mechanical properties of Al_2O_3/$LaPO_4$ composite. *Sci Eng Ceram II* 1999;**2**:341–4.
23. Marshall DB, Morgan PED, Housley RM, Cheung JT. High-temperature stability of the Al_2O_3–$LaPO_4$ system. *J Am Ceram Soc* 1999;**81**(4):951–6.
24. Marshall DB, Davis JB, Morgan PED, Waldrop JR, Porter JR. Properties of La-monazite as an interphase in oxide composites. *Z Metallkd* 1999;**90**(12):1048–52.
25. Min W, Miyahara D, Yokoi K, Yamaguchi T, Daimon K, Hikichi Y, Matsubara T, Ota T. Thermal and mechanical properties of sintered $LaPO_4$–Al_2O_3 composites. *Mater Res Bull* 2001;**36**:939–45.
26. Min W, Daimon K, Matsubara T, Hikichi Y. Thermal and mechanical properties of sintered machinable $LaPO_4$–ZrO_2 composites. *Mater Res Bull* 2002;**37**:1107–15.
27. Mogilevsky P, Hay RS, Boakye EE, Keller KA. Evolution of texture in rhabdophane-derived monazite coatings. *J Am Ceram Soc* 2003;**86**(10):1767–72.
28. Mogilevsky P, Parthasarathy TA, Petry MD. Anisotropy in room temperature microhardness and fracture of $CaWO_4$ scheelite. *Acta Mater* 2004;**52**:5529–37.
29. Morgan PED, Marshall DB. Ceramic composites of monazite and alumina. *J Am Ceram Soc* 1995;**78**(6):1553–63.
30. Morgan PED, Marshall DB, Housley RM. High-temperature stability of monazite-alumina composites. *Mater Sci Eng A Struct* 1995;**1–2**:215–22.
31. Parrish RR. U–Pb dating of monazite and its application to geological problems. *Can J Earth Sci* 1990;**27**:1431–50.
32. Copeland P, Parrish RR, Harrison TM. Identification of inherited radiogenic Pb in monazite and its implications for U–Pb systematics. *Nature* 1988;**333**:760–3.
33. Gardes E. Diffusion du plomb dans la monazite. PhD thesis of Universite Toulouse III, Toulouse, France; 2006.
34. Suzuki K, Adachi M, Kajizuka I. Electron microprobe observations of Pb diffusion in metamorphosed detrital monazites. *Earth Planet Sci Lett* 1994;**128**:391–405.
35. Montel JM, Veschambre M, Nicollet C. Dating monazite with the electron microprobe. *C R Acad Sci Ser II* 1994;**318**(11):1489–95.
36. Braun I, Montel JM, Nicollet C. Electron microprobe dating of monazites from high-grade gneisses and pegmatites of the Kerala Khondalite Belt, southern India. *Chem Geol* 1998;**146**:65–85.
37. Williams ML, Jercinovic MJ. Microprobe monazite geochronology: putting absolute time into microstructural analysis. *J Struct Geol* 2002;**24**:1013–28.
38. Williams ML, Jercinivic MJ, Goncalves P, Mahan K. Format and philosophy for collecting, compiling, and reporting microprobe monazite ages. *Chem Geol* 2006;**225**:1–15.
39. Catlos EJ, Gilley LD, Mark Harrison T. Interpretation of monazite ages obtained via in situ analysis. *Chem Geol* 2002;**188**(3/4):193–215.
40. Vlach SRF. Th–U–Pb_T dating by electron probe microanalysis, Part I. Monazite: analytical procedures and data treatment. *Geol USP* 2010;**10**(1):61–85.
41. Williams ML, Tracy RJ. Preface to collected papers on monazite microprobe geochronology. *Am Miner* 2005;**90**(4):525–6.
42. Cherniak DJ, Zhang XY, Nakamurab M, Watson EB. Oxygen diffusion in monazite. *Earth Planet Sci Lett* 2004;**226**:161–74.
43. Harrison TM, Catlos EJJM. U–Th–Pb dating of phosphate minerals. *Rev Mineral Geochem* 2002;**48**:524–58.
44. Spear FS, Pyle JM, Cherniak D. Limitations of chemical dating of monazite. *Chem Geol* 2009;**266**(3/4):218–30.
45. Krumpel AH, Boutinaud P, van der Kolk E, Dorenbos P. Charge transfer transitions in the transition metal oxides ABO_4:Ln^{3+} and APO_4:Ln^{3+} (A = La, Gd, Y, Lu, Sc; B = V, Nb, Ta; Ln = lanthanide). *J Lumin* 2010;**130**(8):1357–65.
46. Dong H, Liu Y, Yang P, Wang W, Lin J. Controlled synthesis and characterization of $LaPO_4$, $LaPO_4$:Ce^{3+} and $LaPO_4$:Ce^{3+}, Tb^{3+} by EDTA assisted hydrothermal method. *Solid State Sci* 2010;**12**(9):1652–60.
47. Chen G, Holsa J, Peterson JR. A luminescence study of single-crystal $EuPO_4$ at high pressure. *J Phys Chem Solids* 1997;**58**(12):2031–7.
48. Yan ZG, Zhang YW, You LP, Sia R, Yan CH. Controlled synthesis and characterization of monazite type monocrystalline nanowires of mixed lanthanide orthophosphates. *Solid State Commun* 2004;**130**:125–9.
49. Yu M, Lin J, Zhou YH, Pang ML, Han XM, Wang SB. Luminescence properties of $RP_{1-x}V_xO_4$: A (R = Y, Gd, La; A = Sm^{3+}, Er^{3+}, x = 0, 0. 5, 1) thin films prepared by Pechini sol–gel process. *Thin Solid Films* 2003;**444**:245–53.
50. de Sousa Filho PC, Serra OA. Red, green and blue lanthanum phosphate phosphors obtained via surfactant-controlled hydrothermal synthesis. *J Lumin* 2009;**129**:1664–8.
51. Hou Z, Wang L, Lian H, Chai R, Zhang C, Cheng Z, Lin J. Preparation and luminescence properties of Ce^{3+} and/or Tb^{3+} doped $LaPO_4$ nanofibers and microbelts by electrospinning. *J Solid State Chem* 2009;**182**: 698–708.
52. Escobar ME, Baran EJ. Tetragonal form of lanthanum ortho-vanadate. *Z Anorg Allg Chem* 1978;**441**:273–7.
53. Escobar ME, Baran EJ. Precipitation of rare-earth arsenates in aqueous-solutions. *Zeit Chem* 1980;**20**:225–31.
54. Park SW, Yang HK, Chung JW, Chen Y, Moon BK, Choi BC, Jeong JH, Kim JH. Photoluminescent properties of $LaVO_4$:Eu^{3+} by structural transformation. *Physica B* 2010;**405**:4040–4.
55. Yang M, You H, Zheng Y, Liu K, Jia G, Song Y, Huang Y, Zhang L, Zhang H. Hydrothermal synthesis and luminescent properties of novel ordered sphere $CePO_4$ hierarchical architectures. *Inorg Chem* 2009;**48**: 11559–65.

56. Nuñez NO, Liviano SR, Ocaña M. Citrate mediated synthesis of uniform monazite $LnPO_4$ (Ln = La, Ce) and Ln:$LaPO_4$ (Ln = Eu, Ce, Ce+ Tb) spheres and their photoluminescence. *J Colloid Interface Sci* 2010;**349**(2):484–91.
57. Zhang S, Wang L, Peng H, Li G, Chen K. Influence of P-doping on the morphologies and photoluminescence properties of $LaVO_4$:Tb^{3+} nanostructures. *Mater Chem Phys* 2010;**123**:714–8.
58. Isasi J, Veiga ML, Fernandez F, Pico C. Synthesis and structural characterization of solid solutions: $Li_{3x}La_{(1-x)}VO_4$ ($0 \leq x \leq .3$) monazite-type. *J Mater Sci* 1996;**31**(17):4689–92.
59. Hui SQ, Petric A, Gong WH. Stability and conductivity of perovskite oxides under anodic conditions. In: *Proceedings of the solid oxide fuel cells conference (SOFC VI), vol. 99*. 1999. p. 632–9.
60. Varma S, Wani BN, Gupta NM. Synthesis, characterisation, and redox behaviour of mixed orthovanadates $La_{1-x}Ce_xVO_4$. *Mater Res Bull* 2002;**37**:2117–27.
61. Jia CJ, Sun LD, Luo F, Jiang XC, Wei LH, Yan CH. Structural transformation induced improved luminescent properties for $LaVO_4$:Eu nanocrystals. *Appl Phys Lett* 2004;**84**(26):5305–7.
62. Varma S, Wani BN, Sathyamoorthy A, Gupta NM. On the role of lattice distortion in the catalytic properties of substituted orthovanadates $La_{1-x}Fe_xVO_4$. *J Phys Chem Sol* 2004;**65**:1291–6.
63. Jia CJ, Sun LD, You LP, Jiang XC, Luo F, Pang YC, Yan CH. Selective synthesis of monazite- and zircon-type $LaVO_4$ nanocrystals. *J Phys Chem B* 2005;**109**(8):3284–90.
64. Fan W, Song X, Bu Y, Sun S, Zhao X. Selected-control hydrothermal synthesis and formation, Mechanism of monazite- and zircon-type $LaVO_4$ nanocrystals. *J Phys Chem B* 2006;**110**(46):23247–54.
65. Fan W, Bu Y, Song X, Sun S, Zhao X. Selective synthesis and luminescent properties of monazite and zircon-type $LaVO_4$:Ln (Ln = Eu, Sm, and Dy) nanocrystals. *Cryst Growth Des* 2007;**7**(11):2361–6.
66. Liu G, Duan X, Li H, Dong H, Zhu L. Novel polyhedron-like t-$LaVO_4$:Dy^{3+} nanocrystals: hydrothermal synthesis and photoluminescence properties. *J Cryst Growth* 2008;**310**(22):4689–96.
67. Dinh CT, Huong PV, Olazcuaga R, Fouassier C. Syntheses, structures and Raman spectra of luminescent gadolinium phosphates. *J Optoelectron Adv Mater* 2000;**2**(2):159–69.
68. Fang YP, Xu AW, Song RQ, Zhang HX, You LP, Yu JC, Liu HQ. Systematic synthesis and characterization of single-crystal lanthanide orthophosphate nanowires. *J Am Chem Soc* 2003;**125**(51): 16025–34.
69. Zhang Y, Guan H. Hydrothermal synthesis and characterization of hexagonal and monoclinic $CePO_4$ single-crystal nanowires. *J Cryst Growth* 2003;**256**:156–61.
70. Yu M, Lin J, Wang SB. Effects of x and R^{3+} on the luminescent properties of Eu^{3+} in nanocrystalline $YV_xP_{1-x}O_4$:Eu^{3+} and RVO_4:Eu^{3+} thin-film phosphors. *Appl Phys A* 2005;**80**:353–60.
71. Mao CJ, Wu XC, Zhu JJ. Shape-controlled synthesis of $PbCrO_4$ micro/nanostructures and their luminescent properties. *J Nanosci Nanotechnol* 2010;**10**(8):4906–13.
72. Aoki Y, Habazaki H, Konno H. Interconversion between rare-earth metal (III) chromates (V) and low-crystalline phases by reduction with methanol and oxidation in air. *Chem Mater* 2003;**15**(12):2419–28.
73. Cheng B, Guo H, Yu J, Zhao X. Facile preparation, characterization and optical properties of rectangular $PbCrO_4$ single-crystal nanorods. *J Alloys Compd* 2007;**431**:L4–7.
74. Mahapatra S, Madras G, Row TNG. Structural and photocatalytic activity of lanthanide (Ce, Pr, and Nd) molybdovanadates. *J Phys Chem C* 2007;**111**(17):6505–11.
75. Wang W, Xu C, Zhen L, Shao W. Single-crystalline $PbCrO_4$ nanorods: room temperature, surfactant free synthesis, characterization and optical property. *J Cryst Growth* 2007;**299**(1):86–93.
76. Mahapatra S, Vinu R, Row TNG, Madras G. Kinetics of photoconversion of cyclohexane and benzene by $LnVO_4$ and $LnMo_{0.15}V_{0.85}O_4$ (Ln = Ce, Pr and Nd). *Appl Catal A* 2008;**351**:45–53.
77. Mayolet A. Etude des processus d'absorption et de transfert d'énergie au sein de matériaux inorganiques luminescents dans le domaine UV et VUV. PhD Thesis of University Paris-Sud-11 1995;IPNO-T-95.09.
78. Gallini S, Jurado JR, Colomer MT. Combustion synthesis of nanometric powders of $LaPO_4$ and Sr-substituted $LaPO_4$. *Chem Mater* 2005;**17**(16):4154–61.
79. Gallini S, Jurado JR, Colomer MT. Synthesis and characterization of monazite-type Sr:$LaPO_4$ prepared through coprecipitation. *J Eur Ceram Soc* 2005;**25**:2003–7.
80. Sivakumar V, Varadaraju UV. Environmentally benign novel green pigments: $Pr_{1-x}Ca_xPO_4$ (x = 0–0.4). *Bull Mater Sci* 2005;**28**(3):299–301.
81. Amezawa K, Tomii Y, Yamamoto N. High temperature protonic conduction in $LaPO_4$ doped with alkaline earth metals. *Solid State Ionics* 2005;**176**:135–41.
82. Danilovic N, Luo JL, Chuang KT, Sanger AR. Effect of substitution with Cr^{3+} and addition of Ni on the physical and electrochemical properties of $Ce_{0.9}Sr_{0.1}VO_3$ as a H_2S-active anode for solid oxide fuel cells. *J Power Sources* 2009;**194**(1):252–62.
83. Konno H, Tachikawa H, Furusaki A, Furuichi R. Characterization of lanthanum(III) chromium(V) tetraoxide by X-ray photoelectron-spectroscopy. *Anal Sci* 1992;**8**(5):641–6.
84. Boatner LA, Beall GW, Abraham MM, Finch CB, Huray PG, Rappaz M. Monazite and other lanthanide orthophosphates as alternate actinide waste forms. In: Northrup Jr CJM, editor. *Scientific basis for nuclear waste management*, vol. 2. New York: Plenum Publishing Corporation; 1980. p. 289–96.
85. Boatner LA, Sales BC. Radioactive waste forms for the future: monazite. In: Lutze W, Ewing RC, editors. *Radioactive waste forms for the future*. Amsterdam: Elsevier; 1988. p. 495–564.
86. Ewing RC, Lutze W. High-level nuclear waste immobilization with ceramics. *Ceram Trans* 1991;**17**(5):287–93.
87. Lumpkin GR. Ceramic waste forms for actinides. *Elements* 2006;**2**(6):365–72.
88. Matzke H, Rondinella VV, Wiss T. Materials research on inert matrices: a screening study. *J Nucl Mater* 1999;**274**:47–53.
89. Ewing RC. Nuclear waste froms for actinides. *Proc Natl Acad Sci USA* 1999;**96**(7):3432–9.
90. Omel'yanenko BI, Livshits TS, Yudintsev SV, Nikonov BS. Natural and artificial minerals as matrices for immobilization of actinides. *Geol Ore Deposit* 2007;**49**(3):179–93.
91. Tomilin SV, Lukinykh AN, Lizin AA, Bychkov AV, Yakovlev VV, Konovalov VI. Investigation of the incorporation of fission product surrogates and process impurities into ceramics. *Atom Energy* 2007;**102**(4): 271–6.
92. Terra O, Dacheux N, Audubert F, Podor R. Immobilization of tetravalent actinides in phosphate ceramics. *J Nucl Mater* 2006;**352**:224–32.
93. Veilly E, du Fou de Kerdaniel E, Roques J, Dacheux N, Clavier N. Comparative behavior of britholites and monazite/brabantite solid solutions during leaching tests: a combined experimental and DFT approach. *Inorg Chem* 2008;**47**:10971–9.
94. Aloy AS, Kovarskaya EN, Koltsova TI, Samoylov SE, Rovny SI, Medvedev GM. Immobilisation of Am-241 formed under plutonium metal conversion into monazite-type ceramic. In: Lardine LJ, Borisov GB, editors. Review of excess weapons plutonium disposition. LLNL Contract work in Russia, UCRL-ID-149341, 2002, p. 141–5.
95. Abraham MM, Boatner LA, Quincy TC, Thomas DK, Rappaz M. Preparation and compaction of synthetic monazite powders. *Radioact Waste Manage* 1980;**1**(2):181–91.
96. Fiquet O, Croixmarie Y. Method for making optionally actinide-doped monazite compounds and use thereof for conditioning actinide and lanthanide enriched radioactive waste. European Patent EP 0,862,542 B1; 2002.
97. Anthony JW. Hydrothermal synthesis of monazite. *Am Mineral* 1957;**42**:904.
98. Anthony JW. Crystal morphology of thorium-bearing synthetic monazite. *Am Mineral* 1965;**50**:1421–31.
99. Clavier N, Dacheux N, Podor R. Synthesis, characterization, sintering, and leaching of β-TUPD/monazite radwaste matrices. *Inorg Chem* 2006;**45**(1):220–9.
100. Clavier N, Dacheux N, Wallez G, Quarton M. Improvement of the preparation of sintered pellets of thorium phosphate-diphosphate and

associated solid solutions from crystallized precursors. *J Nucl Mater* 2006;**52**:209–16.
101. He Y, Lü Y, Zhang Q. Characterization of monazite glass–ceramics as wasteform for simulated a-HLLW. *J Nucl Mater* 2008;**376**:201–6.
102. Hyatt NC, Stennett MC, Maddrell ER, Lee WE. Single phase ceramic wasteforms for plutonium disposition. *Adv Sci Technol* 2006;**45**: 2004–11.
103. Montel JM, Lhote F, Claude JM. Monazite end members and solid solutions—synthesis, unit-cell characteristics and utilisation as microprobe standards. *Mineral Mag* 1989;**53**(369):120–3.
104. Volkovich VA, Griffiths TR, Thied RC. Formation of lanthanide phosphates in molten salts and evaluation for nuclear waste treatment. *Phys Chem Chem Phys* 2003;**5**(14):3053–60.
105. Bregiroux D, Audubert F, Bernache-Assollant D. The role of the milling step on the sintering behaviour of monazite powder $LaPO_4$, densification and resulting microstructure. *Adv Sci Technol* 2006;**454**:633–8.
106. Bregiroux D, Lucas S, Champion E, Audubert F, Bernache-Assollant D. Sintering and microstructure of rare earth phosphate ceramics $REPO_4$ with RE = La, Ce or Y. *J Eur Ceram Soc* 2006;**26**:279–87.
107. Bregiroux D, Belin R, Valenza P, Audubert F, Bernache-Assollant F. Plutonium and americium monazite materials: solid state synthesis and X-ray diffraction study. *J Nucl Mater* 2007;**366**(1/2):52–7.
108. Bregiroux D, Audubert F, Charpentier T, Sakellariou D, Bernache-Assollant D. Solid-state synthesis of monazite-type compounds $LnPO_4$ (Ln = La to Gd). *Solid State Sci* 2007;**9**:432–9.
109. Hikichi Y, Nomura T, Tanimura Y, Suzuki S, Miyamoto M. Sintering and properties of monazite-type $CePO_4$. *J Am Ceram Soc* 1990;**73**(12):3594–6.
110. Rajesha K, Sivakumara B, Pillaia PK, Mukundana P, Warriera KGK, Nair VR. Synthesis of nanocrystalline lanthanum phosphate for low temperature densification to monazite ceramics. *Mater Lett* 2004;**58**:1687–91.
111. Mooney RCL. Crystal structures of a series of rare earth phosphates. *J Chem Phys* 1948;**16**:1003.
112. Feigelson RS. Synthesis and single-crystal growth of rare-earth orthophosphates. *J Am Ceram Soc* 1964;**47**:257–8.
113. Ghouse KM. Refinement of crystal structure of heat-treated monazite crystal. *Indian J Pure Appl Phys* 1968;**6**:265–8.
114. Pepin GJ, Vance ER. Crystal data for rare earth orthophosphates of the monazite structure-type. *J Inorg Nucl Chem* 1981;**43**(II):2807–9.
115. Mullica DF, Milligan WO, Grossie DA, Beall GW, Boatner LA. Ninefold coordination in $LaPO_4$—pentagonal interpenetrating tetrahedral polyhedron. *Inorg Chim Acta* 1984;**95**:231–6.
116. Mullica DF, Grossie DA, Boatner LA. Structural refinements of praseodymium and neodymium ortho-phosphate. *J Solid State Chem* 1985;**58**:71–7.
117. Beall GW, Boatner LA, Mullica DF, Milligan WO. The structure of cerium ortho-phosphate, a synthetic analog of monazite. *J Inorg Nucl Chem* 1981;**43**:101–5.
118. Ni Y, Hugues JM, Mariano AN. Crystal chemistry of the monazite and xenotime structures. *Am Mineral* 1995;**80**:21–6.
119. Mullica DF, Grossie DA, Boatner LA. Coordination geometry and structural determinations of $SmPO_4$, $EuPO_4$ and $GdPO_4$. *Inorg Chim Acta* 1985;**109**:105–10.
120. Boatner LA. Synthesis, structure, and properties of monazite, pretulite and xenotime. *Rev Mineral Geochem* 2002;**48**:87–121.
121. Weigel F, Scherer V, Henschel H. Chemistry of promethium. I. Crystal structure of promethium phosphate and related compounds. *Radiochim Acta* 1965;**4**:18–23.
122. Callejas G, Blanco M, Cabrera S, Prieto O, Luna I, Choque V, Crespo P. Simulation of the crystal structure of low temperature monazite $LaPO_4$ phase from x-ray diffraction diffusion pattern. *Revista Boliviana de Quimica* 2000;**17**(1):22–7.
123. Thiriet C, Konings RJM, Javorsky P, Magnani N, Wastin F. The low temperature heat capacity of $LaPO_4$ and $GdPO_4$, the thermodynamic functions of the monazite-type $LnPO_4$ series. *J Chem Thermodyn* 2005;**37**:131–9.
124. Jardin R, Pavel CC, Raison PE, Bouëxière D, Santa-Cruz H, Konings RJM, Popa K. The high-temperature behaviour of $PuPO_4$ monazite and some other related compounds. *J Nucl Mater* 2008;**378**: 167–71.
125. Mullica DF, Grossie DA, Boatner LA. Structural refinements of praseodymium and neodymium ortho-phosphate. *J Solid State Chem* 1985;**58**(1):71–7.
126. Horchani-Naifer K, Férid M. Crystal structure, energy band and optical characterizations of praseodymium monophosphate $PrPO_4$. *Inorg Chim Acta* 2009;**362**(6):1793–6.
127. Mullica DF, Grossie DA, Boatner LA. Structural refinements of praseodymium and neodymium orthophosphate. *J Solid State Chem* 1985;**58**(1):71–7.
128. Mullica DF, Grossie DA, Boatner LA. Coordination geometry and structural determinations of samarium orthophosphate, europium orthophosphate, and gadolinium orthophosphate. *Inorg Chim Acta* 1985;**109**(2):105–10.
129. Kurbanov KhM, Efremov VA, Orlovskii VP. Crystal structure of neodymium phosphate ($NdPO_4$). *Kristallografiya* 1986;**31**(4):800–2.
130. Milligan WO, Mullica DF, Beall GW, Boatner LA. The structures of 3 lanthanide ortho-phosphates. *Inorg Chim Acta* 1983. G:133–6.
131. Milligan WO, Mullica DF, Beall GW, Boatner LA. Structures of $ErPO_4$, $TmPO_4$ and $YbPO_4$. *Acta Cryst C* 1983;**39**:23–4.
132. Milligan WO, Mullica DF, Beall GW, Boatner LA. Structures of YPO_4, $ScPO_4$ and $LuPO_4$. *Inorg Chim Acta* 1982;**60**:39–43.
133. Ushakov SV, Helean KB, Navrotsky A, Boatner LA. Thermochemistry of rare-earth orthophosphates. *J Mater Res* 2001;**16**(9):2623–33.
134. Kijkowska R, Cholewka E, Duszak B. X-ray diffraction and Ir-absorption characteristics of lanthanide orthophosphates obtained by crystallisation from phosphoric acid solution. *J Mater Sci* 2003;**38**(2):223–8.
135. Terra O, Clavier N, Dacheux N, Podor R. Preparation and characterization of lanthanum–gadolinium monazites as ceramics for radioactive waste storage. *New J Chem* 2003;**27**:957–67.
136. Jonasson RG, Vance ER. DTA study of the rhabdophane to monazite transformation in rare earth (La-Dy) phosphates. *Thermochim Acta* 1986;**108**:65–72.
137. Glorieux B, Matecki M, Fayon F, Coutures JP, Palau S, Douy A, Peraudeau G. Study of lanthanum orthophosphates polymorphism, in view of actinide conditioning. *J Nucl Mater* 2004;**326**:156–62.
138. Cherniak DJ, Pyle J, Rakovan J. Synthesis of REE and Y phosphates by Pb-free flux methods and their utilization as standards for electron microprobe analysis and in design of monazite chemical U–Th–Pb dating protocol. *Am Mineral* 2004;**89**(10):1533–9.
139. Lehmann O, Meyssamy H, Kmpe K, Schnablegger H, Haase M. Synthesis, growth, and Er^{3+} luminescence of lanthanide phosphate nanoparticles. *J Phys Chem B* 2003;**107**(30):7449–53.
140. Bregiroux D, Terra O, Audubert F, Dacheux N, Serin V, Podor R, Bernache-Assollant D. Solid state synthesis of monazite-type compounds containing tetravalent elements. *Inorg Chem* 2007;**46**:10372–82.
141. Boakye EE, Mogilevsky P, Hay RS, Fair GE. Synthesis and phase composition of lanthanide phosphate nanoparticles $LnPO_4$ (Ln = La, Gd, Tb, Dy, Y) and solid solutions for fiber coatings. *J Am Ceram Soc* 2008;**91**(12):3841–9.
142. Bjorklund CW. The preparation of PuP_2O_7 and $PuPO_4$. *J Am Ceram Soc* 1958;**85**:1001–3.
143. Bamberger CE, Haire RG, Hellwege HE, Begun GM. Synthesis and characterization of crystalline phosphates of plutonium(III) and plutonium(IV). *J Less Common Met* 1984;**97**:349–56.
144. Keller C, Walter KH. Darstellung, gitterkonstanten und chemische eigenschaften einiger ternärer oxide des plutoniums, americiums und curiums vom typ $Me^{III}X^{V}O_4$. *J Inorg Nucl Chem* 1965;**27**:1253–60.
145. Rai D, Felmy AR, Mason MJ. Solubility and ion activity product of $AmPO_4$, xH_2O. *Radiochim Acta* 1992;**56**:7–14.
146. Weigel F, Haug H. Zur Kenntnis des Curium(III) phosphats. *Radiochim Acta* 1965;**4**(4):227–8.
147. Weigel F, Scherer V, Henschel H. Unit-cells of monazite-type rare-earth phosphates. *J Am Ceram Soc* 1965;**48**(7):383–4.
148. Haire RG, Hellwege HE, Hobart DE, Young JP. Synthese, lattice parameters and solid state absorption spectra of the first transplutonium orthophosphates. *J Less Common Met* 1983;**93**:358–9.

149. Hobart DE, Begun GM, Haire RG, Hellwege HE. Raman spectra of the transplutonium orthophosphates and trimetaphosphates. *J Raman Spectrosc* 1983;**14**(1):59–62.
150. Drozdzynski J. Methods of preparation of uranium(+3) compounds from solutions. *Inorg Chim Acta* 1979;**32**:L83–5.
151. Romero B, Bruque S, Aranda MAG, Iglesias JE. Syntheses, crystal structures, and characterization of bismuth phosphates. *Inorg Chem* 1994;**33**(9):1869–74.
152. Roming M, Feldmann C. Synthesis and characterisation of nanoscaled $BiPO_4$ and $BiPO_4$:Tb. *J Mater Sci* 2009;**44**(5):1412–5.
153. Xue F, Li H, Zhu Y, Xiong S, Zhang X, Wang T, Liang X, Qian Y. Solvothermal synthesis and photoluminescence properties of $BiPO_4$ nano-cocoons and nanorods with different phases. *J Solid State Chem* 2009;**182**(6):1396–400.
154. Cho IS, Kim JR, Kim DW, Hong KS. Phase transformation and microwave dielectric properties of $BiPO_4$ ceramics. *J Electroceram* 2006;**16**:379–83.
155. Shannon RD. Revised effective ionic radii and systematic studies of interatomic distances in halides and chalcogenides. *Acta Crystallogr* 1976;**A32**:751–67.
156. De Biasi RS, Fernandes AAR, Oliveira JCS. Cell volumes of $LaPO_4$–$CePO_4$ solid solutions. *J Appl Cryst* 1987;**20**:319–20.
157. Yang P, Quan Z, Li C, Hou Z, Wang W, Lin J. Solvothermal synthesis and luminescent properties of monodisperse $LaPO_4$:Ln (Ln = Eu^{3+}, Ce^{3+}, Tb^{3+}) particles. *J Solid State Chem* 2009;**182**:1045–54.
158. Hou Z, Wang L, Lian H, Chai R, Zhang C, Cheng Z, Lin J. Preparation and luminescence properties of Ce^{3+} and/or Tb^{3+}-doped $LaPO_4$ nanofibers and microbelts by electrospinning. *J Solid State Chem* 2009;**182**: 698–708.
159. Kitamura N, Amezawa K, Tomii Y, Yamamoto N, Hanada T. Protonic conduction in Sr-doped $(La_{1-x}Sm_x)PO_4$. *Solid State Ionics* 2004;**75**:563–7.
160. Ferhi M, Horchani-Naifer K, Férid M. Hydrothermal synthesis and photoluminescence of the monophosphate $LaPO_4$:Eu(5%). *J Lumin* 2008;**128**(11):1777–82.
161. Yang M, You H, Jia G, Huang Y, Song Y, Zheng Y, Liu K, Zhang L. Selective synthesis of hexagonal and monoclinic $LaPO_4$:Eu^{3+} anorods by a hydrothermal method. *J Cryst Growth* 2009;**311**:4753–8.
162. Yaiphaba N, Ningthoujam RS, Shanta Singh N, Vatsa RK, Rajmuhon Singh N. Probing of inversion symmetry site in Eu^{3+}-doped $GdPO_4$ by luminescence study: concentration and annealing effect. *J Lumin* 2010;**130**:174–80.
163. Popa K, Konings RJM, Geisler T. High-temperature calorimetry of $(La_{1-x}Ln_x)PO_4$ solid solutions. *J Chem Thermodyn* 2007;**39**:236–9.
164. Lenggoro IW, Xia B, Mizushima H, Okuyama K, Kijima N. Synthesis of $LaPO_4$:Ce, Tb phosphor particles by spray pyrolysis. *Mater Lett* 2001;**50**:92–6.
165. Wang ZL, Quan ZW, Lin J, Fang J. Polyol-mediated synthesis and photoluminescent properties of Ce^{3+} and/or Tb^{3+}-doped $LaPO_4$ nanoparticles. *J Nanosci Nanotechnol* 2005;**5**(9):1532–6.
166. Bao J, Yu R, Zhang J, Wang D, Deng J, Chen J, Xing X. Oxalate-induced hydrothermal synthesis of $CePO_4$:Tb nanowires with enhanced photoluminescence. *Scripta Mater* 2010;**62**:133–6.
167. Li F, Wang M, Mi C, Yi K, Xu S. Polyol-mediated synthesis and luminescence properties of $CePO_4$:Tb^{3+} nanospindles. *J Alloys Compd* 2009;**486**(1/2):37–9.
168. Jung HK, Oha JS, Seoka SI, Lee TH. Preparation and luminescence properties of $LaPO_4$:Er, Yb nanoparticles. *J Lumin* 2005;**114**:307–13.
169. Han G, Wang Y, Wu C, Zhang J. Hydrothermal synthesis and vacuum ultraviolet-excited luminescence properties of novel Dy^{3+}-doped $LaPO_4$ white light phosphors. *Mater Res Bull* 2009;**44**(12):2255–7.
170. Mullica DF, Sappenfield EL, Boatner LA. Monazite- and zircon-type structures of seven mixed (Ln/Ln)PO_4 compounds. *Inorg Chim Acta* 1996;**44**:247–52.
171. Podor R, Cuney M. Experimental study of Th-bearing $LaPO_4$ (780 °C, 200 MPa): implications for monazite and actinide orthophosphate stability. *Am Mineral* 1997;**82**:765–71.
172. Van Emden B, Thornber MR, Graham J, Lincoln FJ. Solid solution behaviour of synthetic monazite and xenotime structure refinement of powder data. *Adv X-ray Anal* 1998;**40**:402–12.
173. Maslennikova TP, Osipov AV, Mezentseva LP, Drozdova IA, Kuchaeva SK, Ugolkov VL, Gusarov VV. Synthesis, mutual solubility, and thermal behavior of nanocrystals in the $LaPO_4$–YPO_4–H_2O system. *Glass Phys Chem* 2010;**36**(3):351–7.
174. Mogilevsky P. On the miscibility gap in monazite–xenotime systems. *Phys Chem Miner* 2007;**34**:201–14.
175. Mogilevsky P, Boakye EE. Solid solubility and thermal expansion in a $LaPO_4$–YPO_4 system. *J Am Ceram Soc* 2007;**90**(6):1899–907.
176. Rovnyi SI, Medvedev GM, Aloy AS, Koltsova TI, Samoylov SE. REE and TRU incorporation into monazite structure ceramics. *Mater Res Soc Symp Proc* 2004;**824**:237–41.
177. Popa K, Colineau E, Wastin F, Konings RJM. The low-temperature heat capacity of $(Pu_{0.1}La_{0.9})PO_4$. *Solid State Commun* 2007;**144**(1/2):74–7.
178. Zhang Y, Vance ER. Plutonium in monazite and brabantite: diffuse reflectance spectroscopy study. *J Nucl Mater* 2008;**375**:311–4.
179. Anderson EB, Burakov BE. Ceramics for the immobilization of plutonium and americium: current progress of R&D of the V.G. Khlopin Radium Institute. *Mater Res Soc Symp Proc* 2004;**807**:207–12.
180. Kitsay AA, Garbuzov VM, Burakov BE. Synthesis of actinide-doped ceramics: from laboratory experiments to industrial scale technology. *Mater Res Soc Symp Proc* 2004;**807**:237–42.
181. Hernández T, Vila R, Jurado JR, Chinarro E, Molla J, Martín P. Microstructural and electrical features of lithium Ce-monazite. *Solid State Ionics* 2008;**179**:256–62.
182. Li W, Lee J. Microwave-assisted sol–gel synthesis and photoluminescence characterization of $LaPO_4$:Eu^{3+}, Li^+ nanophosphors. *J Phys Chem C* 2008;**112**(31):11679–84.
183. Schwarz L, Finke B, Kloss M, Rohmann A, Sasum U, Haberland D. Investigations on the electronic structure of double phosphates of the type $M_3RE(PO_4)_2$ (RE = rare earths, lanthanides)). *J Lumin* 1997;**72–74**:257–9.
184. Szczygiel I, Znamierowska T. Phase equilibria in the system $CePO_4$–$NaPO_3$. *J Therm Anal Calorim* 1991;**37**:705–11.
185. Orlova AI, Kitaev DB, Lukinich AN, Tomilin SB, Lizin AA, Kulikov IA, Samsonov VE. Phosphate monazite- and $NaZr_2(PO_4)_3$ (NZP)-like ceramics containing uranium and plutonium. *Czech J Phys* 2003;**53**:A665–70.
186. Kharlamova AA, Orlova AI, Volkov YF.*3rd Russian conference on radiochemistry—radiochemistry 2000*. 2000. p. 61–2 [cited by Volkov et al., 2002].
187. Burnaeva AA, Volkov, Yu F, Kryukova AI, Korshunov IA, Skiba OV. Dimorphism and crystallochemical features of sodium plutonium(IV) phosphate of the composition $NaPu_2(PO_4)_3$. *Radiokhimiya* 1992;**34**(5):13–21.
188. Orlova AI. Isomorphism in crystalline phosphates of the $NaZr_2(PO_4)_3$ structural type and radiochemical problems. *Radiochemistry* 2002;**44**(5):423–45.
189. Kazakevicius E, Salkus T, Kezionis A, Dindune A, Kanepe Z, Ronis J, Orliukas AF. Electrical properties of monazite-type superionic ceramics in the 10^6–1.2×10^9 Hz frequency. *Lith J Phys* 2007;**47**(3):315–9.
190. Kitamura N, Amezawa K, Uchimoto Y, Tomii Y, Hanada T, Yamamoto N. Electrical conduction properties of rare earth orthophosphates under reducing conditions. *Solid State Ionics* 2006;**177**:2369–73.
191. Gomez del Moral E, Fagg DP, Chinarro E, Abrantes JCC, Jurado JR, Mather GC. Impendace analysis of Sr-substituted $CePO_4$ with mixed protonic and p-type electronic conduction. *Ceram Int* 2009;**35**: 1481–6.
192. Ravindran Nair K, Prabhakar Rao P, Amina B, Chadran MR, Koshy P. Novel monazite type rare earth based phosphates ARP_3O_{10}—studies on their preparation, microstructure and dielectric propoerties. *Mater Lett* 2006;**60**:1796–9.
193. Peiffert C, Brouand M, Cuney M, Podor R. La monazite—de l'indicateur de fertilité des granites pour les granites. *Rapport CEA* 1996: 103–8.
194. Podor R. Synthèse et caractérisation des monazites uranifères et thorifères. PhD thesis of Université Henri Poincaré, Nancy (France); 1994 (N°: 94 NAN10404).
195. Boatner LA, Abraham MM, Rappaz M. Analogs of monazite for the storage of radioactive wastes. *Trans Am Nucl Soc* 1980;**35**:186–7.

196. Kelly KL, Beall GW, Young JP, Boatner LA. Valence states of actinides in synthetic monazites. In: Moore JG, editor. *The scientific basis for nuclear waste management*, vol. 3. New York: Plenum; 1981. p. 189–95.
197. Hugues JM, Foard EE, Hubbard MA, Ni Y. The crystal structure of cheralite-(Ce), (LREE, Ca, Th, U)(P, Si)O_4: a monazite-group mineral. *Neues Jb Miner Mon* 1995;**8**:344–50.
198. Linthout K. Tripartite division of the system $2REEPO_4$–$CaTh(PO_4)_2$–$2ThSiO_4$, discreditation of brabantite, and recognition of cheralite as the name for members dominated by $CaTh(PO_4)_2$. *Can Mineral* 2007;**45**:503–8.
199. Popa K, Konings RJM, Boulet P, Bouëxière D, Popa AF. The high temperature behavior of barium zirconium diorthophosphate. *Thermochim Acta* 2005;**436**:51–5.
200. Popa K, Konings RJM, Bouëxière D, Popa AF, Geisler T. Synthesis and characterisation of $BaM^{IV}(PO_4)_2$ in the view of conditioning of the actinides. *Adv Sci Technol* 2006;**45**:2012–7.
201. Popa K, Bregiroux D, Konings RJM, Gouder T, Popa AF, Geisler T, Raison PE. The chemistry of the phosphates of barium and tetravalent cations in the 1:1 stoichiometry. *J Solid State Chem* 2007;**180**(8):2346–55.
202. Rose D, Brabantite. $CaTh(PO_4)_2$ a new mineral of the monazite group. *Neues Jb Miner Mon* 1980;**6**:247–57.
203. Davis DD, Vance ER, McCarthy GJ. Crystal chemistry and phase relations in the synthetic minerals of ceramic waste forms. II. Studies of uranium containing monazites. In: Moore JG, editor. *The scientific basis for nuclear waste management*, vol. 3. New York: Plenum; 1981. p. 197–200.
204. Tabuteau A, Pages M, Livet J, Musikas C. Monazite-like phases containing trans-uranium elements (neptunium and plutonium). *J Mater Sci Lett* 1988;**7**(12):1315–7.
205. Raison PE, Jardin R, Bouëxière D, Konings RJM, Geisler T, Pavel CC, Rebizant J, Popa K. Structural investigation of the synthetic $CaAn(PO_4)_2$ (An = Th and Np) cheralite-like phosphates. *Phys Chem Miner* 2008;**35**(10):603–9.
206. Raison PE, Popa K, Jardin R, Bouëxiere D, Konings RJM, Geisler T, Pavel CC, Rebizant J. Structural investigation of synthetic $CaTh(PO_4)_2$ and $CaNp(PO_4)_2$ by X-ray diffraction. *Acta Crystallogr* 2008;**A64**:C492.
207. Heindl R, Flemke E, Loriers J. *Conf Dig Inst Phys* 1971:22–4 [cited by Pepin et al., 1981].
208. Pepin GJ, Vance ER, McCarthy GJ. The crystal-chemistry of cerium in the monazite structure-type phase of tailored-ceramic nuclear waste forms. *Mater Res Bull* 1981;**16**(6):627–33.
209. Orlova AI, Kitaev DB, Volkov YF, Pet'kov VI, Kurazhkovskaya VS, Spiridonova ML. Double phosphates of Ce(IV) and some mono and bivalent elements. *Radiochemistry* 2001;**43**(3):225–8.
210. Kitaev DB, Volkov YF, Orlova AI. Orthophosphates of tetravalent Ce, Th, U, Np, and Pu with the monazite structure. *Radiochemistry* 2004;**46**(3):211–7.
211. Orlova AI, Kitaev DB, Kazantsev NG, Samoilov SG, Kurazhkovskaya VS, Vopilina EN. Double phosphates of Ce(IV) and some mono- and divalent elements: synthesis and crystal structure. *Radiochemistry* 2002;**4**:326–31.
212. Podor R, Cuney M, Nguyen Trung C. Experimental study of the complete solid solution between (La)-monazite and $(Ca_{0.5}U_{0.5})PO_4$ at 780 °C and 200 MPa. *Am Mineral* 1995;**80**(11/12):1261–8.
213. Devidal JL, Montel JM. Crystal chemistry of the brabantite-monazite group. *J Conf Abst* 1999;**4**, http://www.the-conference.com/JConfAbs/4/518.html.
214. Quarton M, Zouiri M, Freundlich W. Cristallochimie des orthophosphates doubles de thorium et de plomb. *C R Acad Sci Ser II* 1984;**299**(12):785–8.
215. Montel JM, Devidal JL, Avignant D. X-ray diffraction study of brabantite–monazite solid solutions. *Chem Geol* 2002;**191**:89–104.
216. Terra O, Dacheux N, Clavier N, Podor R, Audubert F. Preparation of optimized uranium and thorium bearing brabantite or monazite/brabantite solid solutions. *J Am Ceram Soc* 2008;**91**:3673–82.
217. Dacheux N, Clavier N, Robisson AC, Terra O, Audubert F, Lartigue JE, Guy C. Immobilisation of actinides in phosphate matrices. *C R Chimie* 2004;**7**:1141–52.
218. Deschanels X, Picot V, Glorieux B, Jorion F, Peuget S, Roudil D, Jégou C, Broudic V, Cachia JN, Advocat T, Den Auwer C, Fillet C, Coutures JP, Henning C, Scheinost A. Plutonium incorporation in phosphate and titanate ceramics for minor actinide containment. *J Nucl Mater* 2006;**352**:233–40.
219. Hikichi Y, Hukuo K, Shiokawa J. Solid solutions in the systems monazite ($CePO_4$)–huttonite ($ThSiO_4$) and monazite–$(Ca_{0.5}Th_{0.5})PO_4$. *Nippon Kagaku Kaishi* 1978;**12**:1635–40.
220. Montel JM, Glorieux B, Seydoux-Guillaume AM, Wirth R. Synthesis and sintering of a monazite–brabantite solid solution ceramic for nuclear waste storage. *J Phys Chem Solids* 2006;**67**:2489–500.
221. Glorieux B, Montel JM, Matecki M. Synthesis and sintering of a monazite–brabantite solid solution ceramics using metaphosphate. *J Eur Ceram Soc* 2009;**29**(9):1679–86.
222. Muto T, Meyrowitz R, Pommer AM, Murano T. Ningyoite a new uranous phosphate mineral from Japan. *Am Mineral* 1959;**44**:633–50.
223. Volkov YF, Tomilin KSV, Lukinykh AN, Lizin AA, Orlova AI, Kitaev DB. Synthesis and X-ray diffraction study of mixed-metal orthophosphates with $NaZr_2(PO_4)_3$ and $CePO_4$ structures. *Radiochemistry* 2002;**44**(4):319–25.
224. McCarthy GJ, White WB, Pfoertsch DE. Synthesis of nuclear waste monazites, ideal actinide hosts for geological disposal. *Mater Res Bull* 1978;**13**:1239–45.
225. Orlova AI, Kitaev DB, Kemenov DV, Orlova MP, Kazantsev GN, Samoilov SG, Kurazhkovskaya VS. Synthesis and crystal-chemical properties of phosphates $B^{II}R^{III}M^{IV}(PO_4)_3$ containing f, d, and alkaline-earth elements. *Radiochemistry* 2003;**45**(2):103–9.
226. Orlova MP, Orlova AI, Gobechiya ER, Kabalov YK, Dorokhova GI. Synthesis and structure of new thorium phosphate $CaGdTh(PO_4)_3$. *Crystallogr Rep* 2005;**50**(1):48–51.
227. Gardes E, Jaoul O, Montel JM, Seydoux-Guillaume AM, Wirth R. Pb diffusion in monazite: an experimental study of $Pb^{2+} + Th^{4+} \leftrightarrow 2Nd^{3+}$ interdiffusion. *Geochim Cosmochim Acta* 2006;**70**:2325–36.
228. Konings RJM, Walter M, Popa K. Excess properties of the $(Ln_{2-2x}Ca_xTh_x)(PO_4)_2$ (Ln = La, Ce) solid solutions. *J Chem Therm* 2008;**40**(8):1305–8.
229. Popa K, Konings RJM, Wiss T, Leiste H. Hydrothermal alteration of $Ba_xM^{IV}{}_xCe_{2-2x}(PO_4)_2$ M^{IV} = Zr, Hf as hosts for minor actinides. *J Radioanal Nucl Chem* 2007;**273**(3):563–7.
230. Podor R. Raman spectra of the actinide-bearing monazites. *Eur J Mineral* 1995;**7**:1353–60.
231. Zubkova NV, Kabalov YK, Orlova AI, Kitaev DB, Kurazhkovskaya VS. The synthesis and structure of alkaline earth and cerium (IV) phosphates (Ce,B,◊)PO_4(B = Mg,Ca). *Crystallogr Rep* 2003;**48**(3): 401–5.
232. Orlova AI, Spiridonova ML, Orlova MP, Pet'kov VI, Kabalov YK, Zubkova NV, Kulikov IA, Samoilov SG. Cadmium cerium(IV) phosphate $Cd_{0.5}Ce_2(PO_4)_3$: crystal structure and physicochemical properties. *Russ J Inorg Chem* 2004;**49**(9):1331–7.
233. Orlova AI, Kitaev DB. Anhydrous lanthanide and actinide(III) and (IV) orthophosphates $Me_m(PO_4)_n$: synthesis, crystallization, structure and properties. *Radiochemistry* 2005;**47**(1):14–30.
234. Orlova MP, Kitaev DB, Spiridonova ML, Zubkova NV, Kabalov YK, Orlova AI. Structure refinement of cadmium cerium(IV) phosphate $Cd_{0.5}Ce_2(PO_4)_3$. *Crystallogr Rep* 2005;**50**(6):918–22.
235. El Yacoubi A, Brochu R, Serghini A, Louer M. Synthesis and structural study from X-ray powder diffraction of $Pb_{0.5}Th_2(PO_4)_3$. *Powder Diffr* 1997;**12**(2):76–80.
236. Orlova AI, Volkov YF, Kitaev DB, Pet'kov VI.*3rd Russian conference on radiochemistry*. 2000. p. 60 [cited by Volkov et al., 2002].
237. Nectoux F, Tabuteau A. Sur quelques phosphates de neptunium(IV). *Radiochem Radioanal Lett* 1981;**49**(1):43–8.
238. Volkov YF. Compounds with zircon and monazite structures and possibilities of their use for incorporation of radionuclides. *Radiokhimiya* 1999;**41**:168–74.
239. Volkov YF, Melkaya RF, Spiryakov VI, Timofeev GA. Synthesis and characterization of tetravalent actinide orthophosphates with alkali-metals. *Radiochemistry* 1994;**36**:222–6.
240. Orlova AI, Kitaev DB, Kazantzev NG, Samoilov SG, Kurazhkovskaya VS, Vopilina EN. Double phosphates of Ce(IV) and some mono-

and divalent elements: synthesis and crystal structure. *Radiochemistry* 2002;**44**:326.
241. Matkovic B, Sljukic M. Synthesis and crystallographic data of sodium thorium triphosphate, $NaTh_2(PO_4)_3$, and sodium uranium(IV) triphosphate, $NaU_2(PO_4)_3$. *Croat Chem Acta* 1965;**37**:115–6.
242. Volkov YF, Tomilin SV, Orlova AI, Lizin AA, Spiryakov VI, Lukinykh AN. Rhombohedral actinide phosphates $A^IM^{IV}{}_2(PO_4)_3$ (M^{IV} = U, Np, Pu; A^I = Na, K, Rb). *Radiochemistry* 2003;**45**(4):319–28.
243. Tie S, Su Q, Yu Y. Optical and structural investigation of $KMgLa(PO_4)_2$ phospahte doped with europium. *J Solid State Chem* 1995;**114**:282–5.
244. Jungowska W. The system $LaPO_4$–$CaKPO_4$. *Solid State Sci* 2009;**9**:318–21.
245. Hutton CO. Occurrence, optical properties and chemical composition of huttonite. *Am Mineral* 1951;**36**(1/2):66–9.
246. Kolitsch U, Holtstam D. Crystal chemistry of $REEXO_4$ compounds (X = P, As, V). II. Review of $REEXO_4$ compounds and their stability fields. *Eur J Mineral* 2004;**16**(1):117–26.
247. Locock AJ. Crystal chemistry of actinide phosphates and arsenates. In: Krivovichev SV, Burns PC, Tananaev IG, editors. *Structural chemistry of inorganic actinide compounds*. Elsevier Publishers; 2007. p. 207–78 [Chapter 6].
248. Delien M, Piret P. Kusuite becomes plombean wakefieldite (Ce). *Bull Miner* 1986;**109**(3):305.
249. Witzke T, Kolitsch U, Warnsloh JM, Goske J. Wakefieldite (La), $LaVO_4$, a new mineral species from the Glucksstern Mine, Friedrichrodr, Thuringia, Germany. *Eur J Mineral* 2008;**20**(6):1135–9.
250. Bashir J, Khan MN. X-ray powder diffraction analysis of crystal structure of lanthanum orthovanadate. *Mater Lett* 2006;**60**:470–3.
251. Rice CE, Robinson WR. Lanthanum orthophosphate. *Acta Crystallogr* 1976;**B32**:2232–3.
252. Baran EJ, Aymonino PJ. Orthovanadates and related compounds, 2. Lanthanum orthovanadates. *Z Anorg Allg Chem* 1971;**383**(2):220–5.
253. Bazuev GV, Pletnev RN, Slepukhin VK, Lisson VN, Shveikin GP. Rare earth orthovanadates with the monazite structure. *Inorg Mater* 1978;**14**:554–7.
254. Ropp RC, Carroll B. Dimorphic lanthanum orthovanadate. *J Inorg Nucl Chem* 1973;**35**:1153–7.
255. Bazuev GV, Zhilyaev VA, Shveikin GP. Dimorphism of rare-earth orthophosphates. *Dokl Akad Nauk SSSR* 1976;**218**:833–6.
256. Damon K, Min W, Hikichi Y, Wada N, Matsubara T, Ota T. Low-temperature synthesis of monazite-type lanthanum orthovanadate ($LaVO_4$) from aqueous solution. *J Chem Soc Jpn Chem Ind Chem* 2002;**3**:455–8.
257. Oka Y, Yoa T, Yamamoto N. Hydrothermal synthesis of lanthanum orthovanadates; synthesis and crystal structures of zircon-type $LaVO_4$ and a new compound LaV_3O_9. *J Solid State Chem* 2000;**152**: 486–91.
258. Yoshimura M, Sata T. New monoclinic phase of cerium orthovanadate. *Bull Chem Soc Jpn* 1969;**42**:3195–8.
259. Zhao J, Ma J, Dai C, Liu Y, Song Z, Sun Y, Fang J, Gao C, Liu Z, Sun X. Synthesis of $La_{1-x}Fe_xVO_4$ solid solutions and their photocatalytic activity. *J Alloys Compd* 2010;**507**:35–7.
260. Schwarz H. Die phosphate, arsenate und vanadate der seltenen Erden. *Z Anorg Allg Chem* 1963;**323**:44–56.
261. Sleight AW, Chen HY, Ferretti A, Cox DE. Crystal growth and structure of $BiVO_4$. *Mater Res Bull* 1979;**14**:1571–81.
262. Tokunaga S, Kato H, Kudo A. Selective preparation of monoclinic and tetragonal $BiVO_4$ with scheelite structure and their catalytic propreties. *Chem Mater* 2001;**13**:4624–8.
263. Aldred AT. Crystal chemistry of ABO_4 compounds, where A = Sc, Y, La–Lu. *Acta Crystallogr* 1984;**B40**:569–74.
264. Calestani G, Andretti GD. The crystal-structure of the $Pb_{0.5}Th_{0.5}VO_4$ polymorphs with scheelite-type, zircon-type and huttonite-type structures. *Z Kristallogr* 1984;**168**(1–4):41–51.
265. Nabar MA, Mhatre BG. Studies on triple orthovanadates. VIII. Synthesis and spectrostructural characterization of triple orthovanadates $BaLnTh(VO_4)_3$ (Ln = La or Pr) and $BaLnCe(VO_4)_3$ (Ln = La, Pr, Nd or Sm). *J Alloys Compd* 2001;**323–324**:83–5.
266. Nabar MA, Mahtre BG. Studies on triple orthovanadates: IV. Crystal chemistry of the solid solutions $Ca_{1-x}Ba_xLaTh(VO_4)_3$. *Inorg Chim Acta* 1987;**140**:165–6.
267. Aldred AT. Crystal chemistry of ABO_4 compounds. Geochemical Behavior of Disposed Radioactive Waste. American Chemical Society; 1984 March, p. 305–314 [Chapter 18], doi:10.1021/bk-1984-0246.ch018, ACS Symposium Series, Vol. 246. ISBN 13: 9780841208278eISBN: 9780841210745.
268. Andrehs G, Heinrich W. Experimental determination of REE distributions between monazite and xenotime: potential for temperature-calibrated geochronology. *Chem Geol* 1998;**149**(1/2):83–96.
269. Gratz R, Heinrich W. Monazite–xenotime thermometry. III. Experimental calibration of the partitioning of gadolinium between monazite and xenotime. *Eur J Mineral* 1998;**10**(3):579–88.
270. Seydoux-Guillaume AM, Wirth R, Heinrich W, Montel JM. Experimental determination of thorium partitioning between monazite and xenotime using analytical electron microscopy and X-ray diffraction rietveld analysis. *Eur J Mineral* 2002;**14**(5):869–78.
271. Xiao X, Yan B, Song Y. $GdP_xV_{1-x}O_4$:Eu^{3+} nanophosphor and hydrated $Zn_3(PO_4)_2$:Eu^{3+} nanorod bunch: facile reproducible hydrothermal synthesis, controlled microstructure, and photoluminescence. *Cryst Growth Des* 2009;**9**(1):136–44.
272. Cabella R, Lucchetti G, Marescotti P. Occurrence of LREE- and Y-arsenates from a Fe–Mn deposit, Ligurian Brianconnais Domain, Maritime Alps, Italy. *Can Mineral* 1999;**37**(4):961–72.
273. Graeser S, Schwander H. Gasparite–(Ce) and monazite–(Nd): Two new minerals to the monazite group from the Alps. *Schweiz Mineral Petrogr Mitt* 1987;**67**(1/2):103–13.
274. Kolitsch U, Holtstam D, Gatedal K. Crystal chemistry of $REEXO_4$ compounds (X = P, As, V). I. Paragenesis and crystal structure of phosphatian gasparite–(Ce) from the Kesebol Mn–Fe–Cu deposit, Vastra Gotaland, Sweden. *Eur J Mineral* 2004;**16**(1):111–6.
275. Botto IL, Baran EJ. Characterization of the monoclinic rare earth ortoarsenates. *J Less Common Met* 1982;**83**(2):255–61.
276. Kang DH, Schleid T. Single crystals of $LaAsO_4$ with monazite- and $SmAsO_4$ with xenotime-type structure. *Z Anorg Allg Chem* 2005;**631**(10):1799–802.
277. Dong-Hee K, Hoess P, Schleid T. Xenotime-type $YbAsO_4$. *Acta Crystallogr* 2005;**E61**:270–2.
278. Schmidt M, Müller U, Gil RC, Milke E, Binnewies M. Chemical vapour transport and crystal structure of rare-earth arsenates(V). *Z Anorg Allg Chem* 2005;**631**:1154–62.
279. Brahim A, Mongi MF, Amor H. Cerium arsenate, $CeAsO_4$. *Acta Crystallogr* 2002;**E58**:98–9.
280. Choudhary RNP. Structural and dielectric properties of monoclinic $PrAsO_4$. *J Mater Sci Lett* 1991;**10**:432–4.
281. Gasparite–(Ce), 2001–2005 mineral data publishing, version 1, http://www.handbookofmineralogy.org/pdfs/gasparitece.pdf.
282. Escobar ME, Baran EJ. Precipitation of rare-earth arsenates in aqueous solutions. *Z Chem* 1978;**18**(11):418–9.
283. Weigel F, Scherer V, Promethium IV. Ternary oxides of the type $PmXO_4$. *Radiochim Acta* 1967;**7**:46–50.
284. Bedlivy D, Mereiter K. Structure of alpha-$BiAsO_4$ (rooseveltite). *Acta Crystallogr* 1982;**B38**:1559–61.
285. Nabar MA, Mangaonkar SS. Studies on triple orthovanadates. VII: Spectro-structural studies on dimorphic $CaBiTh(AsO_4)_3$. *J Mater Sci Lett* 1994;**13**:225–6.
286. Nabar MA, Sakhardande RR. Studies on thorium containing triple orthoarsenates: $MRETh(AsO_4)_3$ (M = Mg, Sr, Ba, Cd and Pb, RE = La, Pr, Nd, Sm, Gd, Tb, Dy and Y). *J Alloys Compd* 1999;**285**:82–4.
287. Nabar MA, Sakhardande RR. Monazite to scheelite transition in $CdNdTh(AsO_4)_3$. *J Less Common Met* 1985;**110**(1/2):415–20.
288. Schwarz H. Uber verbindungen des typs $Me^2{}_{0.5}Me^4{}_{0.5}X^5O_4$ mit huttonitoder zirkonstruktur. 1. Phosphate und arsenate (Me^2 = Cd, Ca, Sr, Pb, Ba–Me^4 = Th, X^5 = P, As). *Z Anorg Allg Chem* 1964;**334**: 175.
289. Fukunaga O, Yamaoka S. Phase transformations in ABO_4 type compounds under high pressure. *Phys Chem Miner* 1979;**5**:167–77.

290. Aoki Y, Konno H, Tachikawa H, Inagaki M. Characterization of $LaCrO_4$ and $NdCrO_4$ by XRD, Raman spectroscopy, and ab initio molecular orbital calculations. *Bull Chem Soc Jpn* 2000;**73**:1197–203.
291. Aoki Y, Konno H, Tachikawa H. The electronic and magnetic properties of $LaCrO_4$ and $Nd_{1-x}Ca_xCrO_4$ ($x = 0$–0.2) and the conduction mechanism. *J Mater Chem* 2001;**11**(4):1214–21.
292. Melero EJ. Estudio cristalografico y magnetico de oxidos $RCrO_4$ (R = tierra rara). PhD thesis (Universidad Complutense de Madrid), 2005.
293. Vasilega ND, Kir'yakova IE, Pavlikov VN, Tresvyatskii SG. X-ray studies of polycrystalline lanthanum chromate(V) and strontium chromate(VI). Dopovidi Akademii Nauk Ukrains'koi RSR, Seriya B: Geologichni. *Khimichni ta Biologichni Nauki* 1977;**5**:410–3.
294. Aoki Y, Konno H, Tachikawa H, Inagaki M. Characterization of $LaCrO_4$ and $NdCrO_4$ by XRD, Raman spectroscopy and ab initio molecular orbital calculations. *Bull Chem Soc Jpn* 2000;**73**:1197–203.
295. Tsuda T, Nasu K, Fujimori A, Siratori K. *Electric conduction in oxides (Springer series in solid state physics 94)*. Heidelberg: Springer-Verlag; 1991.
296. Manca SG, Baran EJ. Crystal data for lanthanum chromate(V). *J Appl Cryst* 1982;**15**:102–3.
297. Carter JD, Anderson HU, Shumsky MG. Structure and phase transformation of lanthanum chromate. *J Mater Sci* 1996;**31**(2):551–7.
298. Johnson C, Gemmen R, Orlovskaya N. Nano-structured self-assembled $LaCrO_3$ thin film deposited by RF-magnetron sputtering on a stainless steel interconnect material. *Compos B Eng* 2004;**35**:167–72.
299. Rida K, Benabbas A, Bouremmad F, Pena MA, Sastre E, Martines-Arias A. Effect of calcination temperature on the structural characteritics and catalytic activity for propene combustion of sol–gel derived lanthanum chromite perovskite. *Appl Catal A Gen* 2007;**327**(2):173–9.
300. Kattak CP, Koc DE. Structural studies of the (La, Sr)CrO_3 system. *Mater Res Bull* 1977;**12**:463–72.
301. Miyoshi S, Onuma S, Kaimai A, Matsumoto H, Yashiro K, Kawada T, Mizusaki J, Yokokawa H. Chemical stability of $La_{1-x}Sr_xCrO_3$ in oxidizing atmospheres. *J Solid State Chem* 2004;**177**:4112–8.
302. Wagner AL, Jacobson AJ, Richardson JT, Luss D. Reaction characteristics of $La_{0.84}Sr_{0.16}CrO_3$ formation. *J Mater Sci* 1999;**34**:3035–41.
303. Pistorius CWFT, Pistorius MC. Lattice constants and thermal expansion properties of the chromate and selenates of lead, strontium and barium. *Z Kristallogr* 1962;**117**:259–71.
304. Effenberger H, Pertlik F. 4 monazite type structures—comparison of $SrCrO_4$, $SrSeO_4$, $PbCrO_4$ (crocoite), and $PbSeO_4$. *Z Kristallogr* 1984;**176**(1/2):75–83.
305. Parhi P, Manivannan V. Novel microwave initiated synthesis of Zn_2SiO_4 and $MCrO_4$ (M = Ca, Sr, Ba, Pb). *J Alloys Compd* 2009;**469**: 558–64.
306. Chang W, Shen Y, Xie A, Liu X. Facile controlled synthesis of micro/nanostructure $MCrO_4$ (M = Ba, Pb) by using Gemini surfactant C12-PEG-C12 as a soft template. *Appl Surf Sci* 2010;**256**(13): 4292–8.
307. Jacob KT, Abraham KP. Phase relations in the system Sr–Cr–O and thermodynamic properties of $SrCrO_4$ and $Sr_3Cr_2O_8$. *J Phase Equilb* 2000;**21**(1):46–53.
308. Yin J, Zou Z, Ye J. Photophysical and photocatalytic properties of new photocatalysts $MCrO_4$ (M = Sr, Ba). *Chem Phys Lett* 2003;**378**:24–8.
309. Knight KS. A high temperature structural phase transition in crocoite ($PbCrO_4$) at 1068 K: crystal structure refinement at 1073 K and thermal expansion tensor determination at 1000 K. *Mineralog Mag* 2000;**64**(2):291–300.
310. Brill R. The lattice of lead chromate. *Z Knst* 1933;**77**:506.
311. Prevost-Czeskleba H, Endres H. Structure of strontium selenate, $SrSeO_4$. *Acta Crystallogr* 1984;**C40**:18–20.
312. Wildner M, Giester G. Crystal structures of $SrSeO_3$ and $CaSeO_3$ and their respective relationships with molybdomenite- and monazite-type compounds—an example for stereochemical equivalence of $ESeO_3$ groups (E = lone electron pair) with tetrahedral TO_4 groups. *Neues Jb Miner Abh* 2007;**184**(1):29–37.
313. Crichton WA, Müller H, Merlini M, Roth T, Detlefs C. Monazite structure from dehydrated $CaSeO_4 \cdot 2H_2O$. *Mineral Mag* 2010;**74**(1):127–39.
314. Parise JB, Antao SM, Martin CD, Crichton W. Diffraction studies of order–disorder at high pressures and temperatures. *Adv X-ray Anal* 2005;**48**:14–26.
315. Crichton WA, Parise JB, Antao SM, Grzechnik A. Evidence for monazite-, barite-, and $AgMnO_4$ (distorted barite)-type structures of $CaSO_4$ at high pressure and temperature. *Am Mineral* 2005;**90**(1):22–7.
316. Ma YM, Zhou Q, He Z, Li FF, Yang KF, Cui QL, Zou GT. High-pressure and high-temperature study of the phase transition in anhydrite. *J Phys Condens Mater* 2007;**19**:425221–9.
317. Bradbury SE, Williams Q. X-ray diffraction and infrared spectroscopy of monazite-structured $CaSO_4$ at high pressures: Implications for shocked anhydrite. *J Phys Chem Solids* 2009;**70**(1):134–41.
318. Borg IY, Smith DK. A high pressure polymorph of $CaSO_4$. *Contrib Mineral Petrol* 1975;**50**:127–33.
319. Suquet H, Launay S. A crystallochemical study of chrome yellow pigments. *Eur J Solid State Inorg Chem* 1988;**25**(5/6):589–98.
320. Crane MJ, Leverett P, Shaddick LR, Williams PA, Kloprogge JT, Frost RL. The $PbCrO_4$–$PbSO_4$ system and its mineralogical significance. *Neues Jb Miner Mon* 2001;**11**:505–19.
321. Schenker RP, Brunold TC, Gdel HU. Synthesis and optical spectroscopy of MnO_4^{2-}-doped crystals of Cs_2CrO_4, $SrCrO_4$, CsBr, and CsI. *Inorg Chem* 1998;**37**(5):918–27.
322. Keller C. Untersuchung ueber die germinate und silicate des types ABO_4 de vieuvertigen elemente thorium bis americium. *Nukleonik* 1963;**5**: 41–8.
323. Myasoedov BF, Kirby HW, Tananaev IG. Protactinium. In: Morss LR, Edelstein NM, Fuger J, editors. *The chemistry of the actinide and transactinide elements*. Netherlands: Springer; 2006. p. 161–252.
324. Pointeau V, Deditius AP, Miserque F, Renock D, Becker U, Zhang J, Clavier N, Dacheux N, Poinssot C, Ewing RC. Synthesis and characterisation of coffinite. *J Nucl Mater* 2009;**393**(3):449–58.
325. Speer JA. The actinide orthosilicates. *Rev Mineral Geochem* 1980;**5**(1):113–35.
326. Speer JA, Cooper BJ. Crystal structure of synthetic hafnon, $HfSiO_4$, comparison with zircon and the actinide orthosilicates. *Am Miner* 1982;**67**:804–8.
327. Frondel C. Systematic mineralogy of uranium and thorium. *US Geol Surv Bull* 1948;**1064**:151–2.
328. Frondel C. *Systematic mineralogy of uranium and thorium*. Washington, DC: US Govt Print Off.; 1958.
329. Pabst A, Hutton CO, Osborne C. Huttonite, a new monoclinic thorium silicate; its occurrence, analysis and properties. *Am Mineral* 1951;**36**:60–9.
330. Frondel C, Collette RL. Hydrothermal synthesis of zircon, thorite and huttonite. *Am Mineral* 1957;**42**(11/12):759–65.
331. Harlov DE, Wirth R, Hetherington CJ. The relative stability of monazite and huttonite at 300–900 degrees C and 200–1000 MPa: metasomatism and the propagation of metastable mineral phases. *Am Mineral* 2007;**92**(10):1652–64.
332. Berzelius JJ. Untersuchung eines newen Minerals und einer darin erhaltenen zuver unbekannten Erde. *Annalen der Physik und Chemie (Poggendorf)* 1829;**16**:385–415 [also in Svenska Akad Handl 1829;1:1–30].
333. Shein IR, Shein KI, Ivanovskii AL. Thorite versus huttonite: stability, electronic properties and X-ray emission spectra from first-principle calculations. *Phys Chem Miner* 2006;**33**:545–52.
334. Taylor M, Ewing RC. Crystal structures of $ThSiO_4$ polymorphs—huttonite and thorite. *Acta Crystallogr B* 1978;**34**:1074–9.
335. Mazeina L, Ushakov SV, Navrotsky A, Boatner LA. Formation enthalpy of $ThSiO_4$ and enthalpy of the thorite → huttonite phase transition. *Geochim Cosmochim Acta* 2005;**69**(19):4675–83.
336. Seydoux AM, Montel JM. Experimental determination of the thorite-huttonite phase transition. EUGIX, Terra Nova 9, Abstract supplement 1, 42119 (cited by Mazeina et al., 2005).
337. Finch CB, Harris LA, Clark GW. The thorite–huttonite phase transformation as determined by growth of synthetic thorite + huttonite single crystals. *Am Mineral* 1964;**49**(5/6):782–5.
338. Dachille F, Roy R. Effectiveness of shearing stresses in accelerating solid-phase reactions at low temperatures and high pressures. *J Geol* 1964;**72**:243–7.

339. Dusausoy Y, Ghermani NE, Podor R, Cuney M. Synthesis and crystal-structure of the low-temperature form of $CaU(PO_4)_2$. *Eur J Mineral* 1996;**8**(4):667–73.
340. Starynkevitch I. The chemical formula of monazite and several analyses of Russian monazites. *Doklady Akad Nauk SSSR* 1922;**31**:28–30.
341. Bowie SHU, Horne JET. Cheralite a new mineral of the monazite group. *Mineral Mag* 1953;**30**:93–9.
342. Pavlenko AS, Orlova LP, Akhmanova MV. Cerphosphorhuttonite a monazite-group mineral. *Trudy Mineral Muzeya Akad Nauk SSSR* 1965;**16**:166–74.
343. Kucha H. Continuity in the monazite–huttonite series. *Mineral Mag* 1980;**43**(332):1031–4.
344. Della Ventura G, Mottana A, Parodi GC, Raudsepp M, Dellatreccia F, Caprilli E, Rossi P, Fiori S. Monazite–huttonite solid solutions from the vico volcanic complex, Latium, Italy. *Mineral Mag* 1996;**60**: 751–8.
345. Peiffert C, Cuney M. Hydrothermal synthesis of the complete solid solution between monazite ($LaPO_4$) and huttonite ($ThSiO_4$) at 780 °C and 200 MPa. Journal of Conference Abstracts; 1999. Conference «Stabilisation des déchets et environnement: vers la définition d'objectifs de stabilisation des déchets industriels par la prise en compte de l'impact potentiel sur la santé et l'environnement» 4, 522, http://www.the-conference.com/JConfAbs/4/518.html.
346. Montel JM, Devidal JL, Gibert F, Cuney M, Brouand M, Cuney M, et al. Utilisation des phosphates comme matrices de stockage des déchets radioactifs. Programme INSU Matériaux; 1999, 10 pp.
347. Kohler J. Syntheses and structures of novel complex Yb(II) fluorides: $YbBeF_4$, $YbAlF_5$ and $LiYbAlF_6$. *Solid State Sci* 1999;**1**:545–53.
348. Muller O, Roy R. *Crystal chemistry of non-metallic materials, vol. 4, the major ternary structural families*. New York/Heidelberg/Berlin: Springer-Verlag; 1974.
349. Manjon FJ, Errandonea D, Lopez-Solano J, Rodriguez-Hernandez P, Radescu S, Mujica A, Munoz A, Garro N, Pellicer-Porres J, Segura A, Ferrer-Roca Ch, Kumar RS, Tschauner O, Aquilanti G. Crystal stability and pressure-induced phase transitions in scheelite AWO_4 (A = Ca, Sr, Ba, Pb, Eu) binary oxides. II. Towards a systematic understanding. *Phys Status Solidi B* 2007;**244**(1):295–302.
350. Bastide JP. Systématique simplifiée des composés ABX_4 ($X = O^{2-}$, F^-) et evolution possible de leurs structures cristallines sous pression. *J Solid State Chem* 1987;**71**(1):115–20.
351. Finch RJ, Hanchar JM. Structure and chemistry of zircon and zircon-group minerals. *Rev Mineral Geochem* 2003;**53**:1–25.
352. Errandonea D, Manjón FJ. Pressure effects on the structural and electronic properties of ABX_4 scintillating crystals. *Prog Mater Sci* 2008;**53**(4):711–73.
353. Carron MK, Rose ME, Murata KJ. Relation of ionic radius to structures of rare-earth phosphates, arsenates and vanadates. *Am Mineral* 1958;**43**:985–9.
354. Macey BJ. The crystal chemistry of MTO_4 compounds with the zircon, scheelite and monazite structure types. Master thesis, Virginia Tech; 1995, 69 pp.
355. Popa K, Wallez G, Raison PE, Bregiroux D, Konings RJM. $SrNp(PO_4)_2$: an original ordered modification of cheralite. *Inorg Chem* 2010;**49**(15):6904–8.
356. Loskutov VV, Vorobzhanskaya EV, Liberman ZA. Structural diagram of compound ABO_4. *Sov Phys Crystallogr* 1977;**22**:726–8.
357. Gratz R, Heinrich W. Monazite–xenotime thermobarometry: experimental calibration of the miscibility gap in the binary system $CePO_4$–YPO_4. *Am Mineral* 1997;**82**(7/8):772–80.
358. Spear FS, Pyle JM. Apatite monazite, and xenotime in metamorphic rocks. *Rev Mineral Geochem* 2002;**48**(1):293–335.
359. Mullica DF, Sappenfield EL, Boatner LA. A structural investigation of several mixed lanthanide orthophosphates. *Inorg Chem Acta* 1990;**174**(2):155–9.
360. Mullica DF, Sappenfield EL, Boatner LA. Single crystal analyses of mixed ($Ln/TbPO_4$) orthophosphates. *J Solid State Chem* 1992;**99**:313–8.
361. Mooney RCL. X-ray diffraction study of cerous phosphate and related crystals. I. Hexagonal modification. *Acta Cryst* 1950;**3**:337–40.
362. Kijkowska R. Thermal decomposition of lanthanide orthophosphates synthesized through crystallization from phosphoric acid solution. *Thermochim Acta* 2003;**404**:81–8.
363. Du Fou de Kerdaniel E, Clavier N, Dacheux N, Terra O, Podor R. Actinide solubility-controlling phases during the dissolution of phosphate ceramics. *J Nucl Mater* 2007;**362**:451–8.
364. Schatzmann MT, Mecartney ML, Morgan PED. Synthesis of monoclinic monazite, $LaPO_4$, by direct precipitation. *J Mater Chem* 2009;**19**:5720–2.
365. Zaki M, Aamili A, Sadel A, Zahir M, El-Ghozzi M, Avignant D. Synthesis, crystal chemistry and physical study of a new series of rare earth phosphates with specific open structure. *Ann Chim Sci Mater* 2001;**26**: 35–43.
366. Lucas S, Champion E, Bernache-Assollant D, Leroy G. Rare earth phosphates powders $RePO_4$, nH_2O (Re = La, Ce or Y). II. Thermal behavior. *J Solid State Chem* 2004;**177**:1312–20.
367. Bondar LA, Domanskii AI, Mezentseva LP, Degen MG, Kalinina NE. A physicochemical study of lanthanide orthophosphates. *Zh Neorg Khim* 1976;**21**:2045–50.
368. Hikichi Y, Murayama K, Ohsato H, Nomura T. Thermal changes of rare-earth phosphate minerals. *Nippon Kagaku Kaishi* 1989;**19**(3):117–26.
369. Akers WT, Grove M, Harrison TM, Ryerson PJ. The instability of rhabdophane and its unimportance in monazite paragenesis. *Chem Geol* 1993;**110**:169–76.
370. Rajesh K, Mukundan P, Pillai PK, Nair VR, Warrier KGK. High-surface area nanocrystalline cerium phosphate through aqueous sol–gel route. *Chem Mater* 2004;**16**:2700–5.
371. Matraszek A, Szczygiel I, Macalik L, Hanuza J. Mechanochemical synthesis of cerium orthophosphate. *J Rare Earths* 2009;**27**:598–602.
372. Zollfrank C, Scheel H, Brungs S, Greil P. Europium(III) orthophosphates: synthesis, characterization and optical properties. *Cryst Growth Des* 2008;**8**:766–70.
373. Hikichi Y, Yu CF, Miyamoto M, Okada S. Mechanical conversion of rhbadophane type RPO_4, nH_2O (R = La, Ce, Pr, Nd or Sm, $n \sim 1/2$) to the monazite type analogues. *Mineralogical J* 1991;**15**:349–55.
374. Hikichi Y, Yu CF, Miyamoto M, Okada S. Mechanochemical changes in hydrated rare-earth orthophosphates minerals by grinding. *J Alloys Compd* 1993;**192**:102–4.
375. Diaz-Guillen JA, Fuentes AF, Gallini S, Colomer MT. A rapid method to obtain nanometric particles of rhabdophane $LaPO_4$, nH_2O by mechanical milling. *J Alloys Compd* 2007;**427**:87–93.
376. Hikichi Y, Hukuo K, Shiokawa J. Synthesis of rhabdophane $Ce_{1-x}Y_xPO_4$, nH_2O and its thermal change. *Nippon Kagaku Kaishi* 1979;**6**:733–8.
377. Osipov AV, Mezentseva LP, Drozdova IA, Kuchaeva SK, Ugolkov VL, Gusarov VV. Preparation and thermal transformations of nanocrystals in the $LaPO_4$–$LuPO_4$–H_2O system. *Glass Phys Chem* 2009;**35**:431–5.
378. Ivanov VI, Sin'kova LA. Experimental study of the monazite–xenotime structural relationship in the rare-earth phosphates. *Geokhimiya* 1967;**2**:241–3.
379. Min W, Daimon K, Ota T, Matsubara T, Hikichi Y. Synthesis and thermal reactions of rhabdophane-(Yb or Lu). *Mater Res Bull* 2000;**35**:2199–205.
380. Fisher FG, Meyrowitz R. Brockite, a new calcium thorium phosphate from Wet Mountains, Colorado. *Am Miner* 1962;**47**:1346–56.
381. Atkin D, Basham IR, Bowles JFW. Tristramite, a new calcium uranium phosphate of the rhabdophane group. *Mineral Mag* 1983;**344**:393–6.
382. du Fou de Kerdaniel E, Clavier N, Dacheux N, Podor R. Kinetic and thermodynamic study of the chemistry of neoformed phases duraing the dissolution of phosphate based ceramics. *Mater Res Soc Symp Proc* 2007;**985**:341–6.
383. Huang T, Lee JS, Kung J, Lin CM. Study of monazite under high pressure. *Solid State Commun* 2010;**37–38**:1845–50.
384. Stephens DR. The hydrostatic compression of 8 rocks. *J Geophys Res* 1964;**69**(14):2967–78.
385. Stubican VS, Roy R. High pressure scheelite-structure polymorphs of rare-earth vanadates and arsenates. *Z Kristallog* 1963;**119**:90–7.
386. Range K, Meiester, Klement U. Hochdrunckumwandlungen von Cer(III)orthovanadat (V) $CeVO_4$. *Z Naturforsch B* 1990;**45**(5):598–602.
387. Lacomba-Perales R, Errandonea D, Meng Y, Bettinelli M. High-pressure stability and compressibility of APO_4 (A = La, Nd, Eu, Gd, Er, and Y)

orthophosphates: an x-ray diffraction study using synchrotron radiation. *Phys Rev* 2010;**B81**:064113.
388. López-Solano J, Rodríguez-Hernández P, Muñoz A, Gomis O, Santamaría-Perez D, Errandonea D, Manjón FJ, Kumar RS, Stavrou E, Raptis C. Theoretical and experimental study of the structural stability of $TbPO_4$ at high pressures. *Phys Rev* 2010;**B81**:144126.
389. Meldrum A, Boatner LA, Weber WT, Ewing RC. Radiation damage in zircon and monazite. *Geochim Cosmochim Acta* 1998;**62**(14): 2509–20.
390. Weber WJ, Ewing RC, Catlow CRA, Diaz de la Rubia T, Hobbs LW, Kinoshita C, Matzke Hj, Motta AT, Natasi M, Slje EKH, Vance ER, Zinkle SJ. Radiation effects in crystalline ceramics for the immobilization of high-level nuclear waste and plutonium. *J Mater Res* 1998;**13**: 1434–84.
391. Burakov BE, Yagovkina MA, Garbuzov VM, Kitsay AA, Zirlin VA. Self-irradiation of monazite ceramics: contrasting behaviour of $PuPO_4$ and (La, Pu)PO_4 doped with Pu-238. *Mater Res Soc Symp Proc* 2004;**824**:219–24.
392. Goubard F, Griesmar P, Tabuteau A. Alpha self-irradiation effects in ternary oxides of actinides elements: the zircon-like phases $Am^{III}VO_4$ and $A^{II}Np^{IV}(VO_4)_2$ (A = Sr, Pb). *J Solid State Chem* 2005;**178**:1898–902.
393. Chen C, Liu L, Lin C, Yang Y. High-pressure phase transformation in $CaSO_4$. *J Phys Chem Solids* 2001;**62**:1293–8.
394. Kirfel A, Will G. Charge density in anhydrite, $CaSO_4$, from X-ray and neutron diffraction measurements. *Acta Crystallogr* 1980;**B36**:2881–90.
395. Norlund Christensen A, Olesen M, Cerenius Y, Jensen TR. Formation and transformation of five different phases in the $CaSO_4$–H_2O system: crystal structure of the subhydrate β-$CaSO_4$, $0.5H_2O$ and soluble anhydrite $CaSO_4$. *Chem Mater* 2008;**20**:2124–32.
396. Chang FM, Jansen M. Crystal structure refinement of silver permanganate. *Z Kristallogr* 1984;**169**:295–8.
397. Kay MI, Frazer BC, Almodovar I. Neutron diffraction refinement of $CaWO_4$. *J Chem Phys* 1964;**40**:504–6.
398. Masse R, Durif A. Etude structurale de la forme haute temperature du monophosphate de bismuth $BiPO_4$. *C R Acad Sc Paris II* 1985;**300**:849–51.